



Durham E-Theses

CP(¹) model on a sphere and on a torus

Cova, Ramón José Cova

How to cite:

Cova, Ramón José Cova (1997) *CP(¹) model on a sphere and on a torus*, Durham theses, Durham University. Available at Durham E-Theses Online: <http://etheses.dur.ac.uk/4851/>

Use policy

The full-text may be used and/or reproduced, and given to third parties in any format or medium, without prior permission or charge, for personal research or study, educational, or not-for-profit purposes provided that:

- a full bibliographic reference is made to the original source
- a [link](#) is made to the metadata record in Durham E-Theses
- the full-text is not changed in any way

The full-text must not be sold in any format or medium without the formal permission of the copyright holders.

Please consult the [full Durham E-Theses policy](#) for further details.

CP^1 MODEL ON A SPHERE AND ON A TORUS

Ramón José Cova Cova

A thesis presented for the degree of
Doctor of Philosophy
at the University of Durham

Department of Mathematical Sciences
Centre for Particle Theory
University of Durham
Durham DH1 3LE
England

March 1997

The copyright of this thesis rests
with the author. No quotation
from it should be published
without the written consent of the
author and information derived
from it should be acknowledged.



3 JUL 1997

A MI FAMILIA...

Contents

List of Figures	iii
Foreword	vii
Abstract	viii
1 Introduction	1
2 Soliton theory	14
2.1 Derrick's theorem	15
2.2 Topological considerations	17
2.3 Solitons in one dimension	25
2.4 Solitons in two dimensions	30
2.5 Solitons in three dimensions	34
3 A planar skyrmion model	39
3.1 The non-linear $O(3)$ sigma model	39
3.2 CP^1 formulation	43
3.3 Modified model	47

3.4	Numerical procedure	52
3.5	Results	55
3.5.1	Static case	55
3.5.2	Scattering	66
4	$\mathbb{C}P^1$ model on a torus	77
4.1	The $O(3)$ model on a torus	78
4.2	Basic numerical set up	84
4.3	Solitons of degree one	87
4.3.1	$O(3)$ case	87
4.3.2	Skyrmion case	94
4.4	Solitons of degree 2	106
4.4.1	$O(3)$ case	106
4.4.2	Skyrmion case	110
5	Summary	128
6	Bibliography	135

List of Figures

3.1	Total energy density for one skyrmion at the initial time and the evolution of its height.	60
3.2	The skyrmion-lump shakes off some kinetic energy waves that spread out to the boundary at the speed of light.	61
3.3	As the kinetic waves fade away with time we are left with a stable pure $O(3)$ lump on the lattice.	62
3.4	A repulsive force exists between the two skyrmions.	63
3.5	Development of the energy density for two skyrmions which start from rest.	64
3.6	<u>Above</u> : Total energy density corresponding to two pure $O(3)$ solitons with no initial speed. <u>Below</u> : The same $O(3)$ lumps with different non-zero initial speeds (both curves correspond to head-on collisions that lead to scattering at right angles). Compare with the stable case shown in diagram 3.11.	65
3.7	Collision featuring two skyrmion-lumps with relative initial velocity $\vec{v} = (0.2, 0.0)$	69
3.8	Contour plots for figure 3.7.	71

3.9	Two skyrmion-humps in collision course; their relative initial velocity is $\vec{v} = (0.3, 0.0)$	72
3.10	Contour plots for figure 3.9.	74
3.11	Amplitude of the total energy density corresponding to skyrmion scattering. A speed of 0.2 (0.3) leads to back-to-back (right angles) scattering. In both cases the lowest E_{max} occurs at impact time, when the two lumps coalesce. Compare with the unstable case of figure 3.6.	75
3.12	Non-zero impact parameter collision between skyrmions. The initial velocity is $\vec{v} = (0.3, 0.01)$	76
4.1	The non-periodic field W_1 (dashed line) and its periodised version W_p (solid line) along the line $y = 2$ of the fundamental cell.	97
4.2	The real (above) and imaginary (below) parts of the periodic soliton field W_p . The periodisation procedure creates small folds at the borders.	98
4.3	The first component of the periodic soliton $\vec{\phi}_p$. The components ϕ_2 and ϕ_3 are shown next.	99
4.4	Total energy density at the initial time corresponding to the periodic field W_p . The folds at the edges, brought about by the periodisation procedure, must be eliminated in order to improve the initial conditions.	102

4.5	<u>Above</u> : Total energy density at $t_0=0.8$, corresponding to our prepared, improved initial one-soliton configuration. <u>Below</u> : The maximum value of the total energy density (E_{max}) and the total energy <i>vs.</i> t . The lump grows infinitely tall soon after $t_f \approx 3.5$, and the numerical procedure collapses.	103
4.6	Modified $O(3)$ model for a single-lump with $\theta_1 = 0.001$. <u>Above</u> : Peak of the total energy density <i>vs.</i> t . The lump is now stable. <u>Below</u> : The corresponding total energy is now conserved throughout the numerical evolution. In both diagrams t runs from $t_0=0.8$ [compare with figure 4.5].	104
4.7	Kinetic plots for the single-skyrmion case of figure 4.6. <u>Above</u> : Peak of the kinetic energy density <i>vs.</i> time. <u>Below</u> : The corresponding total kinetic energy. In both diagrams the large values of the kinetic energy are during the preparatory stage ($t=0$ to $t_0=0.8$). Later on, the kinetic energy is derisory.	105
4.8	Total energy density corresponding to $O(3)$ solitons sent towards each other with $\vec{v} = (0.2, 0)$	116
4.9	Total energy density corresponding to $O(3)$ solitons moving away from the centre with $\vec{v} = (0.2, 0)$. The amplitude of the lumps gradually decreases as they approach each other, reaching a minimum when they coalesce.	118
4.10	Graphs corresponding to the scattering shown in figure 4.9.	120
4.11	Conservation of energy and topological index. The slopes at the tail of the curves signal the occurrence of numerical errors as the solitons get too spiky.	121

4.12	$O(3)$ solitons moving away from the centre along the (0,0)-(4,4) diagonal (B). They collide at the corners and scatter at right angles (A). When the model is supplemented by a Skyrme term the lumps are stable, as shown in the accompanying graph $E_{max}(t)$ (broken curve).	122
4.13	$O(3)$ collision for a relatively large impact parameter. The initial velocity is $\vec{v} = (0.3, 0.1)$	123
4.14	Skyrmion scattering ($\theta_1=1/2000$) for $\vec{v} = (0.2, 0)$. After scattering like the $O(3)$ solitons of figure 4.9, the skyrmions do not collapse but go on to collide at $t = 11, 17.5, 25.5$ and so forth. In every occasion they scatter at right angles. This cycle repeats itself indefinitely.	125
4.15	Three dimensional picture corresponding to the second collision of the event depicted in figure 4.14. The four peaks characterise the coalescing state, where the lumps can no longer be individually recognised. Note also that the united skyrmions occupy all the lattice area.	126
4.16	Trajectories of the position of E_{max} corresponding to head-on scattering of skyrmions arbitrarily situated in the basic cell. The labels A-E follow the itinerary of one of the lumps. The polar plot shows $Z = r \sin(\vartheta)$. The distance d is from the lumps to the origin (0,0,0) of equations (4.58).	127

Foreword

This thesis is the result of research done by the author during the period 1993-1996 at the University of Durham, under the supervision of Professor Wojtek Zakrzewski. No part of it has been submitted for any degree, either in this university or anywhere else.

Except for the first and second chapters and wherever a reference is given, this work is believed to be original. The third chapter is based on two published papers [1, 2] and chapter 4 is a substantial extension of a Durham preprint [3] submitted for publication to *Nonlinearity*.

I warmly thank Wojtek for his general support and key supervision throughout. I have also derived great benefit from the internal seminars organised by him, and I would like to acknowledge all the colleagues therein involved. Educational as well have been conversations with Dr. Bennett Palmer in the topic of harmonic maps and with Dr. Michael Young who many times assisted me in software and IT matters relevant to my thesis. I also thank M. Blatter and R. Burkhalter for making available to me a subroutine that computes the Weierstrass σ function.

Finally, I acknowledge the financial support of *Universidad del Zulia* and *Fundación Gran Mariscal de Ayacucho*.

© R. J. Cova 1997

The copyright of this thesis rests with the author. No quotation from it should be published without his prior written consent and information derived from it should be acknowledged.

CP^1 model on a sphere and on a torus

Ramón José Cova Cova

Ph.D. Thesis, 1997

Abstract

The work in this thesis is concerned with the numerical study of some stability and scattering properties of two CP^1 models in three dimensional space-time: The non-linear $O(3)$ model and its modified Skyrme version. Chapter 3 focuses principally on the Skyrme model on compactified plane, the topological sphere. Such model is obtained by supplementing the ordinary $O(3)$ lagrangian with both a Skyrme term and a potential term which, in the present work, has a rather general form. Under the numerical simulation the skyrmions behave stably and scatter either back-to-back or at 90° to the initial direction of motion, depending on the initial velocity. In the $O(3)$ limit the solitons are no longer stable and scatter at 90° irrespective of the speed. In the fourth chapter the $O(3)$ model is studied on a flat torus. Its solitons exhibit the usual instability but can be stabilised by the sole addition of a Skyrme term to the lagrangian. Scattering at right angles is observed in all cases considered, including skyrmions colliding at speeds that would bounce them back were they evolving in compactified plane. The periodic $O(3)$ model has no analytic solutions of degree one, so when a field configuration that resembles a single soliton is numerically evolved, it shrinks to become infinitely thin. Interestingly, such *ansatz* may be regarded as a soliton of unit topological charge in the context of the periodic skyrmion model. Chapter 5 closes with a summary and suggestions for future research.

Chapter 1

Introduction

Elementary particles are described by fields which obey relativistic wave equations. These fields have basic properties that follow from a postulated invariance of the wave equations under certain groups of transformations, the symmetry groups. Examples of these symmetries are the independence of the laws of physics from the origin of time and from the position and orientation of laboratories in ordinary space. Invariance of the wave equations under the groups of time and space translations and rotations leads to conservation of energy and momentum and angular momentum.

The most important invariance principle in quantum field theory (QFT) is the principle of relativity, which imposes that the equations of motion be invariant under the proper orthochronous Poincare group. Wave fields are assumed to belong to representations of this group; their space-time geometrical nature is thus determined and the fields can only be spinors or tensors under the Poincare group (scalars and vectors being tensors of order



zero and one, respectively).

In addition to their Poincare geometrical nature, there exists a rich variety of fields which may be spinors or tensors with respect to certain symmetry groups related to internal quantum numbers like isospin, flavour, colour, *etc.*. These internal degrees of freedom result from the invariance of the wave equations under the so-called gauge transformations which act on the (gauge) field regarded as an entity in an internal space, such as the group $SU(2)$ of phase operator transformations of isospinors. One should bear in mind that, whereas the Poincare invariance of the equations of field theory is universal, invariance under internal symmetry groups (gauge groups) is obeyed by specific models, *e.g.*, quantum chromodynamics (QCD), a $SU(3)$ gauge theory that describes the strong interactions. Internal symmetries can also be approximate, as in flavourdynamics.

Gauge fields play a fundamental role in most unification models, schemes where the nuclear interactions are analogous to quantum electrodynamics (QED) but with consideration to the specific characteristics of a non commutative gauge group. Such a prosperous idea was introduced by Yang and Mills (YM) in 1954 [4]. The utility of gauge fields lies chiefly in their ability to express underlying relations among forces that appear superficially to be quite distinct. Example of an unification model is the standard model (SM), whose gauge group is $SU(3) \times SU(2) \times U(1)$. Roughly, the SM is based on six leptons and six accompanying quarks in three separate levels of energy (generations). It amalgamates strong interactions, electro-weak theory and classical gravitational interactions. The forces responsible for these interactions are transmitted by another set of particles, the gauge bosons (a modern

version of Yukawa's bosons). Despite its success, the SM is considered incomplete since it has many arbitrary parameters: In its simplest version there are over 20, including particle masses and strength of forces. This might be an indication that the model is carrying a bit too much baggage.

Of utmost importance for the formulation of unification models is the Higgs mechanism [5, 6] of mass generation for the weak bosons $-W^\pm, Z^0-$ by spontaneous symmetry breaking. This phenomenon occurs when the basic states of a given system do not enjoy a symmetry of the associated lagrangian. The YM theory did not receive much attention at first, and it was the discovery of the Higgs mechanism in 1966 that awoke interest in it.

Until not so long ago, the only means for obtaining numerical quantities in field theory was the method of perturbations. This method gives excellent results in QED but it is less useful in low-energy QCD due a to a rising coupling constant. Over the past years, however, the development of YM theories has given rise to a promising alternative area of research: Classical non-linear equations that admit non-dissipative non-singular solutions of finite total energy; lump-like structures that propagate without diffusion. These entities, generically referred to as **solitons** owing to their 'solitary wave' and particle-like behaviour allow to model complicated phenomena which lie beyond the scope of linear description. The properties of solitons in the quantum version of these schemes are not analysed through a standard perturbative approach, but via an expansion which is a generalisation of the familiar WKB method in field theory. In this expansion, the quantum solitons receive their leading contributions from their classical counterparts, around which the fluctuations are quantised [7].

The existence of solitons is quite special, since in most equations dispersion effects would lead to the breakup or collapse of a lump. Solitons only emerge from equations where diffusion and non-linear effects exactly balance each other, permitting the travelling lumps to conserve their initial integrity as if the medium were linear and dispersionless. Furthermore, unlike most non-linear theories, the theory of solitons possesses the linear-like feature whereby two solutions can be combined to produce a third one. Not unnaturally, the localised nature of soliton-bearing systems, resembling extended objects with finite energy such as might be the classical limit of hadrons, make them candidates to describe elementary particles. Noteworthy is the fact that solitons appear in most theories with spontaneous symmetry breaking.

The theory of solitons brings together many branches of mathematics, *v.gr.*, topology, differential geometry, group theory and complex analysis. It has applications in many sub-fields in physics, including nuclear and particle theory, condensed matter, hydrodynamics and optics. In biophysics solitons arise in the description of DNA and protein dynamics [8]. Soliton theory illustrates the interaction between physics and mathematics, of how one is drawn from one subject to understand the other [9]. It brings new insight to research in technology, affecting related concepts of noise figure degradation and information entropy increase. In communication theory, for example, the possibility of transmitting optical signals over virtually unlimited lengths using soliton-pulse propagation augurs well, and it certainly checks previous engineering knowledge. Much research has been done, and continues today, on system topologies, management and communication protocols for solitonic

fiber-optic networks, the promised communication highways of the future [10].

The first recorded observation of solitonic behaviour was made by an English shipbuilding engineer on the Edinburgh-Glasgow canal in 1834, although the matter was officially reported a decade later [11]. In 1895 Korteweg and de Vries [12] derived an equation for waves in shallow water, taking into account dispersion but ignoring the dissipation of energy. Known as KdV, the equation due to these two scientists can be written as

$$\frac{d}{dt}u + 6u\frac{d}{dx}u + \frac{d^3}{dx^3}u = 0. \quad (1.1)$$

It has the travelling wave solution

$$u(x, t) = 2k^2 \frac{1}{\cosh^2 k(x - 4k^2t - x_0)}, \quad (1.2)$$

where the amplitude $2k^2$ is equal to half the speed of the wave.

For a long time solitons were treated as an unimportant piece of exotica which one encountered in two-dimensional problems of non-linear waves. It was supposed that when two such waves collided, they fell apart; there was no basis for considering soliton solutions to be sufficiently general.

But things took a turn in 1965 when Zabusky and Kruskal [13], studying a periodic unidimensional anharmonic lattice whose continuum limit is (1.1), discovered via numerical computations that solitons were not destroyed under collisions; they somehow passed through one another, changing places in an elastic interaction. The picture was especially curious when two lumps collided with speeds $v_1 \gg v_2$: The fast, big lump swallows the slow, small one and then emits it again.

The theoretical basis for these properties was found in Princeton three years later [14] when it was shown that equations of the KdV type have an infinite series of conserved quantities in a class of multi-soliton solutions, described by a Schrodinger equation. In 1972 two Russians brought to light yet another class of non-linear Schrodinger equations, possessing these same properties [15].

One of the most powerful methods for solving KdV-like equations involves mapping the non-linear problem into an inverse linear system which resembles the problem of finding the potential of a Schrodinger equation from the scattering and bound-state data of its solutions, rather than the other way around. This procedure, known as the inverse scattering transform [16], can be considered as the non-linear analogue of the Fourier transform. Other effective techniques for constructing multi-soliton solutions are the Backlund transformations [17], whereby multi-solitons are generated via a recursive method, and the Hirota method [18], which relies on reducing the given non-linear equation to a bilinear system through a change of variables.

Now, solitonic solutions of **integrable models** (those for which methods of finding solutions exist) like (1.1) are constrained by the above-said presence of an infinite number of conserved quantities. Such models possess a relatively simple dynamics in which, for instance, collisions occur always elastically, essentially undergoing no more than a phase shift. This kind of models are of enormous interest in soliton theory itself and in several areas of science. But in particle physics, where complicated phenomena as particle annihilation must be accounted for, integrable models are of very limited relevance.

The majority of integrable equations are encountered in unidimensional systems, the panorama presenting itself much more involved as we augment the dimensionality of space. In (2+1) dimensions (2 space, 1 time) for instance, only few integrable systems are known, and none of them enjoys the requisite relativistic invariance. Examples of such systems are the Davey-Stewardson [19] and the Kadomtsev-Petviashvili [20] equations, which are basically simple generalisations of familiar unidimensional equations. The Kadomtsev-Petviashvili equation, for example, is a two-dimensional version of (1.1):

$$\frac{d}{dx} \left(\frac{d}{dt} u + 6u \frac{d}{dx} u + \frac{d^3}{dx^3} u \right) + 3 \frac{d^2}{dy^2} u = 0.$$

Therefore, when the space dimensionality is greater than one, explicit solutions of relativistically invariant **non-integrable models** are mostly restricted to static ones and Lorentz transformations thereof. The dynamics of such systems is studied using numerical simulations and approximation techniques. Possessors of a non-trivial scattering behaviour, whereby a soliton and an anti-soliton can collide and annihilate each other producing radiation, non-integrable solitons are the ones that seem more suitable to fit into the framework of particle physics.

The properties of higher dimensional solitons are closely related to the topological aspects of the gauge fields, instances of more abstract mathematical structures known as connections in fiber bundles. Through topology we can usually explain the complexity of these models even without knowing the analytic expression of their solutions. This is superlatively important for, as already outlined, analytical soliton solutions are certainly not in oversupply.

One of the most interesting result is the appearance of conserved quantities having no dynamic but purely topological origin. Solitonic entities bearing these so-called **topological charges** are frequently referred to as **topological solitons**. These charges invest the solitons with a stability that prevents them from decaying into the basic state(s), and relies on the *global* aspects of the system (its topology). Such global aspects do not depend critically on the self-interaction of the system, and so the circumstances that facilitate the appearance of topological solitons in nature (where they are widely observed) is by large and far less restrictive than in the case of integrable solitons, which owe their stability to the *local*, delicate details of the governing evolution equations. Such details are exigent, and so the occurrence of integrable solitons is scarce.

A notable example of a topological soliton is the 't Hooft-Polyakov monopole (tHP) [21, 22], which dons a fresh look upon the familiar Dirac magnetic monopole. It appears in a whole class of models of weak and electromagnetic interactions; absent in the original scheme of Weinberg-Salam, the tHP monopole does come about in several of its modifications, *e.g.*, in the Georgi-Glashow model.

Another important concept in soliton theory is that of **instantons**: Localised finite-action classical solutions of the Euclidean version of the field equations of any given model. Classically, instantons in D Euclidean dimensions are essentially the same as *static* solitons of the same model in $(D+1)$ Minkowskian dimensions. This is basically because static solutions involve only the spatial coordinates, the Euclidean sub-space of Minkowskian space-time. Consider for example one scalar field ϕ in $(2+1)$ dimensions with a

Minkowskian action given by

$$S_M^{(2+1)} = \int dt \int dx dy [(\partial_t \phi)^2 - (\partial_x \phi)^2 - (\partial_y \phi)^2], \quad (1.3)$$

whose static energy density is

$$E_{static}^{(2+1)} = \int dx dy [(\partial_x \phi)^2 + (\partial_y \phi)^2]. \quad (1.4)$$

The point to note is that (1.4) possesses the same structure as the two-dimensional Euclidean action

$$S_{Euc}^{(2)} = \int dx_4 \int dx [(\partial_4 \phi)^2 + (\partial_x \phi)^2], \quad x_4 = it. \quad (1.5)$$

Clearly, the solutions to (1.4) can be formally employed in the model (1.5) and vice-versa. Observe *en passant* that instantons are also localised in the time coordinate x_4 , hence the name ‘instanton’.

In spite of their classical similitude, the impact of solitons and instantons on the corresponding quantum theory is very different: Solitons lead to extended-particle states and instantons lead to tunnelling effects that can affect the structure of the vacuum state. The contribution of classical instantons to quantum effects is proportional to $\exp(-S_{Euc})$, which cannot be substantial unless the action is finite. This and other important features of Minkowskian QFT can be conveniently explored through instantons. Such methods have been applied in, for example, the problems of a double-well potential [23] and a periodic potential [24].

Returning to the topological charge, it can be interpreted in a natural way: We can imagine the soliton as a subatomic particle carrying the topological charge as one of its constants of motion. Among the most successful models

which have made use of this appealing idea is the (3+1)-dimensional **Skyrme model** in hadron physics [25]. It deals with an effective theory of pions and how to derive baryons and their interactions within such theory. Its soliton solutions, the skyrmions, are thought of as classical protons and neutrons with the conserved topological charge being the baryon number. This model, where just two free parameters are required, leads to qualitative results which are in good qualitative agreement with experimental results of nuclear physics [26]. It is interesting to highlight that solitons in the Skyrme model appear directly, by construction. In contrast, solitons within the framework of grand unified theories come about as an offshoot: They emerge in the form of domain walls, cosmic strings and monopoles through the Kibble mechanism.

In the beginning the Skyrme model received relatively short shrift, partly because of the advent of QCD: The QFT-notion of a free particle described by a quantised mode of a linear equation with its interactions being described through perturbation theory would not give way. Nevertheless, the Skyrme model acquired popularity towards the end of the 70s due to speculations that it might serve as a link between QCD and the familiar old theory (valid in the low-energy regime) where the inter-baryonic forces occur via the exchange of Yukawa π mesons. In this low-energy regime QCD encounters the difficulty of having no small parameter to describe the dynamics of quarks and gluons. But in the limit as the number of colours N tends to infinity, QCD reduces to a theory of effective mesons with interactions of order $1/N$. Amazingly, it transpires that in such a limit baryons may be regarded as solitons of an effective meson theory without any further reference to their quark content [27]. Hence the re-newed interest in the Skyrme model.

In 1983 the model was boosted further, when it was shown that its lagrangian, supplemented with a Wess-Zumino term, reproduces the quantum numbers of baryons in QCD [28]. This latter result comes from simply eliminating a certain discrete symmetry of the skyrmion lagrangian which is not a symmetry of QCD. This is most remarkable.

A scheme that connects the Skyrme model with quarks is the so-called hybrid model [29]. It pictures the space in two parts: A very small volume with only quarks and gluons interacting perturbatively as dictated by QCD, and the rest, large part of the whole containing pions and skyrmions.

The Skyrme system is just one example of a large family of non-linear models known as **chiral** or **sigma models** introduced in the 1960s to describe β -decay and strong interactions where topology played no role [30]. The baryons were no longer lumps of energy but were represented in the context of quantum theory as non-linear fields themselves. The calculations were made utilising the techniques of current algebra.

Soliton-like structures occur abundantly in the context of sigma models. In the plane for instance they bear several properties in common with the more involved (3+1)-dimensional YM schemes. Amongst these properties we have conformal invariance, spontaneous symmetry breaking, asymptotic freedom and existence of soliton solutions. *Obtaining information about the quantum field theory of gauge systems in three-space, starting from classical solutions of the corresponding, less cumbersome, equations of low-dimensional analogues, is one of the ideas behind the study of sigma models.* It goes without saying that quantum solitons are the ones to be applied in particle physics but, as mentioned earlier, they are quantised around their classical

counterparts.

Sigma models are interesting by themselves. Known as harmonic maps, they represent a rich industry of research in pure mathematics, differential geometry in particular. Besides, as we have been illustrating -and shall continue to do as we move on-, there is this ample spectrum of applications of sigma models in nature that motivates one's dedication to the subject. For example, the **non-linear $O(3)$ model** has been used in solid state physics as the continuum limit of the Heisenberg ferromagnet, and also appears to provide mechanisms for high-temperature superconductivity [31] and the quantum Hall effect [32].

In the present thesis we study aspects of the *classical* theory of two particular sigma **CP^1 models** in (2+1) dimensions: The non-linear $O(3)$ model and a modified version of it that can be considered as a low-dimensional analogue of the Skyrme model in three spatial dimensions. Specifically, we are concerned with the stability and scattering properties of the CP^1 solitons. Being non-integrable, the evolution in time of our CP^1 systems must be done via numerical simulations, and so a significant proportion of our work is numerical. Numerical and graphical: We have included a sizable selection of illustrations all along our work.

Our two CP^1 models have links not only with the (3+1) dimensional skyrmion theory, but also with several other important theories in particle physics, like the tHP monopoles and the vortices of the abelian Higgs model. Our class of low-dimensional Skyrme models is similar to these extended entities in that parameters exist in the lagrangian which determine the size

of the extended structures. Moreover, these parameters possess a limit where the interaction forces between the particles vanish: This is the so-called Bogomolny-Prasad-Sommerfield (BPS) limit for the tHP monopoles and the $O(3)$ limit for the planar skyrmion model. Also, the CP^1 models of our concern have scattering properties akin to those observed in the said (3+1) dimensional systems.

In the next chapter we review some relevant mathematics for the exposition ahead. Using a relatively general expression for the potential energy, in chapter 3 we consider the Skyrme model in the usual compactified plane or, topologically equivalent, in the two-sphere. In chapter 4 we envisage the problem of both the $O(3)$ and skyrmion model on a torus, a rather unexplored format in this context. Chapter 5 closes with a summary, some conclusions, and our suggestions for future research.

Hopefully, our work will be of a small contribution to applied mathematics, soliton theory in particular. And it might perhaps awake some interest to extend it to more realistic (3+1) dimensional scenarios, specially the model on the torus laid out in chapter 4.

Chapter 2

Soliton theory

There are non-linear field theories that are integrable in one space-dimension, but all their time-dependent solutions cannot be obtained in general. And for typical systems in higher dimensions there is no systematic method of obtaining even a single non-trivial solution in an analytic form. From the standpoint of physics, there is the additional requirement that such theories must be relativistically invariant. Thus, in soliton theory we analyse static finite-energy configurations and try to obtain as much information as possible without explicitly solving the field equations. In so doing, topological techniques, a virial-like theorem and a relatively simple completing-the-square procedure are of enormous utility. The dynamics of these models is then studied via approximations and numerical techniques.

2.1 Derrick's theorem

Consider the class of Poincare or Lorentz-invariant non-linear scalar field theories in a Minkowski space in $(D + 1)$ dimensions (D space, one time):

$$x_\mu x^\mu = (x^0)^2 - \sum_{i=1}^D (x^i)^2, \quad \mu = 0, 1, 2, \dots, D.$$

And consider those systems described by a lagrangian density of the standard relativistic form

$$\begin{aligned} \mathcal{L} &= C \sum_{a=1}^n \sum_{\mu=1}^D \partial_\mu \phi_a \partial^\mu \phi_a - U(\vec{\phi}) \\ &= C (\partial_\mu \vec{\phi}) \cdot (\partial^\mu \vec{\phi}) - U(\vec{\phi}), \end{aligned} \tag{2.1}$$

where

$$\vec{\phi} \equiv \{\phi_a(x^\mu); a = 1, 2, \dots, n\}$$

denotes a vector in the internal space of the fields. The function U is non-negative and vanishes only at its absolute minima which, without loss of generality, we can normalise to zero. The number C is a constant adjustable to convenience.

We are concerned with the possible existence of non-singular solutions whose energy density at a given time is finite in some finite region of space, and falls to zero at spatial infinity sufficiently fast as to be integrable. Such **localised** energy density has a distinctive lump-like profile usually able to propagate without much change in shape. The corresponding field solution is a **soliton**. One should be aware that in the scientific soliton-community the soliton's energy density (the soliton-lump) is frequently dubbed a 'soliton' as

well (actually, by antonomasia virtually any lump is referred to as a soliton). We shall try to distinguish both usages in this work but, inevitably, our propensity to follow the semantically lax, popular trend will be manifest in some passages.

Now let us look at the static situation where the energy as identified from (2.1) is (the static energy of this system is just its potential energy)

$$\begin{aligned} V(\vec{\phi}) &= C \int (\partial_k \vec{\phi}) \cdot (\partial_k \vec{\phi}) d^D x + \int U(\vec{\phi}) d^D x \\ &= V_1(\vec{\phi}) + V_2(\vec{\phi}), \quad k = 1, \dots, D, \end{aligned} \quad (2.2)$$

in obvious notation. A static solution of the model (2.1) is an extremum condition $\delta V=0$ for (2.2), which leads to the static field equation [take $C = 1/2$]

$$\nabla^2 \vec{\phi} - \frac{d}{d\phi} U = \vec{0}. \quad (2.3)$$

Let $\vec{\phi}_1(\vec{x})$ be a solution to (2.3) and consider the one-parameter family of configurations obtained by re-scaling $\vec{x} \mapsto \gamma \vec{x}$:

$$\vec{\phi}_\gamma(\vec{x}) = \vec{\phi}_1(\gamma \vec{x}). \quad (2.4)$$

With the help of equation (2.2) we get

$$V[\vec{\phi}_\gamma(\vec{x})] = \gamma^{2-D} V_1[\vec{\phi}_1(\vec{x})] + \gamma^{-D} V_2[\vec{\phi}_1(\vec{x})], \quad (2.5)$$

wherefrom

$$\frac{d}{d\gamma} V[\vec{\phi}_\gamma(\vec{x})] = (2-D)\gamma^{1-D} V_1[\vec{\phi}_1(\vec{x})] - D\gamma^{-1-D} V_2[\vec{\phi}_1(\vec{x})]. \quad (2.6)$$

Since $\vec{\phi}_1(\vec{x})$ is a local extremal of V , it must in particular produce

$$\frac{d}{d\gamma} V[\vec{\phi}_\gamma(\vec{x})] |_{\gamma=1} = 0,$$

i.e.,

$$(2 - D)V_1[\vec{\phi}_1(\vec{x})] = DV_2[\vec{\phi}_1(\vec{x})]. \quad (2.7)$$

Inasmuch as both V_1 and V_2 are non-negative, equation (2.7) precludes the existence of non-trivial *static* solutions for the class of models (2.1) when $D \geq 3$ (time-dependent solutions are not precluded). This is the content of the so-called Derrick's theorem [33, 34]. It allows one to tell solely from the form of the lagrangian and the dimensionality of space whether a given theory is a candidate for soliton solutions. If we are seeking solitons in $D > 2$ it is necessary to somehow modify the lagrangian (2.1).

Research has therefore been carried out for different types of non-linear equations with various possible values of D . We are going to examine some of these models below, but first let us acquaint ourselves with how topology steps into the soliton scene.

2.2 Topological considerations

One of the basic tasks of topology is to learn how to discern non homeomorphic figures. With this aim one introduces a class of invariant quantities which do not change with homeomorphic transformations of a given figure. The study of topological spaces is connected with the resolution of questions like: Can one describe a class of invariants of a given manifold?. Does there exist a set of integral invariants, fully characterising a given manifold?. Integral invariants are in their own way 'quantum numbers' of a manifold (a similar problem is envisaged in physics, namely, to characterise a particle

having given its special parameters, *v.gr.*, spin, charge, mass). Among such tasks is the classification of n -dimensional surfaces, compact, connected, orientable and 2-dimensional for example, as those we shall encounter in the present thesis.

The internal degrees of freedom of the field, the soliton field, give rise to an internal space whose manifold (the field solutions) can define a non-trivial mapping onto the manifold of the ‘physical’ D -dimensional space. Each mapping can be characterised by an integral number which is a conserved quantity -associated with the topology of the solutions as outlined above and with nothing to do with Noether’s theorem-.

This type of maps is the subject of homotopy theory. Consider two maps f and g from a manifold \mathcal{N} to a manifold \mathcal{M} :

$$f : \mathcal{N} \mapsto \mathcal{M}, \quad g : \mathcal{N} \mapsto \mathcal{M}.$$

These mappings are homotopic if they can be continuously deformed one into the other:

$$\mathcal{F} : \mathcal{N} \times [1, 0] \mapsto \mathcal{M},$$

with the continuous connecting map \mathcal{F} satisfying

$$\mathcal{F}(x, 0) = f(x), \quad \mathcal{F}(x, 1) = g(x).$$

That is, as the continuous variable t in $\mathcal{F}(x, t)$ varies continuously from 0 to 1 in the interval $[0, 1]$, the function $f(x)$ is deformed continuously into $g(x)$.

Homotopy is an equivalence relation that partitions the manifold of continuous maps from \mathcal{N} to \mathcal{M} into equivalent classes $[f]$. A map from one

homotopy sector cannot be continuously deformed into another sector. Homotopy classes are topological invariants of the pair of spaces above, since they are unchanged under homeomorphism of \mathcal{N} or \mathcal{M} . This must be so, for homeomorphism is a continuous map itself. *In this picture we can think of classical time evolution as a homotopy between initial and final state field configurations, and visualise $[f]$ as the class of fields conserved as time elapses.*

A classification of topological spaces may be achieved by selecting a standard ‘test body’ \mathcal{N} and permitting \mathcal{M} to vary through the family of target spaces under study. The sphere S_n , defined by

$$\sum_{k=1}^{n+1} (x_k)^2 = \text{constant},$$

is a usual choice for \mathcal{N} . Here S_0 corresponds to just two points ($x_1 = \pm \text{constant}$), S_1 is a circle or a ring, S_2 is a sphere and so on. Another interesting, if less common, choice for \mathcal{N} is the two-torus T_2 ; we shall deal with it in chapter 4.

Homotopy classes can be endowed with a group structure via the operation $[f + g] = [f] + [g]$. By $\pi_n(\mathcal{M})$ we denote the homotopy group associated with the maps $S_n \mapsto \mathcal{M}$. These groups are generalisations of the first homotopy group or fundamental group $\pi_1(\mathcal{M})$: It consists of the set of classes of closed paths on \mathcal{M} which are not homotopic to one another. Now, a closed path on \mathcal{M} can be represented as the image of a fixed circle $\mathcal{N} = S_1$. The associated fundamental group $\pi_1(\mathcal{M})$ is then the set of non-homotopic maps $S_1 \mapsto \mathcal{M}$. By replacing the circle by the n -sphere we obtain the higher groups $\pi_n(\mathcal{M})$. As an illustration may serve the fundamental group $\pi_1(S_2) = 0$, which says that on a spherical surface all closed paths are homo-

topic and can be shrunk to a point (simple connectedness). For the two-torus we have $\pi_1(T_2) = Z \oplus Z$, signifying that there exists an infinite number of closed paths which are not homotopic to one another. An arbitrary closed path on T_2 is homotopic to a path passing r times along the parallel of the torus and s times along its meridian, and it is labelled by the pair of integers (r, s) . Note that a path with $r = s = 0$ is contractable to a point. The classes $\pi_1(T_2)$ are relevant, for instance, in characterising general ring-vortex configurations in both Higgs and sigma models [35].

In the usual event when the target manifold is also a sphere, it can be proven that [36] :

$$\begin{aligned} \pi_n(S_n) &= Z, \\ \pi_n(S_m) &= 0, \quad n < m, \\ \pi_n(S_1) &= 0, \quad n > 1. \end{aligned} \tag{2.8}$$

The last two expressions indicate that the homotopy groups involved are trivial: All maps can be deformed one into the other. The interesting case when the group of homotopy classes is isomorphic to the group of integers Z means that each homotopy sector can be labelled by an integer: The topological charge. A theory with non-trivial topology is said to be stable, in the sense that no configuration can evolve out of its original topological class.

The scenario for the expressions (2.8) often emerges in the sigma models from demanding that the energy of the fields involved be finite at spatial infinity, the localised fields playing the role of the homotopic maps. When $D > 1$ the fields must tend to the same value at spatial infinity, regardless of direction. Whence, the spatial degrees of freedom of the fields may be

regarded as a one-point compactification

$$\mathfrak{R}_D \cup \{\infty\} \cong S_D, \quad (2.9)$$

leading to the maps

$$S_D \mapsto S_m. \quad (2.10)$$

The homotopy classification is valid for any localised static field configuration (the set of which spans the so-called configuration space). The same classification holds for localised solutions all right (moduli space), as they are subsets of finite-energy configurations.

In connection with the $O(3)$ model in (2+1) dimensions we shall study the case $S_2 \mapsto S_2$ in chapter 3. The pre-image two-sphere comes from compactifying $\mathfrak{R}_2 \cup \{\infty\} \cong S_2$ and the target two-sphere is the internal manifold where the $O(3)$ fields live. The associated homotopy classification is given by (2.8): $\pi_2(S_2) = \mathbb{Z}$.

At the centre of our interest also lies the CP^1 model with periodic boundary conditions, where the solitons are maps $T_2 \rightarrow S_2$. Here, one no longer requires a one-point compactification procedure since the system is situated in a finite volume from the outset (in this sense, the toroidal model looks more physical than the one on the sphere). With regards to the homotopy classification of the toroidal model, it is known [37] that the topological index associated with $T_2 \mapsto S_2$ is given by the integers excluding ± 1 , meaning that the model on the torus possesses no single-soliton solutions.

In any of the above cases the topological index Q can be computed using the expression

$$Q = (\text{constant}) \int_{\mathcal{N}} (\phi^* w), \quad (2.11)$$

where ϕ^*w is a suitable volume-form on \mathcal{N} . The mapping

$$\phi^* : \mathcal{M} \mapsto \mathcal{N}$$

is the pull-back map [38] induced by

$$\phi : \mathcal{N} \mapsto \mathcal{M}.$$

The constant in (2.11) normalises Q to an integer. Further insight into the topological charge, usually called the Brouwer degree in pure mathematics, will be gained as we apply it to particular models as we move on.

A large number of soliton-bearing models can be conveniently considered in the context where the target manifold has the structure of a coset space [39]. The idea is to find a continuous group G of symmetries acting on the manifold \mathcal{M} in such a way that, given a point $p \in \mathcal{M}$, the action of G over p produces the whole of \mathcal{M} . This transitivity property is technically stated as

$$\forall p_1, p_2 \in \mathcal{M}, \exists g \in G \mid gp_1 = p_2.$$

Given this, a homomorphism between \mathcal{M} and G (or some related group) could probably be established. However, note that the said procedure will yield \mathcal{M} more than once in general, the aim being to obtain it only once. The gist of the matter then lies on the question: When do two elements $g_1, g_2 \in G$ yield the same point p of \mathcal{M} ? Observing that

$$g_1p = g_2p \rightarrow g_2^{-1}g_1p = p,$$

we realise that the answer is: When $g_2^{-1}g_1$ leaves p unaltered, *i.e.*, when $h = g_2^{-1}g_1 \in H(p)$, the isotropy group of p :

$$H(p) = \{h \in G \mid hp = p\}.$$

But $h = g_2^{-1}g_1 \rightarrow g_2h = g_1$, meaning that two elements of G operate on p to produce the same point of \mathcal{M} iff they belong to the same left coset of G with respect to $H(p)$. Now we recall from group theory that G may be partitioned into disjoint cosets, with the characteristic -suitable for our objective- that every element of G belongs to *one and only one* left coset of G with respect to $H(p)$. This guarantees that \mathcal{M} will be obtained only once when acted upon by the coset space $G/H(p)$. The identification we desire is then

$$\begin{aligned}\mathcal{M} &= G/H(p) \\ &= \{gH(p) \mid g \in G\},\end{aligned}\tag{2.12}$$

description independent of the choice of p if, as usual in physics, \mathcal{M} is homogeneous.

The manifold \mathcal{M} can now be seen to adopt a variety of forms. Notably:

- Grassmannian sigma-models in $2mn$ dimensions [40, 41]:

$$\begin{aligned}\mathcal{M} &= \frac{SU(m+n)}{SU(m) \times SU(n) \times U(1)} \\ &= \mathcal{G}_{m,n}.\end{aligned}\tag{2.13}$$

They require mn ($2mn$) complex (real) fields. -The case $\mathcal{G}_{1,n}$ is known as the complex projective space CP^n [41, 42, 43]:

$$\begin{aligned}\mathcal{M} &= \frac{SU(n+1)}{SU(n) \times U(1)} \\ &= CP^n.\end{aligned}\tag{2.14}$$

- S_n or $O(n)$ sigma-models [41, 44]: The fields take values on the sphere S_{n-1} , the acting symmetry group being $SO(n-1)$. Given a point p

of the target manifold, the rotations that leave it invariant are those about the direction of p itself; so its isotropy group is $SO(n-1)$. We then have

$$\begin{aligned}\mathcal{M} &= \frac{SO(n)}{SO(n-1)} \\ &= S_{n-1}.\end{aligned}\tag{2.15}$$

Other than giving a systematic classification of important solitonic models, the coset description (2.12) permits the calculation of the associated homotopy groups in a relatively easy fashion. For example, using the result $\pi_2(G/H) = \pi_1(H)$, valid when G is both connected [$\pi_0(G) = 0$] and simply connected [$\pi_1(G) = 0$], we obtain from (2.14)

$$\begin{aligned}\pi_2(CP^n) &= \pi_1(SU(n) \times U(1)) \\ &= \pi_1(SU(n)) \oplus \pi_1(U(1)) \\ &= \pi_1(U(1)) \\ &= Z \quad [U(1) = S_1],\end{aligned}\tag{2.16}$$

a special case of (2.8). In particular, since CP^1 is isometric to S_2 , the above result for $n = 1$ applies to $O(3)$ as well. These two specific models are essentially the same. As a generalisation for arbitrary n , however, CP^n is more appropriate than is $O(n)$, by virtue of continuing to give topological soliton solutions for arbitrary n in the plane. This is not difficult to infer: In two spatial dimensions the case $O(n > 3)$ produces, from expressions (2.10) and (2.15), $S_2 \mapsto S_{n>2}$. Whereupon (2.8) tells us that the associated homotopy group is the trivial $\pi_2(S_{n>2}) = 0$, which cannot accommodate

topological objects. On the other hand, the non-trivial CP^n result (2.16) holds for all n .

Next, we briefly review some examples of solitons in various dimensions.

2.3 Solitons in one dimension

The simplest models governed by (2.1) involve one single real scalar field dwelling in a line. An interesting example is the so-called ϕ^4 theory [22, 45, 46], which plays an important role in gauge theories. It corresponds to a Higgs-like function U of the form

$$U(\phi) = \frac{\lambda}{4} \left(\phi^2 - \frac{m^2}{\lambda} \right)^2, \quad (2.17)$$

where λ, m are positive constants.

The static equation of motion for this system readily follows from inserting (2.17) into (2.3). The resulting equation is solved by

$$\phi(x) = \pm \frac{m}{\sqrt{\lambda}} \tanh\left(\frac{mx}{\sqrt{2}}\right), \quad (2.18)$$

solution known as the kink (by convention, the solution with the minus sign is frequently referred to as the anti-kink).

Finite-energy solutions must obey the boundary conditions

$$\lim_{x \rightarrow \pm\infty} \phi(x) \rightarrow \pm \frac{m}{\sqrt{\lambda}}, \quad (2.19)$$

which are the minima of the potential energy.

The kink provides an example of spontaneous symmetry breaking: Its lagrangian is invariant under reflections $\phi \rightarrow -\phi$ (the internal degree of

freedom of the system) whereas the two fundamental states $\pm m/\sqrt{\lambda}$ are not; rather, they are transformed into one another under reflections. Other symmetries of the kink are those involving the parity operation $x \rightarrow -x$ and space translations $x \rightarrow x + x_0$.

The homotopic maps for this model are the correspondence between the two vacuum states (S_0) and the points at infinity (a 0-sphere as well). We have four topological classes, namely, the kink sector, the anti-kink sector, and the two vacua. These sectors are characterised by the pair of indices

$$[\phi(-\infty), \phi(\infty)] : \left[-\frac{m}{\sqrt{\lambda}}, \frac{m}{\sqrt{\lambda}}\right], \left[\frac{m}{\sqrt{\lambda}}, -\frac{m}{\sqrt{\lambda}}\right], \left[\frac{m}{\sqrt{\lambda}}, \frac{m}{\sqrt{\lambda}}\right], \left[-\frac{m}{\sqrt{\lambda}}, -\frac{m}{\sqrt{\lambda}}\right]. \quad (2.20)$$

The topological index can be defined as the ‘charge’

$$Q = \int_{-\infty}^{\infty} k_0(x) dx, \quad k_0(x) = \frac{\sqrt{\lambda}}{2m} \frac{d\phi}{dx}, \quad (2.21)$$

of the conserved ‘current’

$$k^\mu = \frac{\sqrt{\lambda}}{2m} \epsilon_{\mu\nu} \partial^\nu \phi(x), \quad \mu, \nu = 0, 1, \quad (2.22)$$

where $\epsilon_{\mu\nu}$ is the Levi-Civita pseudotensor. We see that the topological charge is ± 1 for the kink and zero for the minima $\pm m/\sqrt{\lambda}$. The system possesses topological stability, in the sense that a kink will not decay into either of the minima because it is not homotopic to any of them. Also note that (2.21) looks like (*constant*) $\int d\phi$, which is nothing but (2.11) with $\phi^* w = d\phi$ a one-form.

Even though we might not be able to explicitly calculate the evolution of the system, of what happens after, say, a kink and an anti-kink collide,

we know that the resulting field configuration will always be within one of the four homotopy sectors shown above. For instance, an anti-kink coming from the far left and an kink approaching from the far right belong to the $Q=-1+1=0$ class, and there will remain after the impact.

As it actually happens, explicit solutions of the time-dependent ϕ^4 model are not available. Its dynamics, studied through numerical simulations, indicate that the kinks do not retain their shapes under collisions. Also, they seem to repel each other when started off at rest, a characteristic present as well in (2+1) dimensional skyrmions.

The particle-like nature of (2.18) can be further substantiated by deriving an Einsteinian mass-energy formula between static and moving kinks. Since the model is Lorentz-invariant, travelling solutions can be obtained by Lorentz-transforming (2.18):

$$\phi_v = \pm \frac{m}{\sqrt{\lambda}} \tanh\left(\frac{m}{\sqrt{2}} \frac{x - vt}{\sqrt{1 - v^2}}\right), \quad -1 < v < 1. \quad (2.23)$$

We emphasise that this solution is not what we mean by an explicit time-dependent object derived from the full equation of motion, moving independently from other solutions. Now, from equations (2.2) and (2.18) we get

$$\begin{aligned} V(\phi) &= \frac{1}{2} \int_{-\infty}^{\infty} (\partial_x \phi)^2 dx + \int_{-\infty}^{\infty} U(\phi) dx \\ &= \frac{m^4}{2\lambda} \int_{-\infty}^{\infty} \frac{1}{\cosh^4\left(\frac{m}{\sqrt{2}}x\right)} dx \\ &= \frac{2\sqrt{2}m^3}{3\lambda}. \end{aligned} \quad (2.24)$$

The energy expression for (2.23) is related to (2.24) by the mass-energy

formula:

$$V_v(\phi) = \frac{V(\phi)}{\sqrt{1-v^2}}. \quad (2.25)$$

A schematic plot of the integrand in expression (2.24) gives a lump of matter positioned around $x = 0$, able to cruise along unscathed upon boosting.

The ϕ^4 model also illustrates what we mentioned in the previous chapter about solitons only stemming from equations that possess a special, fine balance among their terms. If, instead of (2.17), we take the look-alike $(\phi^2 + \alpha\phi^4)^2$, say, then no soliton solutions are produced.

Also worthy of remark is the non-perturbative character of the kink: Since it is singular when $\lambda \rightarrow 0$, a QFT-like perturbation expansion in λ is no longer feasible. As touched on in chapter 1, the quantum theory of solitons resorts to a semi-classical expansion that quantises around the classical solutions.

Amongst other important models in $D = 1$ appear the KdV (1.1), the $O(3)$ (2.15) [47, 48] and sine-Gordon [49] systems. They are fully-integrable and have several interesting properties, *v.gr.*, possession of an infinite number of conserved quantities, presence of inverse scattering transform and Backlund transformations.

Let us now introduce a useful procedure, first suggested in [50], for constructing static solutions. By completing squares, the static energy for uni-dimensional systems can be cast into

$$\begin{aligned} V(\phi) &= \frac{1}{2} \int_{-\infty}^{\infty} [\partial_x \phi \pm \sqrt{2U(\phi)}]^2 dx \mp \int_{-\infty}^{\infty} \partial_x \phi \sqrt{2U(\phi)} dx \\ &= \frac{1}{2} \int_{-\infty}^{\infty} [\partial_x \phi \pm \sqrt{2U(\phi)}]^2 dx \mp \int_{\phi(-\infty)}^{\phi(\infty)} \sqrt{2U(\phi)} d\phi. \end{aligned} \quad (2.26)$$

Wherefore the inequality (sometimes referred to as the Bogomolny bound)

$$V(\phi) \geq \left| \int_{\phi(-\infty)}^{\phi(\infty)} \sqrt{2U(\phi)} d\phi \right|, \quad (2.27)$$

which imposes a lower limit to the energy of any static configuration in a given homotopy sector Q . The condition for equality minimises V and occurs iff

$$\partial_x \phi \pm \sqrt{2U(\phi)} = 0, \quad (2.28)$$

expression that is often called the Bogomolny equation. It is of first order, easier to solve than its parent second order equation. Upon inserting the quartic function (2.17) into (2.28) the field (2.18) readily follows.

Solutions of the Bogomolny equation automatically satisfy the original second order equation, but the reverse is not generally true. But for the kink model the double implication does hold. The kink, the anti-kink and the fundamental states ‘saturate’ the bound (2.27), and all other Q -sectors are empty. This feature occurs in all Poincare-invariant soliton systems in one dimension [51].

As applied to one-dimensional situations the artillery of topological techniques seems too simple to merit the bother. It is educational, though, to display such methods here, for the same ideas apply in more complicated scenarios in higher dimensions.

Finally, note that from (2.6) one derives:

$$\frac{d^2}{d\gamma^2} V[\vec{\phi}_\gamma(\vec{x})] = (2 - D)(1 - D)\gamma^{-D} V_1[\vec{\phi}_1(\vec{x})] + D(D + 1)\gamma^{-2-D} V_2[\vec{\phi}_1(\vec{x})]. \quad (2.29)$$

Taking into account that for $D = 1$ equation (2.7) gives

$$V_1[\vec{\phi}_1(x)] = V_2[\vec{\phi}_1(x)] > 0, \quad (2.30)$$

we deduce

$$\frac{d^2}{d\gamma^2} V[\vec{\phi}_\gamma(x)] \Big|_{\gamma=1} = 2 V_2[\vec{\phi}_1(x)] > 0. \quad (2.31)$$

Therefore, $\gamma = 1$ corresponds to a minimum of the potential energy and hence a soliton in $D = 1$ is stable. Its finely-balanced scaling behaviour is brought forth by equation (2.5):

$$V[\phi_\gamma(x)] = \gamma V_1[\phi_1(x)] + \frac{1}{\gamma} V_2[\phi_1(x)]. \quad (2.32)$$

As we shall see in the next section, the situation is entirely different in two spatial dimensions.

2.4 Solitons in two dimensions

Derrick's theorem for planar systems entails $V_2(\vec{\phi}_1) = 0$, in which case the lagrangian (2.1) reduces to

$$\mathcal{L} = C (\partial_\mu \vec{\phi}) \cdot (\partial^\mu \vec{\phi}), \quad \mu = 0, 1, 2. \quad (2.33)$$

An illustration is provided by the $O(4)$ chiral model. It consists of a real vector

$$\vec{\phi} = (\phi_0, \phi_1, \phi_2, \phi_3) \quad (2.34)$$

restricted to take values on the 3-sphere S_3 :

$$\vec{\phi} \cdot \vec{\phi} = \phi_0^2 + \phi_k \phi_k = 1, \quad (2.35)$$

summation over $k=1,2,3$ understood. The model is clearly invariant under the $O(4)$ rotation group in internal space. The equation of motion that stems

from (2.33)-(2.35) is

$$\partial_\mu \partial^\mu \vec{\phi} + (\partial_\mu \vec{\phi} \cdot \partial^\mu \vec{\phi}) \vec{\phi} = \vec{0}. \quad (2.36)$$

It is customary to take as the basic field the $SU(2)$ quaternion

$$\begin{aligned} J &= \begin{bmatrix} \phi_0 + i\phi_3 & \phi_2 + i\phi_1 \\ -\phi_2 + i\phi_1 & \phi_0 - i\phi_3 \end{bmatrix} \\ &= \phi_0 \tau_0 + i\tau_k \phi_k, \end{aligned} \quad (2.37)$$

where τ_0 is the 2×2 identity matrix and τ_k are the Pauli matrices. Laborious but straightforward manipulation yields

$$\partial_\mu J \partial^\mu J^{-1} = \begin{bmatrix} (\partial_\mu \vec{\phi}) \cdot (\partial^\mu \vec{\phi}) & 0 \\ 0 & (\partial_\mu \vec{\phi}) \cdot (\partial^\mu \vec{\phi}) \end{bmatrix},$$

in terms of which the lagrangian density (2.33) becomes

$$\mathcal{L} = \frac{C}{2} Tr(\partial_\mu J \partial^\mu J^{-1}), \quad (2.38)$$

with Tr denoting the trace of the matrix.

Written in this form the invariance of the model under the so-called $SU(2) \times SU(2)$ chiral transformations is manifest. Since the chiral group and the four-dimensional rotations have the same Lie algebra, the $O(4)$ model is equivalently referred to as $SU(2)$ chiral. Noteworthy as well is that upon expanding (2.38) around the vacuum, which we can take as equal to τ_0 , one obtains a lagrangian of the Klein-Gordon type: An effective meson model. This is in connection with our earlier remark about skyrmions springing from a theory of pions. Couched in quantum terminology, the pions would be represented by the fluctuations of the field J around τ_0 . The lagrangian (2.38) is the starting point of the Skyrme model.

With regards to the homotopy of the chiral model in two spatial dimensions first note that finiteness of the energy compactifies the plane into the unit 2-sphere as per (2.10). Since the internal manifold is a 3-sphere we then have a trivial homotopy [$\pi_2(S_3) = 0$] wherein no topological extended objects can be accommodated.

Now, the only localised solutions to (2.38) are those corresponding to J being anti-hermitian [$\phi_0 = 0$], the $O(3)$ subspace of $O(4)$ [52]. In this case topological solitons do arise because $\pi_2(S_2) = \mathbb{Z}$. Consequently, one frequently focuses on the $O(3)$ model from the outset rather than on $O(4)$.

An interesting modification of the chiral system is the Ward model [53], where we have time-dependent lumps which do not lie in general in an $O(3)$ subspace. This model is integrable but at the expense of destroying the relativistic invariance of the pure chiral scheme. Both trivial [53] and non-trivial (ninety degrees) [54] scattering have been observed in the Ward model.

An important example of a soliton in two spatial dimensions is the vortex in the abelian Higgs model, mentioned in the first chapter as possessor of interesting similarities with the models dealt with in the present work. Vortices illustrate the mechanism for obtaining dual strings from gauge theories [55] and, upon suitable change of semantics, the vortex system turns into the Ginzburg-Landau model [56] in the statistical mechanics of a superconductor placed in a magnetic field. Here the magnetic flux is quantised by the topological charge.

A prototype presentation of the vortex lagrangian is (note the quartic

kink-like potential):

$$\mathcal{L}_{vortex} = -\frac{1}{4}F^{\alpha\beta}F_{\alpha\beta} + (D_\alpha\phi)^*(D^\alpha\phi) - \frac{\eta}{2}(|\phi|^2 - \frac{m^2}{\eta})^2, \quad (2.39)$$

where ϕ is a complex scalar field, $F_{\alpha\beta}$ is the familiar electromagnetic tensor, D_α is the covariant derivative and m, η are constants. The tHP monopole model is a non-abelian extension of (2.39).

The procedure followed to obtain (2.31) can also be applied here. One finds

$$\frac{d^2}{d\gamma^2}V[\vec{\phi}_\gamma(\vec{x})] \Big|_{\gamma=1} = 6V_2[\vec{\phi}_1(\vec{x})] = 0, \quad (2.40)$$

unveiling the presence of zero modes. From (2.5) we further obtain

$$V[\vec{\phi}_\gamma(\vec{x})] = V_1[\vec{\phi}_1(\vec{x})], \quad (2.41)$$

confirming the scale-free nature of bidimensional sigma models. Wherefore, planar solitons have no preferred scale and at the expense of no energy at all they can alter their size under small perturbations. In this sense they are unstable. In particular, such instability occurs in the planar $O(3)$ model, but it is corrected in its Skyrme version.

Historically interesting is the fact that in the 1960s the quantum version of (2.33) interpreted ϕ_0 as the creation operator of a σ -particle and $\vec{\phi}$ designated a pion operator. The name ‘sigma’ was thus coined for most models of a structure similar to (2.38). The notation in terms of sigma and pion fields is still widely used.

2.5 Solitons in three dimensions

In accordance with Derrick's theorem non-trivial static solitons in three or more spatial dimensions cannot exist for models based upon a lagrangian (2.1). Adopting a more general standpoint one can circumvent such a problem, though. For instance, one can permit the interaction of the scalar field $\vec{\phi}$ with gauge fields, idea that leads to monopole theories. Another option is to stick to scalar fields, only, and add extra terms to (2.1). This latter idea was implemented by Skyrme [25]: He added an extra term to the $O(4)$ model in four-dimensional space-time. The Skyrme lagrangian is given by

$$\begin{aligned} \mathcal{L}_{skyrme} = & C_1(\partial_\mu \vec{\phi}) \cdot (\partial^\mu \vec{\phi}) - C_2[(\partial_\mu \vec{\phi} \cdot \partial^\mu \vec{\phi})^2 + \\ & (\partial_\mu \vec{\phi} \cdot \partial_\nu \vec{\phi})(\partial^\mu \vec{\phi} \cdot \partial^\nu \vec{\phi})], \quad \mu, \nu = 0, 1, 2, 3, \end{aligned} \quad (2.42)$$

where the real vector $\vec{\phi}$ is of the form (2.34). The constants C_j are free parameters which in principle can be calculated from QCD; in practice their values are fitted by phenomenological considerations.

In chiral notation the above lagrangian is nowadays frequently written as

$$\mathcal{L}_{skyrme} = -\frac{F_\pi^2}{16} Tr(R_\mu R^\mu) + \frac{1}{32e^2} Tr([R_\mu, R_\nu][R^\mu, R^\nu]), \quad R_\mu = (\partial_\mu J)J^\dagger, \quad (2.43)$$

where the $SU(2)$ quaternion J is the 3-D analogue of (2.37):

$$J = \sigma(x^\mu)\tau_0 + i\vec{\tau} \cdot \vec{\pi}(x^\mu), \quad \vec{\pi} = (\pi_1, \pi_2, \pi_3). \quad (2.44)$$

The unitarity of J is guaranteed by the ordinary ligature on the fields:

$$\sigma^2 + \vec{\pi}^2 = 1. \quad (2.45)$$

The routine finite-energy analysis exacts that localised lumps must tend to an absolute minimum of the integrand of the potential [using a particular choice of the parameters in (2.43)]

$$V_{skyrme} = - \int \left\{ \frac{1}{2} \text{Tr}(R_j R_j) + \frac{1}{32} \text{Tr}([R_j, R_k][R_j, R_k]) \right\} d^3 x, \quad j, k = 1, 2, 3, \quad (2.46)$$

at spatial infinity. Electing the 2×2 identity matrix as the vacuum, the finite-energy argument translates into

$$\lim_{|\vec{x}| \rightarrow \infty} J(\vec{x}) = \tau_0, \quad (2.47)$$

which effectively compactifies \mathfrak{R}_3 to a three-sphere. At any given time, finite-energy fields are maps $J : S_3 \mapsto S_3$ whose associated homotopy classification is dictated by $\pi_3(S_3) = \mathbb{Z}$.

The topological index for this model is interpreted as the baryon number:

$$\begin{aligned} Q_{skyrme} &= \int B^0 d^3 x, \\ &= \frac{1}{24\pi^2} \int \epsilon^{0jkl} \text{Tr}(R_j R_k R_l) d^3 x, \end{aligned} \quad (2.48)$$

of the topological current [compare with (2.22)],

$$B^\mu = \frac{1}{24\pi^2} \epsilon^{\mu\nu\lambda\gamma} \text{Tr}(R_\nu R_\lambda R_\gamma). \quad (2.49)$$

Completing the square in (2.46) we get

$$- \frac{1}{2} \int \text{Tr} \sum_j \left\{ R_j \pm \frac{1}{4} \epsilon_{jkl} [R_k, R_l] \right\}^2 d^3 x \mp 12\pi^2 Q_{skyrme}, \quad (2.50)$$

the Bogomolny bound in the present case being

$$V_{skyrme} \geq 12\pi^2 |Q_{skyrme}|. \quad (2.51)$$

The equality in the above expression occurs iff

$$R_j \pm \frac{1}{4}\epsilon_{jkl}[R_k, R_l] = 0, \quad (2.52)$$

for which no non-trivial analytic solutions have been found. Its simplest numerical solution corresponds to a quaternion J of the form

$$J(\vec{x}) = \cos[f(|\vec{x}|)] + i \frac{\sin[f(|\vec{x}|)]}{|\vec{x}|} \vec{x} \cdot \vec{\tau}, \quad (2.53)$$

where the profile function $f(|\vec{x}|)$ is subject to $f(0) = \pi$ and $f(\infty) = 0$. It sets the skyrmion energy to the value $1.232 \times 12\pi^2$, which exceeds the minimal energy in (2.51) [57]. Some scholars [58, 59] have been able to produce a value of $V_{skyrmie}$ closer to the minimal value by using instanton holonomies to generate skyrmion fields. So, the approximate solution (2.53) is a local minimum rather than an absolute one.

The first application of skyrmions in nuclear physics was the extraction of a nucleon-nucleon interaction energy of separated $Q = 1$ lumps [60, 61], idea later extended to $Q = 2$. The deuteron for instance, being the simplest nucleus, has been described as a quantised two-skyrmion by a number of people, using very particular approximations [62, 63, 64, 65]. As commented in the prolegomena, the results extracted from the Skyrme model are in qualitative accord with reality [66]. Approximate skyrmions on a cubic lattice belonging to $Q=3,4,5,6$ have been reported in [67]. And more recently, high-technology multi-skyrmion scattering has been investigated using an economical approximation based on a solution of the sine-Gordon type [68].

The evident progress that has been made in deriving multi-configurations in three spatial dimensions bodes well for the longevity of the model, but still

the multi-skyrmion problem is very hard to attack. Analytical solutions even for the simplest single-soliton case are not available.

Consequently, one is naturally led to investigate simpler models which still possess key features of the four dimensional ones. Through such low-dimensional analogues one hopes that a better understanding of the underlying mechanism of soliton dynamics will be attained, thenceforth assisting in the analysis of the more realistic, but too involved, (3+1) case. Skyrme himself used a (1+1) dimensional model (sine-Gordon) [69] as calisthenics to his (3+1) invention [25]. In the present work, we study two tractable, yet still rich, skyrmion models in (2+1) dimensions.

Finally, we present a Derrick-like argument in three spatial dimensions: Under dilations $\vec{x} \rightarrow \gamma\vec{x}$ the potential (2.46) goes to

$$V[J(\gamma\vec{x})] = \gamma^{2-D}V_1[J(\vec{x})] + \gamma^{4-D}V_{sk}[J(\vec{x})], \quad (2.54)$$

where V_1 , V_{sk} denote the first and second terms is the right-hand-side of (2.46). Equation (2.54) is the analogue of equations (2.4)-(2.5). Differentiating we get

$$\frac{d}{d\gamma}V[J(\gamma\vec{x})] = (2-D)\gamma^{1-D}V_1[J(\vec{x})] + (4-D)\gamma^{3-D}V_{sk}[J(\vec{x})]. \quad (2.55)$$

Setting the left hand side equal to zero for $\gamma=1$ there follows

$$(4-D)V_{sk}(J) = (D-2)V_1(J), \quad (2.56)$$

according to which the existence of solitons in $D = 3$ is now licit. Note also that plugging the value $D = 3$ into (2.54) we find

$$V[J(\gamma\vec{x})] = \gamma^{-1}V_1[J(\vec{x})] + \gamma V_{sk}[J(\vec{x})], \quad (2.57)$$

characteristic of a stable lump if we recall the kink result (2.32).

The whys and wherefores of the additional Skyrme term in the lagrangian are clearly to stabilise the solitons. In the pure chiral limit [$V_{sk}=0$], equation (2.57) says that for any configuration J the energy can always be decreased by dilations $\gamma > 1$. In the limit as the latter goes to infinity the size of the lump collapses to zero. But a non-zero Skyrme term gives a minimal value of the potential energy equal to

$$V_{minimal} = 2\sqrt{V_{sk}V_1}. \quad (2.58)$$

There are other important examples of solitons in three spatial dimensions, including YM instantons, monopoles and dyons, this latter objects being carriers of both magnetic and electric charge.

Chapter 3

A planar skyrmion model

3.1 The non-linear $O(3)$ sigma model

One of the simplest Lorentz-invariant models in (2+1) dimensions is the $O(3)$ model. It involves three real scalar fields $\vec{\phi}(x^\mu) \equiv \{\phi_a(x^\mu), a = 1, 2, 3\}$ with the constraint that $\forall x^\mu \equiv (x^0, x^1, x^2) = (t, x, y)$ [speed of light set equal to unity] the fields lie on the unit sphere $S_2^{(\Phi)}$:

$$\vec{\phi} \cdot \vec{\phi} = 1. \quad (3.1)$$

Subject to this constraint, the lagrangian density reads

$$\begin{aligned} \mathcal{L}_{O(3)} &= \frac{1}{4} \sum_{a=1}^3 \sum_{\mu=0}^2 \partial_\mu \phi_a \partial^\mu \phi_a \\ &= \frac{1}{4} (\partial_\mu \vec{\phi}) \cdot (\partial^\mu \vec{\phi}). \end{aligned} \quad (3.2)$$

The model is invariant under global $O(3)$ rotations in internal space, feature disclosed earlier in the coset description (2.15).

The dynamics of the $O(3)$ fields is governed by

$$\partial^\mu \partial_\mu \vec{\phi} - (\vec{\phi} \cdot \partial_\mu \partial^\mu \vec{\phi}) \vec{\phi} = \vec{0}, \quad (3.3)$$

which for the static case reduces to

$$\nabla^2 \vec{\phi} - (\vec{\phi} \cdot \nabla^2 \vec{\phi}) \vec{\phi} = \vec{0}. \quad (3.4)$$

Were it not for the constraint imposed on $\vec{\phi}$, the second term in the left-hand-side of the above equations would not be present, and the static non-singular solutions would be trivial. The condition (3.1) enriches the system, leading to finite-energy non-singular solutions: Solitons. Furthermore, the interaction of the system is of a pure geometrical nature; it is defined by equation (3.1) which determines the curvature of the internal space Φ . This is a particularity of the chiral or sigma models.

It is straightforward to see that the kinetic and potential energies are given by

$$K_{O(3)} = \frac{1}{4} \int (\partial_t \vec{\phi}) \cdot (\partial_t \vec{\phi}) dx dy, \quad (3.5)$$

$$\begin{aligned} V_{O(3)} &= \frac{1}{4} \int (\partial_i \vec{\phi}) \cdot (\partial_i \vec{\phi}) dx dy \quad [i = 1, 2] \\ &= \frac{1}{4} \int (\partial_r \vec{\phi}, \frac{1}{r} \partial_\theta \vec{\phi}) \cdot (\partial_r \vec{\phi}, \frac{1}{r} \partial_\theta \vec{\phi}) r dr d\theta. \end{aligned} \quad (3.6)$$

The problem is completely specified by giving the boundary conditions. As usual we take, $\forall t$,

$$\lim_{r \rightarrow \infty} \vec{\phi}(r, \theta) = \vec{\phi}^{(0)}, \quad (3.7)$$

where the unit vector $\vec{\phi}^{(0)}$ is independent of the polar angle θ . This condition ensures a finite potential energy: In effect, its finiteness demands

$$\begin{aligned} \lim_{r \rightarrow \infty} r |\nabla \vec{\phi}| &= \lim_{r \rightarrow \infty} \sqrt{(r \partial_r \vec{\phi})^2 + (\partial_\theta \vec{\phi})^2} \\ &\rightarrow 0, \end{aligned} \tag{3.8}$$

which implies (3.7).

It is interesting to note that the classical vacua [$V_{O(3)}=0$] ought to be represented by $\vec{\phi}^{(0)}$ for all $\vec{x} \equiv (x, y)$. Since such unit vector can point in any direction, we have a continuous family of zero-energy solutions connected by $O(3)$ rotations in internal space. As in the kink model described in section (2.3), this is an example of spontaneous symmetry breaking.

The boundary condition (3.7) defines a one-point compactification of \mathfrak{R}_2 , allowing us to consider $\vec{\phi}$ on the extended plane $\mathfrak{R}_2 \cup \{\infty\}$, topologically equivalent to $S_2^{(x)}$ (the superscript indicating that the sphere refers to compactified plane). Consequently, the field configurations we want are maps

$$S_2^{(x)} \mapsto S_2^{(\Phi)}$$

which, according to (2.8), can be labelled by an integral topological index. An expression for this index is readily found by pulling back the differential form

$$\begin{aligned} w &= \vec{\phi} \cdot d\vec{S}^{(\Phi)} \\ &= (\phi_1, \phi_2, \phi_3) \cdot (d\phi_2 \wedge d\phi_3, d\phi_3 \wedge d\phi_1, d\phi_1 \wedge d\phi_2) \end{aligned} \tag{3.9}$$

from the internal sphere to the ‘physical’ sphere via equation (2.11). Using coordinates (x, y) in the latter, expansion of w yields

$$\phi^* w = \begin{vmatrix} \phi_1 & \partial_x \phi_1 & \partial_y \phi_1 \\ \phi_2 & \partial_x \phi_2 & \partial_y \phi_2 \\ \phi_3 & \partial_x \phi_3 & \partial_y \phi_3 \end{vmatrix} dx \wedge dy. \tag{3.10}$$

Relaxing the wedge notation and setting the constant in (2.11) equal to $1/4\pi$ we get

$$Q_{O(3)} = \frac{1}{4\pi} \int_{S_2^{(x)}} \vec{\phi} \cdot (\partial_x \vec{\phi} \times \partial_y \vec{\phi}) dx dy, \quad (3.11)$$

quantity sometimes called the **winding number** because it gives the number of times that $\vec{\phi}$ ranges over the internal sphere as (x, y) ranges over the compactified plane once. We can convince ourselves of that by observing that (3.9) is nothing but the element of area of the unit sphere $S_2^{(\Phi)}$: Expanding w in terms of local space polar coordinates (ϑ, φ) in internal space and parametrising

$$\vec{\phi} = (\sin \vartheta \cos \varphi, \sin \vartheta \sin \varphi, \cos \vartheta),$$

we find the all familiar

$$w = \sin \vartheta d\vartheta d\varphi.$$

The topological charge now stems from

$$\int_{S_2^{(x)}} \phi^* w = Q_{O(3)} \int_{S_2^{(\Phi)}} w,$$

hence equation (3.11). Note as well that $Q_{O(3)}$ may be considered as the zero component of the topological current [compare with equations (2.21)-(2.22) and (2.48)-(2.49)]

$$k^\mu = \epsilon^{\mu\nu\xi} \epsilon^{abc} \phi_a \partial_\nu \phi_b \partial_\xi \phi_c, \quad (3.12)$$

where ϵ^{jkl} is the familiar Levi-Civita pseudo-tensor.

3.2 CP^1 formulation

It will be propitious to use a formulation of the model where the soliton solutions adopt a simple form. This so-called CP^1 formulation involves just one independent complex field, W , related to the fields $\vec{\phi}$ via the stereographic projection

$$W = \frac{\phi_1 + i\phi_2}{1 - \phi_3}. \quad (3.13)$$

Introducing complex coordinates $z = x + iy$ and $\bar{z} = x - iy$ on the extended plane and using the handy notation $\partial_z W = W_z$, $\partial_z(\partial_{\bar{z}}W) = W_{z\bar{z}}$, *etc.*, the equation of motion (3.4) becomes

$$W_{z\bar{z}} - \frac{2\bar{W}W_zW_{\bar{z}}}{|W|^2 + 1} = 0, \quad (3.14)$$

where \bar{W} is the complex conjugate of W .

In terms of W the potential energy and the topological index read

$$V_{O(3)} = 2 \int_{S_2^{(x)}} \frac{|W_z|^2 + |W_{\bar{z}}|^2}{(|W|^2 + 1)^2} dx dy, \quad (3.15)$$

$$Q_{O(3)} = \frac{1}{\pi} \int_{S_2^{(x)}} \frac{|W_z|^2 - |W_{\bar{z}}|^2}{(|W|^2 + 1)^2} dx dy. \quad (3.16)$$

Clearly

$$V_{O(3)} = \begin{cases} 2\pi Q_{O(3)} + 4 \int_{S_2^{(x)}} \frac{|W_{\bar{z}}|^2}{|W|^2 + 1} dx dy \\ 2\pi[-Q_{O(3)}] + 4 \int_{S_2^{(x)}} \frac{|W_z|^2}{|W|^2 + 1} dx dy \end{cases} \quad (3.17)$$

→

$$V_{O(3)} \geq 2\pi|Q_{O(3)}|. \quad (3.18)$$

The static solitons or instanton solutions correspond to the equality in (3.18): Solutions with $Q_{O(3)} > 0$ (solitons) and solutions with $Q_{O(3)} < 0$ (anti-solitons) obey, respectively,

$$W_{\bar{z}} = 0, \quad W_z = 0. \quad (3.19)$$

These are nothing but the Cauchy-Riemann conditions for W being an analytic function of z or \bar{z} [in terms of $\vec{\phi}$ equations (3.19) read

$$\partial_i \vec{\phi} \pm \epsilon_{ij} \vec{\phi} \times \partial_j \vec{\phi} = \vec{0}, \quad (3.20)$$

clearly simpler than equation (3.4)].

The most general static solutions of the planar $O(3)$ model are of the form

$$W(z) = \lambda \prod_{j=1}^{\kappa} \frac{z - a_j}{z - b_j}, \quad W(\bar{z}) = \lambda \prod_{j=1}^{\kappa} \frac{\bar{z} - a_j}{\bar{z} - b_j}, \quad (3.21)$$

where λ is a free parameter. The degree κ of the polynomials is numerically equal to $|Q_{O(3)}|$.

For a degree-one soliton, the potential energy density is

$$\varepsilon = 2 \frac{|\lambda(a - b)|^2}{\{|z - b|^2 + |\lambda|^2|z - a|^2\}^2}. \quad (3.22)$$

It possesses a bell-like shape whose maximum value

$$\varepsilon_{max} = 8 \frac{(|\lambda|^2 + 1)^2}{|\lambda(a - b)|^2} \quad (3.23)$$

is positioned at

$$z_{max} = \frac{a|\lambda|^2 + b}{|\lambda|^2 + 1}. \quad (3.24)$$

In any given topological sector the potential energy is minimised when one of the Cauchy conditions is satisfied. A solution of (3.19) automatically

solves the original second order equation (3.14), but the converse need not be true. However, all the static finite-energy solutions of (3.14) are exhausted by equation (3.19) [70, 71]. This is a special asset of the CP^1 model on the sphere which is absent in its generalisation (2.14). The latter possesses static solutions like $W(z, \bar{z})$ which are non-meromorphic and correspond to saddle points of the energy [72]. Furthermore, in the CP^1 model itself with *periodic* boundary conditions there are solutions to (3.14) which disobey (3.19). We shall have occasion to expand on this matter in chapter 4.

The simplest one-soliton solution has the form

$$W = \lambda(z - a),$$

configuration that has been numerically studied in [73]. When viewed as an evolving structure in (2+1) dimensions this soliton is unstable under any small perturbation, either explicit (*e.g.*, by setting the soliton into motion) or implicit (as inevitably introduced by the discretisation procedure). This behaviour has been seen not only in the full simulation of the model but also in the approximation known as the collective coordinate approach [74]. The said instability, which eventually collapses the numerical procedure by infinitely shrinking or expanding the soliton, is associated with the conformal invariance of the $O(3)$ lagrangian in two dimensions: The solitons can change their size at the expense of no energy at all. This statement follows from equations (2.40)-(2.41).

With regards to collisions, two-soliton solutions of the form

$$W = \lambda(z - a)(z - b), \quad \lambda \frac{(z - a)(z - b)}{z - c},$$

have been found to scatter at right angles with the initial direction of motion in the centre of mass frame, the instability taking over a short while afterwards [75].

Nonetheless, it has been demonstrated [76] that the instability of the discretised $O(3)$ model can be cured by the addition of two extra terms to the lagrangian. The first one resembles the term introduced by Skyrme in his nuclear model in four dimensional space-time, and the second one is an additional potential-like term. The solitonic configurations of this modified model give stable extended structures which repel each other and scatter at 90° when sent towards each other with sufficient speed. In the present chapter we follow [76] and study a version of such modified, Skyrme-like model, corresponding to a more general choice of the potential term in the lagrangian.

Note that a finite mesh introduces a scale into the model and, by imposing appropriate boundary conditions, it is possible to have a stable $O(3)$ lump on the lattice. But of course this is not a very useful scheme from the standpoint of a general field theoretical context.

3.3 Modified model

Our modified model corresponds to a lagrangian density

$$\begin{aligned}
\mathcal{L}_{sky} &= \mathcal{L}_{O(3)} \\
&- \frac{1}{4}\theta_1[(\partial^\mu \vec{\phi} \cdot \partial_\mu \vec{\phi})^2 - (\partial^\mu \vec{\phi} \cdot \partial^\nu \vec{\phi})(\partial_\mu \vec{\phi} \cdot \partial_\nu \vec{\phi})] \\
&- \frac{1}{4}\theta_2[-2\text{Re}(\lambda)\phi_1 - 2\text{Im}(\lambda)\phi_2 + (1 - |\lambda|^2)\phi_3 \\
&+ (1 + |\lambda|^2)]^4, \quad \theta_1, \theta_2 \in \mathfrak{R}^+,
\end{aligned} \tag{3.25}$$

where $\mathcal{L}_{O(3)}$ is given by equation (3.2).

The kinetic and potential energies can be read-off from (3.25):

$$\begin{aligned}
K_{sky} &= \frac{1}{4} \int dx dy \{ (\partial_t \vec{\phi} \cdot \partial_t \vec{\phi}) [1 + 2\theta_1 (\partial_x \vec{\phi} \cdot \partial_x \vec{\phi} + \partial_y \vec{\phi} \cdot \partial_y \vec{\phi})] \\
&- 2\theta_1 [(\partial_t \vec{\phi} \cdot \partial_x \vec{\phi})^2 + (\partial_t \vec{\phi} \cdot \partial_y \vec{\phi})^2] \},
\end{aligned} \tag{3.26}$$

$$\begin{aligned}
V_{sky} &= \frac{1}{4} \int dx dy \{ \partial_x \vec{\phi} \cdot \partial_x \vec{\phi} + \partial_y \vec{\phi} \cdot \partial_y \vec{\phi} \\
&+ 2\theta_1 [(\partial_x \vec{\phi} \cdot \partial_x \vec{\phi})(\partial_y \vec{\phi} \cdot \partial_y \vec{\phi}) - (\partial_x \vec{\phi} \cdot \partial_y \vec{\phi})^2] \\
&+ \theta_2 [-2\text{Re}(\lambda)\phi_1 - 2\text{Im}(\lambda)\phi_2 + (1 - |\lambda|^2)\phi_3 \\
&+ (1 + |\lambda|^2)]^4 \}.
\end{aligned} \tag{3.27}$$

It can be verified that the potentials corresponding to the terms θ_1 and θ_2 scale like

$$\begin{aligned}
V_{\theta_1}[\vec{\phi}(\gamma x, \gamma y)] &= \gamma^2 V_{\theta_1}[\vec{\phi}(x, y)], \\
V_{\theta_2}[\vec{\phi}(\gamma x, \gamma y)] &= \gamma^{-2} V_{\theta_2}[\vec{\phi}(x, y)],
\end{aligned} \tag{3.28}$$

so that the expression resembling (2.57) is

$$V_{sky}[\vec{\phi}(\gamma \vec{x})] = V_{O(3)}[\vec{\phi}(\vec{x})] + \gamma^2 V_{\theta_1}[\vec{\phi}(\vec{x})] + \gamma^{-2} V_{\theta_2}[\vec{\phi}(\vec{x})], \tag{3.29}$$

where the scale-free potential $V_{O(3)}$ corresponds the pure $O(3)$ model. The θ -terms break the conformal invariance and their combined effect stabilises the solitons. If the size of the solitons is appropriately chosen, it is now energetically unfavourable for them to change it. Also note that the skyrmion lagrangian is no longer $O(3)$ invariant, but it still respects the requirement of relativistic invariance. The θ_1 term is the Skyrme-like term and it prevents the solitons from shrinking, whereas the θ_2 term resembles a potential that prevents their expansion. Judicious choices of the θ_2 term, which unlike the Skyrme term is nonunique [77], opens up the possibility of writing different interesting versions of the skyrmion model, a realisation of which is our proposition (3.25). The form of the θ_2 term in our Skyrme lagrangian density is precisely the one that will make the field $W(z)$ of degree one in (3.21) a solution of the equation of motion (see below). As commented earlier on, we are interested in a version of the model in which the most general expression for a single-soliton be a solution. So, a method for obtaining a suitable potential term in the planar skyrmion system is to ask oneself what the potential should be in order to have the desired soliton configuration as a solution of the equation of motion. Upon inserting the field in question into the governing static equation, one can work out the required θ_2 expression, as well as the relation between the θ s and the parameter λ , which determines the size of the extended structures.

In the W -formulation the lagrangian density (3.25) acquires the form

$$\begin{aligned}
\mathcal{L}_{sky} &= \frac{|W_t|^2 - |W_x|^2 - |W_y|^2}{(|W|^2 + 1)^2} \\
&- \frac{2\theta_1}{(|W|^2 + 1)^4} [(\bar{W}_t W_x - W_t \bar{W}_x)^2 + (\bar{W}_t W_y - W_t \bar{W}_y)^2 \\
&- (\bar{W}_x W_y - W_x \bar{W}_y)^2] - 4\theta_2 \frac{|W - \lambda|^8}{(|W|^2 + 1)^4}, \tag{3.30}
\end{aligned}$$

the ensuing equation of motion being

$$\begin{aligned}
0 &= W_{tt} - W_{xx} - W_{yy} - \frac{2\bar{W}}{|W|^2 + 1} [(W_t)^2 - (W_x)^2 - (W_y)^2] \\
&+ \frac{4\theta_1}{(|W|^2 + 1)^2} \{2\bar{W}_{tx} W_t W_x + 2\bar{W}_{ty} W_t W_y - 2\bar{W}_{xy} W_x W_y \\
&- \bar{W}_{tt} [(W_x)^2 + (W_y)^2] + \bar{W}_{xx} [(W_y)^2 - (W_t)^2] + \bar{W}_{yy} [(W_x)^2 - (W_t)^2] \\
&+ W_{tt} (|W_x|^2 + |W_y|^2) + W_{xx} (|W_t|^2 - |W_y|^2) + W_{yy} (|W_t|^2 - |W_x|^2) \\
&- W_{tx} (\bar{W}_t W_x + W_t \bar{W}_x) - W_{ty} (\bar{W}_t W_y + W_t \bar{W}_y) + W_{xy} (\bar{W}_x W_y + \bar{W}_y W_x) \\
&+ \frac{2W}{|W|^2 + 1} [(\bar{W}_t W_x - W_t \bar{W}_x)^2 + (\bar{W}_t W_y - W_t \bar{W}_y)^2 - (\bar{W}_x W_y - W_x \bar{W}_y)^2] \} \\
&+ 4\theta_2 \frac{|W - \lambda|^6}{(|W|^2 + 1)^3} [\bar{\lambda} W^2 + (1 - |\lambda|^2)W - \lambda]. \tag{3.31}
\end{aligned}$$

For the static case we may write more conveniently

$$\begin{aligned}
0 &= W_{z\bar{z}} - \frac{2\bar{W}W_zW_{\bar{z}}}{|W|^2 + 1} \\
&+ \frac{4\theta_1}{(|W|^2 + 1)^2} [2\bar{W}_{z\bar{z}} W_z W_{\bar{z}} - \bar{W}_{zz} (W_z)^2 - \bar{W}_{\bar{z}\bar{z}} (W_{\bar{z}})^2 + W_{zz} \bar{W}_z W_{\bar{z}} \\
&+ W_{\bar{z}\bar{z}} \bar{W}_{\bar{z}} W_z - W_{z\bar{z}} (|W_z|^2 + |W_{\bar{z}}|^2) + \frac{2W}{|W|^2 + 1} (|W_z|^2 - |W_{\bar{z}}|^2)^2] \\
&+ 4\theta_2 \frac{|W - \lambda|^6}{(|W|^2 + 1)^3} [\bar{\lambda} W^2 + (1 - |\lambda|^2)W - \lambda]. \tag{3.32}
\end{aligned}$$

Ignoring anti-solitonic terms like $W_{\bar{z}}$ in (3.32), some re-arrangement produces

$$\begin{aligned}
0 = & \{ 8\theta_1|W_z|^4 - 4\theta_2|\mathcal{V}|^2 + [-4\theta_1(W_z)^2\bar{W}_{zz} + \theta_2\mathcal{V}\frac{d\bar{\mathcal{V}}}{d\bar{W}}] \bar{W} \} W \\
& + [-4\theta_1(W_z)^2\bar{W}_{zz} + \theta_2\mathcal{V}\frac{d\bar{\mathcal{V}}}{d\bar{W}}], \quad \mathcal{V} \equiv (W - \lambda)^4, \quad (3.33)
\end{aligned}$$

from which it is directly checked that the configuration

$$W = \lambda \frac{z - a}{z - b}, \quad (3.34)$$

where

$$\lambda = \frac{\sqrt[4]{2\theta_1/\theta_2}}{a - b}, \quad a, b \in \mathcal{C}, \quad (3.35)$$

solves the equations of motion. The field (3.34) is the familiar general expression for a single CP^1 soliton but with λ fixed by (3.35). A soliton with its size thus fixed we will call a ‘skyrmion’ [an anti-skyrmion is derived by complex conjugation of (3.34)]. As touched on in the introductory chapter, theories like the tHP monopoles also have a parameter in the lagrangian which determines the size of the corresponding solitons.

The skyrmion’s potential or static energy density E is found by inserting (3.34) into

$$\begin{aligned}
E = & 2 \frac{|W_z|^2 + |W_{\bar{z}}|^2}{(|W|^2 + 1)^2} + 8\theta_1 \frac{(|W_z|^2 - |W_{\bar{z}}|^2)^2}{(|W|^2 + 1)^4} \\
& + 4\theta_2 \frac{|W - \lambda|^8}{(|W|^2 + 1)^4}, \quad (3.36)
\end{aligned}$$

whose maximum value is calculated via

$$\begin{aligned}
E_{max} &= \varepsilon_{max} \left[1 + \frac{\theta_1}{2} \varepsilon_{max} + \frac{\theta_2 |\lambda(a - b)|^4}{4} \varepsilon_{max} \right], \\
\varepsilon_{max} &= 8 \frac{(|\lambda|^2 + 1)^2}{|\lambda(a - b)|^2}. \quad (3.37)
\end{aligned}$$

Through relation (3.35) it is possible to cast (3.37) into the simpler

$$E_{max} = \varepsilon_{max}(1 + \theta_1 \varepsilon_{max}). \quad (3.38)$$

The position of E_{max} is still determined by formula (3.24). Observe also that in the $O(3)$ limit where the θ s go to zero we have $E_{max} = \varepsilon_{max}$, equation (3.23).

For the case tackled in [76] one has [put $\mathcal{V} = 1$ instead of $\mathcal{V} = (W - \lambda)^4$ in equation (3.33)]

$$E_{max} = 2|\lambda|^2 + 8\theta_1|\lambda|^4 + 4\theta_2, \quad \lambda = \sqrt[4]{\frac{\theta_2}{2\theta_1}},$$

the complex coordinate of which is just $z_{max} = a$.

In order to study processes involving two skyrmions we are going to consider fields of the appearance

$$W = \lambda \frac{z - a}{z - b} \frac{z + c}{z + d}. \quad (3.39)$$

They do not satisfy identically the field equation (3.32) and hence describe two solitons in an approximate manner. For objects of the simpler form $\lambda(z - a)(z - b)$ it is possible to find a relationship similar to (3.35) such that the model actually have static two-skyrmion solutions [78]. Inspection of equation (3.33) reveals that such an expression for a configuration (3.39) is quite involved to obtain. For instance, the term

$$-4\theta_1(W_z)^2 \bar{W}_{zz} + \theta_2 \mathcal{V} \frac{d\bar{\mathcal{V}}}{d\bar{W}}$$

in (3.33) gives, with the help of (3.39) [take $a = c$, $b = d \in \Re$ for simplicity],

$$-16\theta_1 \left[\frac{b}{\lambda(a^2 - b^2)} \right]^3 \sqrt{\mathcal{V}} \frac{d\bar{\mathcal{V}}}{d\bar{W}} + \theta_2 \mathcal{V} \frac{d\bar{\mathcal{V}}}{d\bar{W}}, \quad \mathcal{V} \equiv (W - \lambda)^3 \left(W - \lambda \frac{a^2}{b^2} \right),$$

where it is uncertain how to define a relation like (3.35) so that a two-skyrmion solution is produced.

3.4 Numerical procedure

The fields W are treated as the basic initial configurations, their analytic values being used at each lattice site in the discrete approximation of the model. After giving some initial speed to the W fields, we pass on to the ϕ -formulation by means of equation (3.13). Then $\vec{\phi}$ is numerically evolved according to the full equation (3.31), written in terms of $\vec{\phi}$.

It is quite common for ϕ_3 to have values near to 1, in which case W in (3.13) becomes too large for numerical comfort. So in our simulations we have preferred, instead of (3.13), the projection

$$W' = \frac{1 - \phi_3}{\phi_1 + i\phi_2}, \quad (3.40)$$

clearly a more numerically tractable selection. The dynamics of the system is unchanged because

$$\mathcal{L}(W') = \mathcal{L}(W).$$

Most of the numerical simulations were carried out in the workstations at Durham but, when the disk space was full-up, the computers at *Universidad del Zulia* were of key assistance.

Our simulations employ the fourth-order Runge-Kutta method and approximate the spatial derivatives by finite-differences. The laplacian is evaluated using the standard nine-point formula. We use double-precision arith-

metrics on a 200×200 ($n_x = n_y = 200$) lattice with spatial and time steps $\delta x = \delta y = 0.02$ and $\delta t = 0.005$.

Unavoidable numerical truncation errors introduced at various stages of the calculations gradually shift the fields away from the unit sphere (3.1), thereby building-up numerical inaccuracies in the evolution equations. So we rescale

$$\vec{\phi} \rightarrow \frac{\vec{\phi}}{\sqrt{\vec{\phi} \cdot \vec{\phi}}}$$

every few iterations. The error associated with this procedure is of the order of the accuracy of our calculations. Each time, just before the rescaling operation, we evaluate the quantity

$$\mu \equiv \vec{\phi} \cdot \vec{\phi} - 1$$

at each lattice point. Treating the maximum of the absolute value of μ as a measure of the numerical error, we found that $|\mu|_{max} \approx 10^{-8}$. This magnitude is useful as a guide to determine how reliable a given numerical result is. Usage of an unsound numerical procedure like, say, taking $\delta x < \delta t$ in the Runge-Kutta evolution, shows itself as a rapid growth of $\max|\mu|$; such increase also occurs when the solitons become exceedingly thin.

We also include along the boundary a narrow strip to absorb the various radiation waves, reducing their effect on the skyrmions via the reflections from the boundary. The absorption is implemented by setting

$$\partial_t \vec{\phi} \rightarrow \chi \partial_t \vec{\phi},$$

where the damping function χ has the form

$$\chi(j) = \begin{cases} 1, & j \in [0, j_1], \\ 1 - \frac{j - j_1}{j_2 - j_1}(1 - \chi_0), & j \in [j_1 + 1, j_2 - 1], \\ \chi_0, & j \in [j_2, n_x] \quad (\chi_0 = 0.95), \end{cases}$$

where the absorbing band is small, no more than about 10 % of mesh-points. As time elapses, the absorption of radiation manifests itself through a small decrease of the total energy, which gradually stabilises as the radiation waves are gradually absorbed. The damping device is specially useful when studying soliton stability but it is dispensable when considering collision processes.

For the parameters we have chosen the values:

$$\begin{aligned} a &= c = 0.75, & b &= d = 0.05, \\ \theta_1 &= 0.015006250, & \theta_2 &= 0.1250. \end{aligned} \tag{3.41}$$

The global $U(1)$ symmetry of (3.34) has been used to choose λ real. From (3.35) and (3.41) it follows that $\lambda=1$, a calculational-friendly number as can be inferred from (3.27).

Noteworthy is the fact that the finite-difference expressions for the derivatives of fields like λz and λz^2 , used in previous works, are exact. This is no longer true for our choices (3.34) and (3.39), whose numerical versions are in this sense more perturbed. It turns out that this factor has no telling effect in the qualitative behaviour of the system.

3.5 Results

3.5.1 Static case

Firstly consider the situation where the skyrmions have zero initial velocity. Our single-skyrmion field is

$$W = \frac{z - 0.75}{z - 0.05}, \quad (3.42)$$

a typical picture of which energy density is displayed in the upper half of figure 3.1.

Our simulations show that the energy density corresponding to this soliton evolves only very slightly and does not change its shape. At the initial time the amplitude of the energy density has the numerical value of ≈ 128.47 , which quickly re-adjusts and stabilises itself around 129.5. This last number agrees very well with the analytical result as calculated from equation (3.37) [or (3.38)] and (3.41):

$$E_{max} \approx 65.3 + 31.99 + 31.99 = 129.3. \quad (3.43)$$

In the lower half of the figure 3.1 a graph showing the stable evolution of E_{max} is exhibited.

In figure 3.2 we show some pictures of the radiation waves emitted by the soliton-hump. They propagate out to the boundary at the speed of light, leaving the central region of the lattice essentially free of kinetic energy. The smallness of the kinetic energy indicates that our soliton is almost perfectly static. This is in fact numerically observed: At the initial time the lump of energy is situated at $z_{max}=(0.40,0)$ and by $t=10$ it has slowly shifted to

(0.4013,0). Note that the theoretical value of z_{max} , as per formula (3.24), is precisely (0.40,0).

Although small enough as to cause no preoccupation in the problem under study, the said kinetic energy is considerably larger than the one emitted by the solitons of the model with $\mathcal{V} = 1$ in (3.33). This is not surprising since our choice of potential leads to a more perturbed, complicated discrete representation of the analytic soliton fields than in the $\mathcal{V} = 1$ case.

A cursory glance at (3.25) shows that by simply equating $\theta_1 = \theta_2 = 0$ we recover the unmodified $O(3)$ model:

$$\lim_{\theta_1, \theta_2 \rightarrow 0} \mathcal{L}_{sky} \rightarrow \mathcal{L}_{O(3)} \quad (3.44)$$

[we underline *en passant* that this limit resembles the BPS limit in the tHP monopole theory].

Our simulations for this limiting case show that (3.42) represents a static $O(3)$ solution which behaves stably on the mesh, corroborating the results found in [73]. It possesses an oscillating quasi-periodic energy density whose amplitude decreases as time goes by, eventually becoming quite small (recall there is an absorbing set-up operating along a small band near the edges of the grid). However, the source of such stability resides on the scale set by the finite net, where the kinetic waves are reflected in such a way as to stabilise the hump. In fact, upon effectively moving the boundaries to infinity, the discrete $O(3)$ system is unstable [73]. This kind of lattice-stabilisation is clearly of no applicability within a general field theoretical framework. By contrast, the skyrmion scheme has an intrinsic scale that renders a stable soliton regardless, being therefore alluring from a general perspective. A

depiction of the said $O(3)$ lattice-stability is given in figure 3.3.

Without the absorption arrangement the kinetic waves, rather than peetering out as in the previous figure, keep travelling from the soliton-lump out to the boundary and inward back again. The energy density in this case exhibits a periodic behaviour, with the amplitude of its oscillations being about constant in time; the question of stability under these circumstances meets with difficulties. Hence the importance of the absorbing band that gradually extinguishes the radiation, as seen in figure 3.3.

We now shift our attention to the approximate two-soliton configuration

$$W = \frac{z - 0.75}{z - 0.05} \frac{z + 0.75}{z + 0.05}, \quad (3.45)$$

which gives two skyrmion-lumps of equal size initially well separated from each other (so that they have a minimal overlapping) but still far away from the borders of the mesh (thus avoiding reflections from the boundaries as much as possible). Since the above field is not an exact solution of the model it should undergo some evolution even for $v = 0$.

The energy density corresponding to the *ansatz* (3.45) at $t = 0$ is illustrated in the upper part of figure 3.4. We can see that the amplitude starts at a value somewhat bigger than twice the value for a single soliton. As soon as the evolution commences the skyrmions shake off some radiation and alter their size by getting broader. In so doing, they slowly move away from each other, uncovering the presence of a repulsive force between them; this is apparent from figure 3.4. During this process the peak E_{max} decreases and undergoes damped oscillations around the analytical result (3.43); by $t \approx 8$ the oscillations are quite small and the energy stabilises near the theoretical

value. A feel for this course of events can be developed through figure 3.5, where the graph of the maximum of the energy density is plotted *versus* time. It is re-assuring that this kind of weak repulsion, also characteristic of the kink model described in the anterior chapter, has been observed using a collective coordinate method as well [79].

By taking a value of the parameter λ which does not satisfy (3.35) we can introduce explicit perturbations into the system, other than the implicit ones brought about by the discretisation procedure. We have checked that our skyrmions are indeed stable under all such disturbances. If the initial λ is much greater (smaller) than the value dictated by (3.35), unity in our case, the initial amplitude of the solitons will be manifestly above (below) the analytic value (3.43). But the pattern is always the same: Maintaining its shape unscathed, the skyrmion-hump corrects its height to around 129.5, emitting kinetic waves in so doing.

In the limit (3.44) we have verified that the repulsion between the lumps disappears, and these remain motionless in their initial positions [as in the upper half of figure 3.4] throughout the simulation if started off from rest. However, the solitons are now unstable and their energy density increases non-stoppingly: Their breadth goes down to the order of the lattice spacing, eventually collapsing the numerics. A prototype picture after this time would reveal the soliton-lumps not so much thin as blown asunder.

In the upper half of figure 3.6 we show the said rise of the peak of the energy density corresponding to (3.45) in the $O(3)$ limit. It is pedagogical to compare the unstable behaviour of these two static solitons with the stable performance of the $O(3)$ single-soliton shown in figure 3.3. One may natu-

rally ask himself why the two lumps, having been given no initial velocity either, behave unstably. The answer relies on the fact that the discrete representation of the two-solitons (3.45) brings forth an extra perturbation which spells unfavourably in terms of stability, the boundary-reflected radiation being now incapable of balancing things out. This result is very important, for if the kinetic waves reflected from the boundary stabilised the two $O(3)$ solitons as in the single-lump case, then it would be necessary to study the behaviour of the skyrmion model in an infinite lattice, to make sure that its extended objects are stable regardless. But given the actual circumstances, such study would be only academic.

Total energy density

$E_{\max}=128.47; t=0$

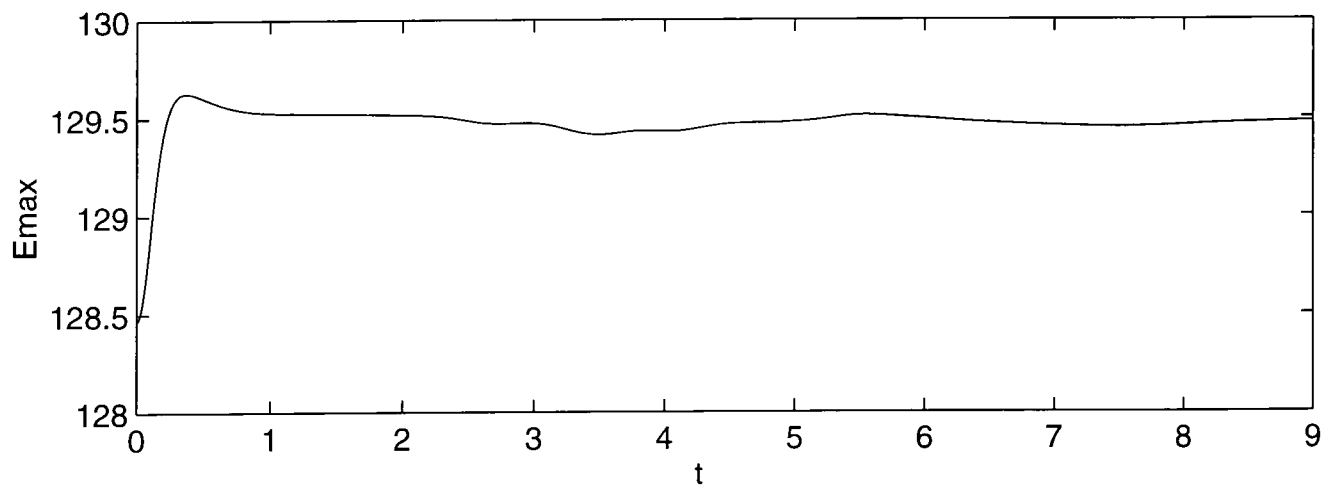
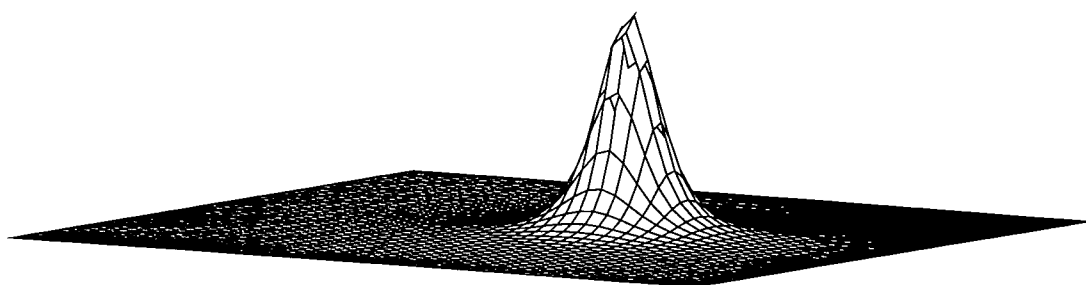
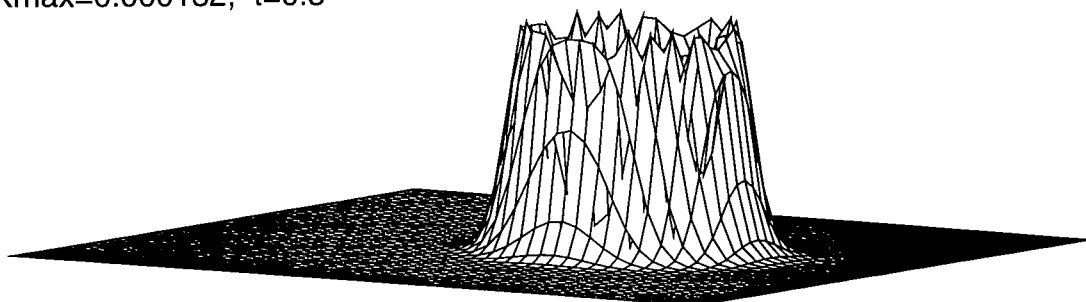


Figure 3.1: Total energy density for one skyrmion at the initial time and the evolution of its height.

Kinetic energy density

$K_{\max}=0.000132$; $t=0.5$



$K_{\max}=0.0000438$; $t=1.5$

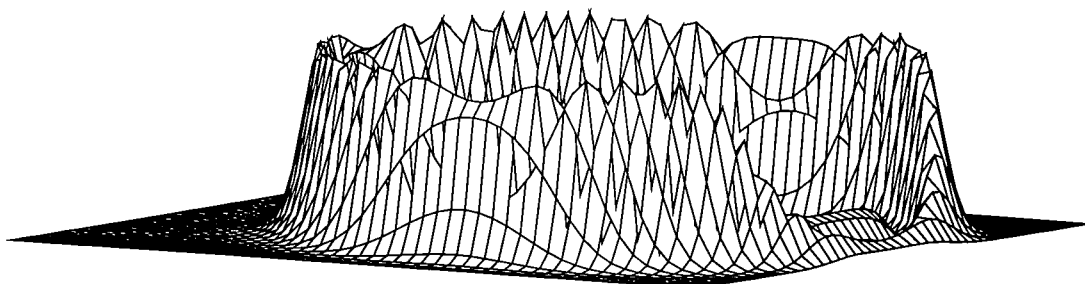


Figure 3.2: The skyrmion-lump shakes off some kinetic energy waves that spread out to the boundary at the speed of light.

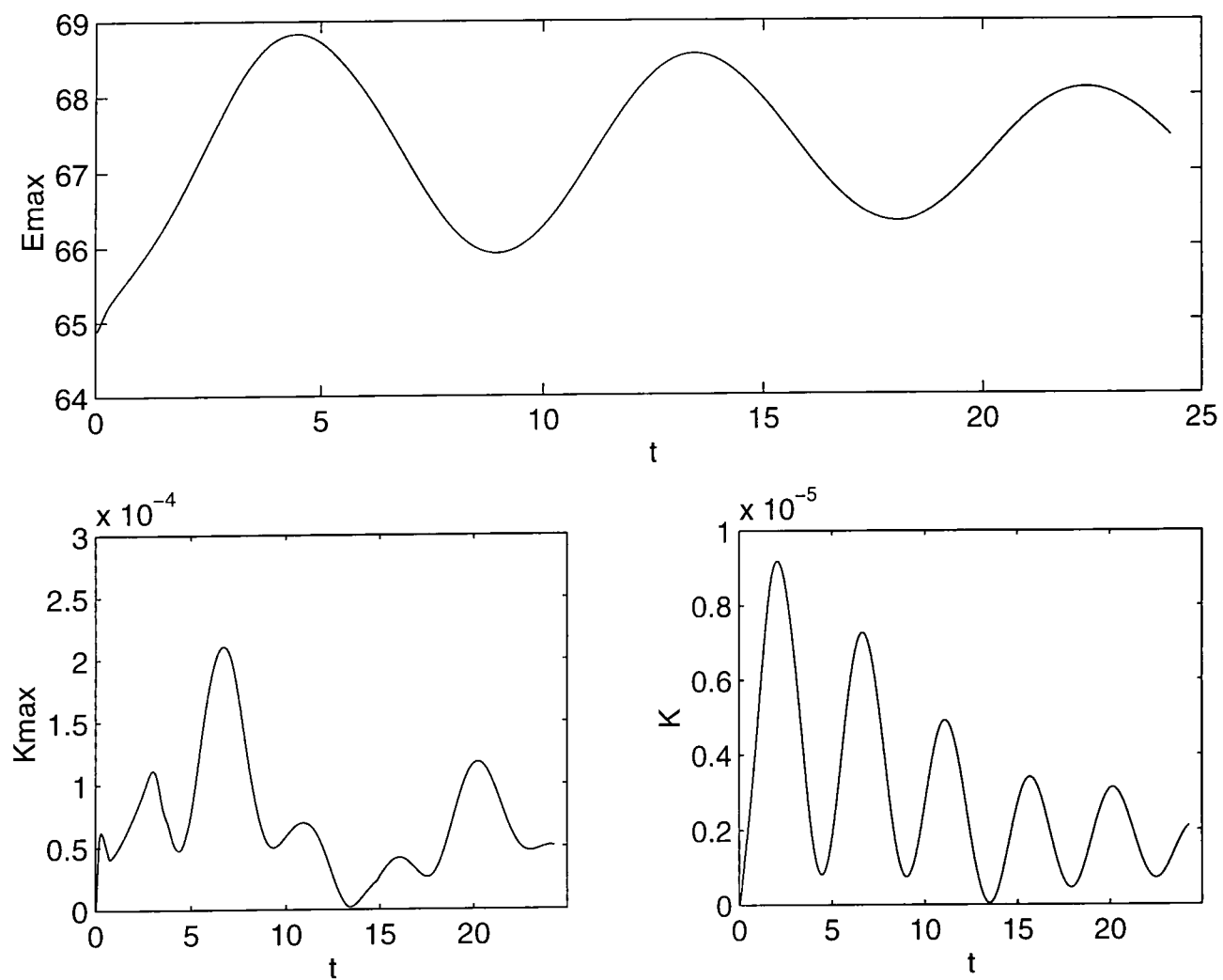
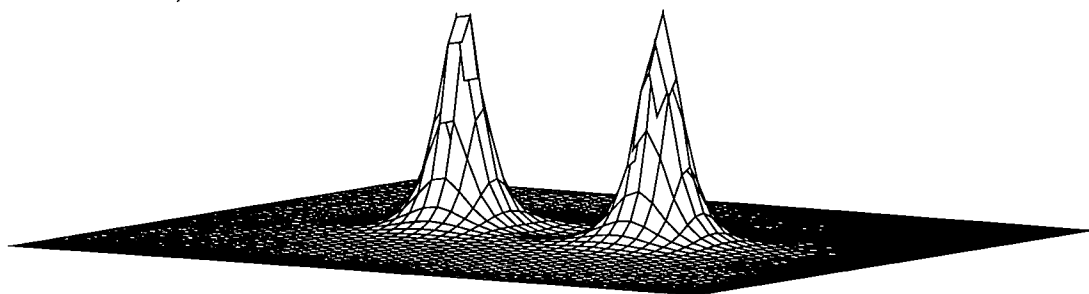


Figure 3.3: As the kinetic waves fade away with time we are left with a stable pure $O(3)$ lump on the lattice.

Total energy density

$E_{\max}=268.4$; $t=0$



$E_{\max}=134.8$; $t=8$

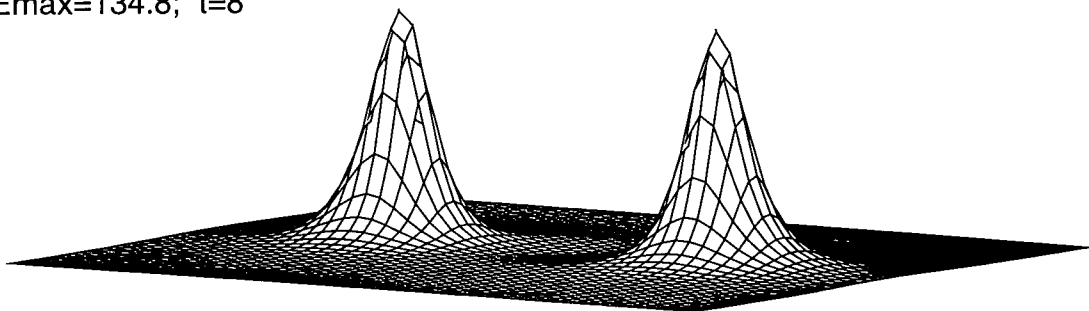


Figure 3.4: A repulsive force exists between the two skyrmions.

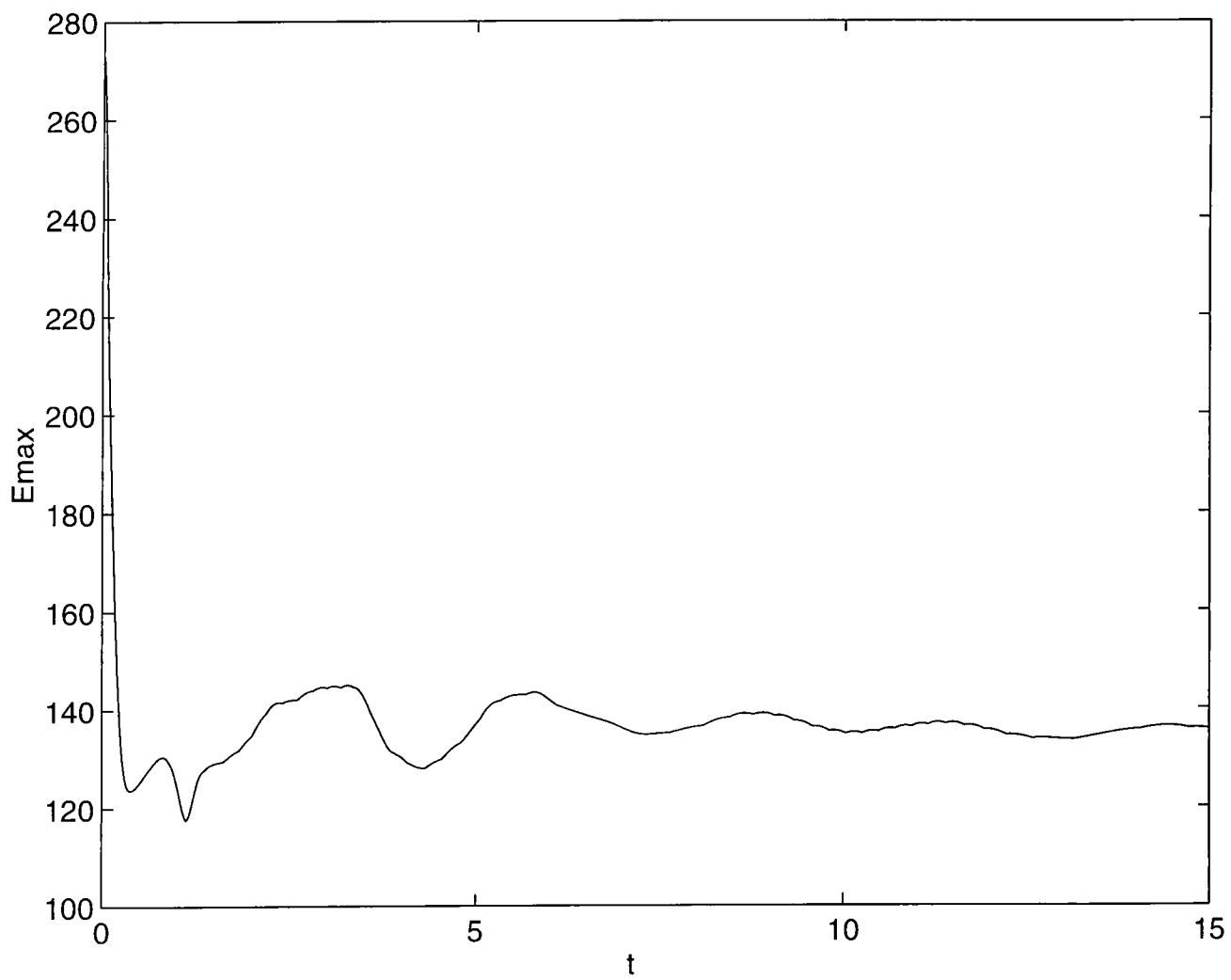


Figure 3.5: Development of the energy density for two skyrmions which start from rest.

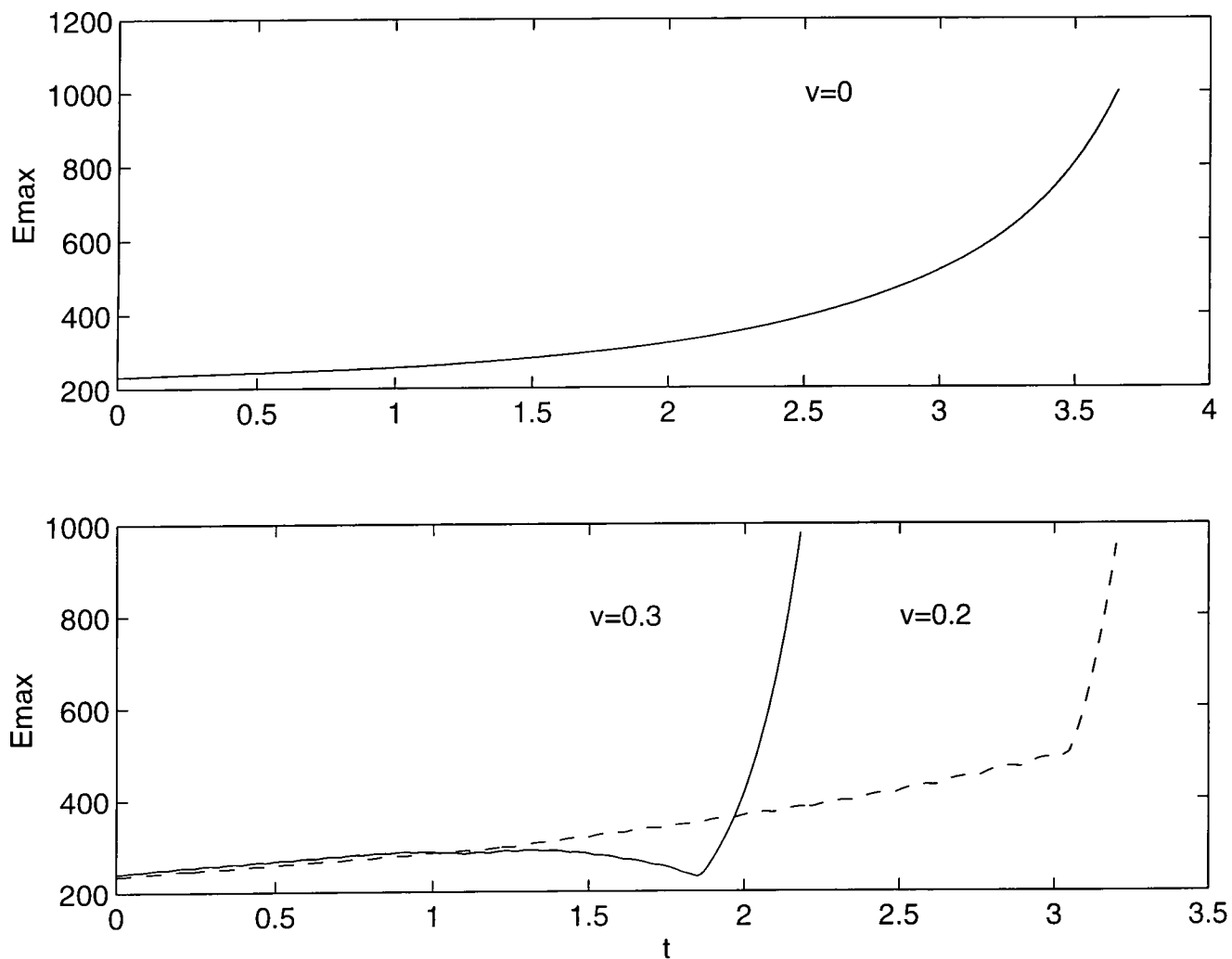


Figure 3.6: Above: Total energy density corresponding to two pure $O(3)$ solitons with no initial speed. Below: The same $O(3)$ lumps with different non-zero initial speeds (both curves correspond to head-on collisions that lead to scattering at right angles). Compare with the stable case shown in diagram 3.11.

3.5.2 Scattering

We now study the scattering behaviour of our two-skyrmion field (3.45) for different initial velocities. Let us consider head-on collisions.

There is always an initial burst of radiation as the skyrmion-lumps rearrange themselves towards their stable size. At small speeds the two humps approach each other, but the repulsive force between them results in their motion being reversed. This situation can be viewed in figure 3.7, where we present some pictures of the total energy density for skyrmions sent towards each other along the horizontal axis with a relative initial speed of 0.2; the corresponding contour plots are shown in figure 3.8.

A qualitatively similar behaviour is observed for speeds up to approximately 0.3. For $v \approx 0.3$ and higher the skyrmions acquire enough kinetic energy to overcome their mutual repulsion; during their collision they form a complicated ringish state (at which stage they attain a minimum height and hence maximum width) and re-emerge at 90° to the original direction of motion in the centre-of-mass frame. The emerging skyrmions are initially shrinking but, after they have travelled some distance, they expand once more. The final state is achieved after some oscillations of the energy density. In figure 3.9 we present a quartet of 3-D pictures of this 90° -scattering; the corresponding contour plots may be seen in figure 3.10.

The existence of a critical velocity above (below) which the lumps scatter at right angles (backwards) is a major difference between the pure $O(3)$ model and its modified Skyrme version: Going to the limit (3.44) we have been able to confirm that this critical velocity ceases to exist and 90° -scattering

occurs as long as $v > 0$: Events unfold very much like the skyrmion situation of figure 3.10 but now the system is no longer stable. The soliton-humps continue to grow thin, increasing in height, to eventually break down the numerical procedure as an aftermath. In the bottom half of figure 3.6 these episodes are illustrated with typical $E_{max}(t)$ plots. They are to be compared with their skyrmion counterpart plots in figure 3.11, which correspond to both the back-to-back (180°) and 90° scattering cases already discussed. It is noteworthy that a CP^1 -like scattering behaviour, and the existence of a critical velocity as well, are exhibited by some other important soliton models, *e.g.*, the ϕ^4 kink [80], the vortex model [81] and the tHP monopoles [82].

The fact that in our model the radiation emitted by the solitons is relatively large (as compared to other versions of the model) is immaterial for the modified $O(3)$ model because the lumps are stable anyway and can be studied for as long as necessary. But in the unstable, pure $O(3)$ scheme, such larger perturbation shows itself in a quicker collapse of the numerics, making the analysis of scattering processes more difficult to follow. For instance, the shrinking of the $O(3)$ solitons exemplified in figure 3.6 takes place significantly faster than fields of the aspect

$$(z - a)(z - b), \quad \frac{(z - a)(z - b)}{z - c},$$

studied in reference [75]. In any case, in all the situations considered the collisions are quasi-elastic (in the $O(3)$ case the quasi-elastic process is as long as the numerics runs smoothly).

For collisions with small but non-zero impact parameter the results are not at variance with prognostication: The skyrmion-lumps scatter either

bouncing back or at nearly right-angles to the initial direction of motion, depending on the velocity. A 90° event is pictured in figure 3.12. In general, the larger the impact parameter, the smaller the scattering angle, and the more the lumps conserve their identity during the process.

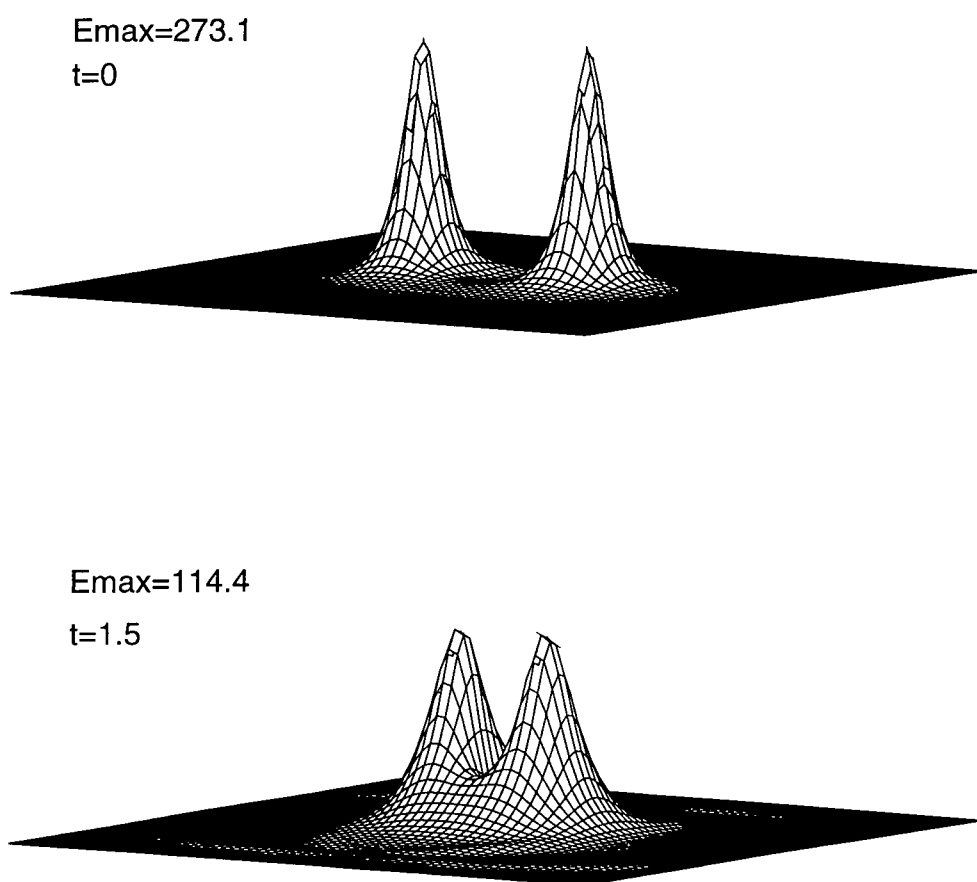


Figure 3.7: Collision featuring two skyrmion-lumps with relative initial velocity $\vec{v} = (0.2, 0.0)$.

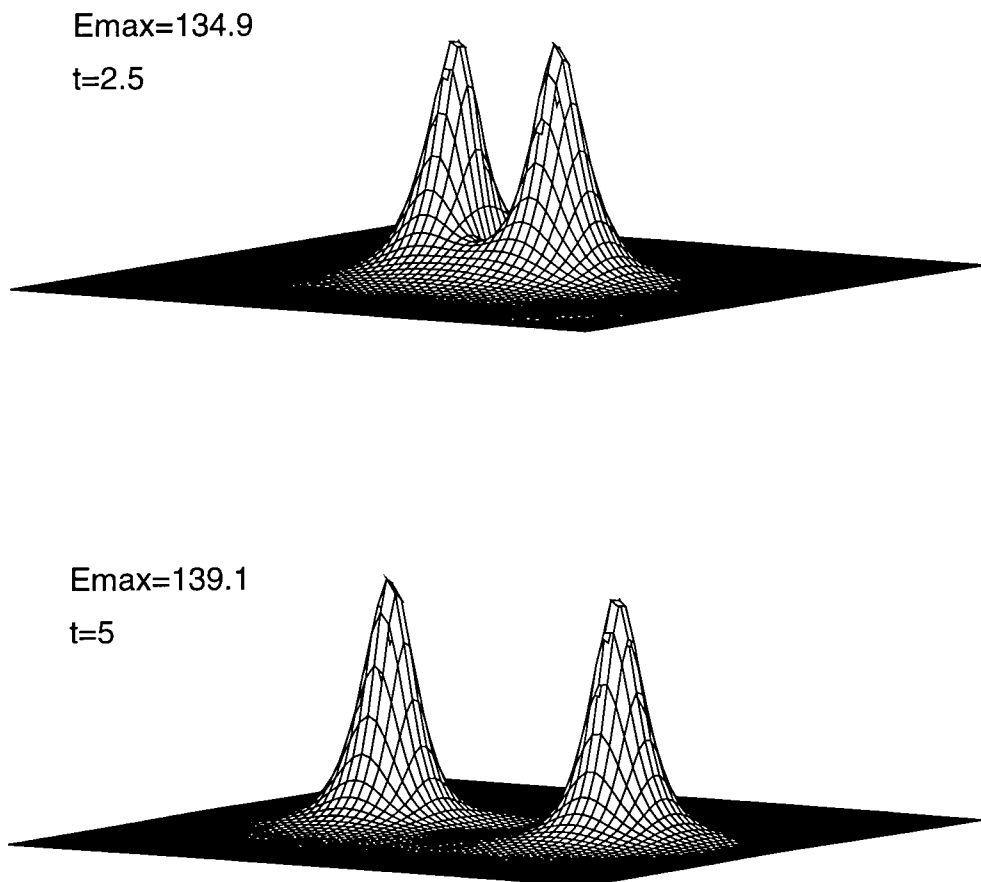


Figure 3.7: Continued. A speed of 0.2 is not big enough to overcome the repulsion between the lumps and back-to-back scattering occurs.

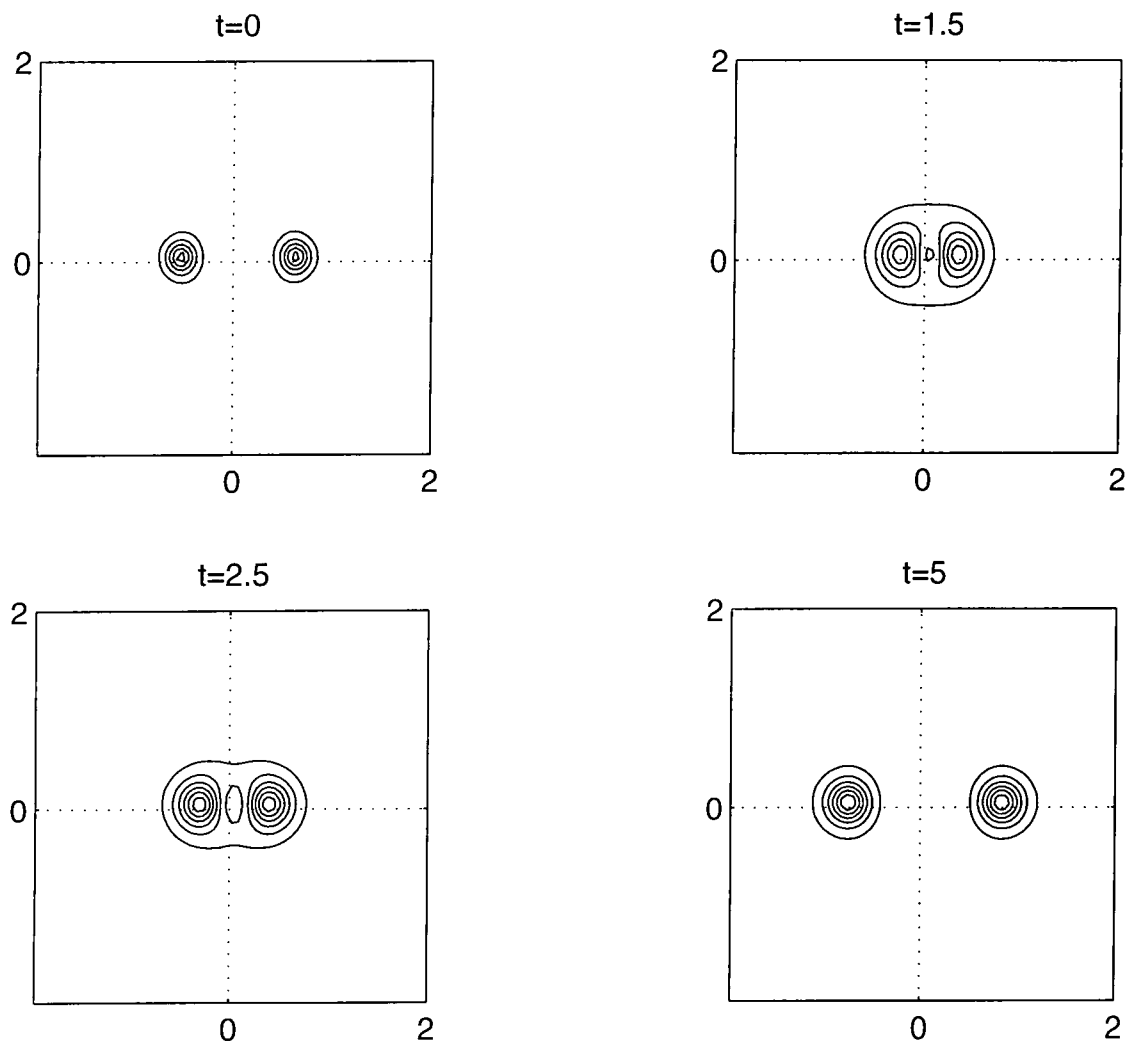


Figure 3.8: Contour plots for figure 3.7.

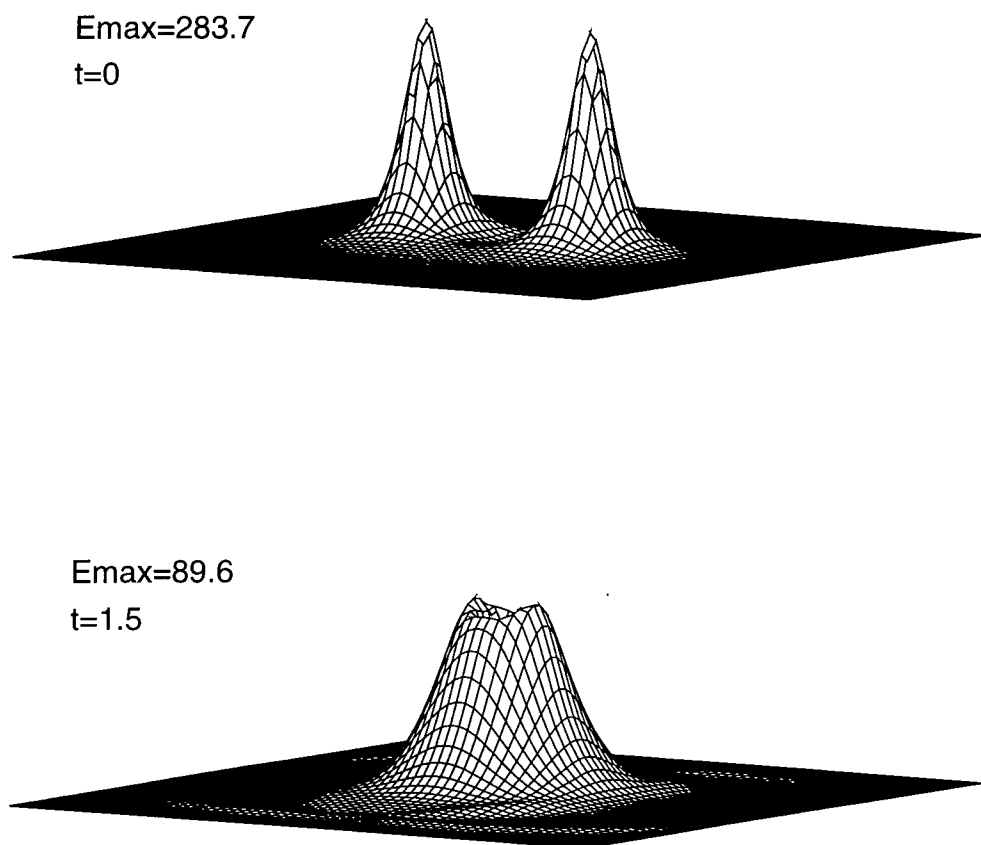


Figure 3.9: Two skyrmion-humps in collision course; their relative initial velocity is $\vec{v} = (0.3, 0.0)$.

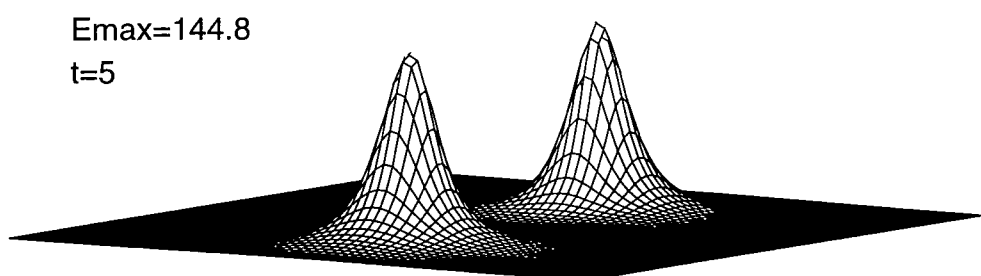
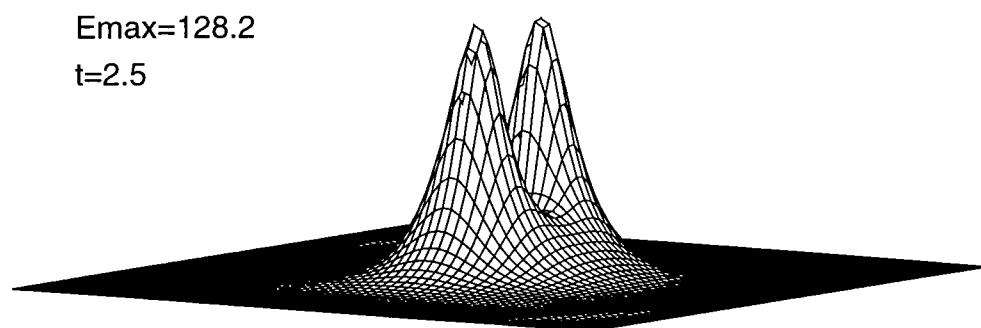


Figure 3.9: Continued. Above the critical value, now the speed leads to 90 degree skyrmion scattering.

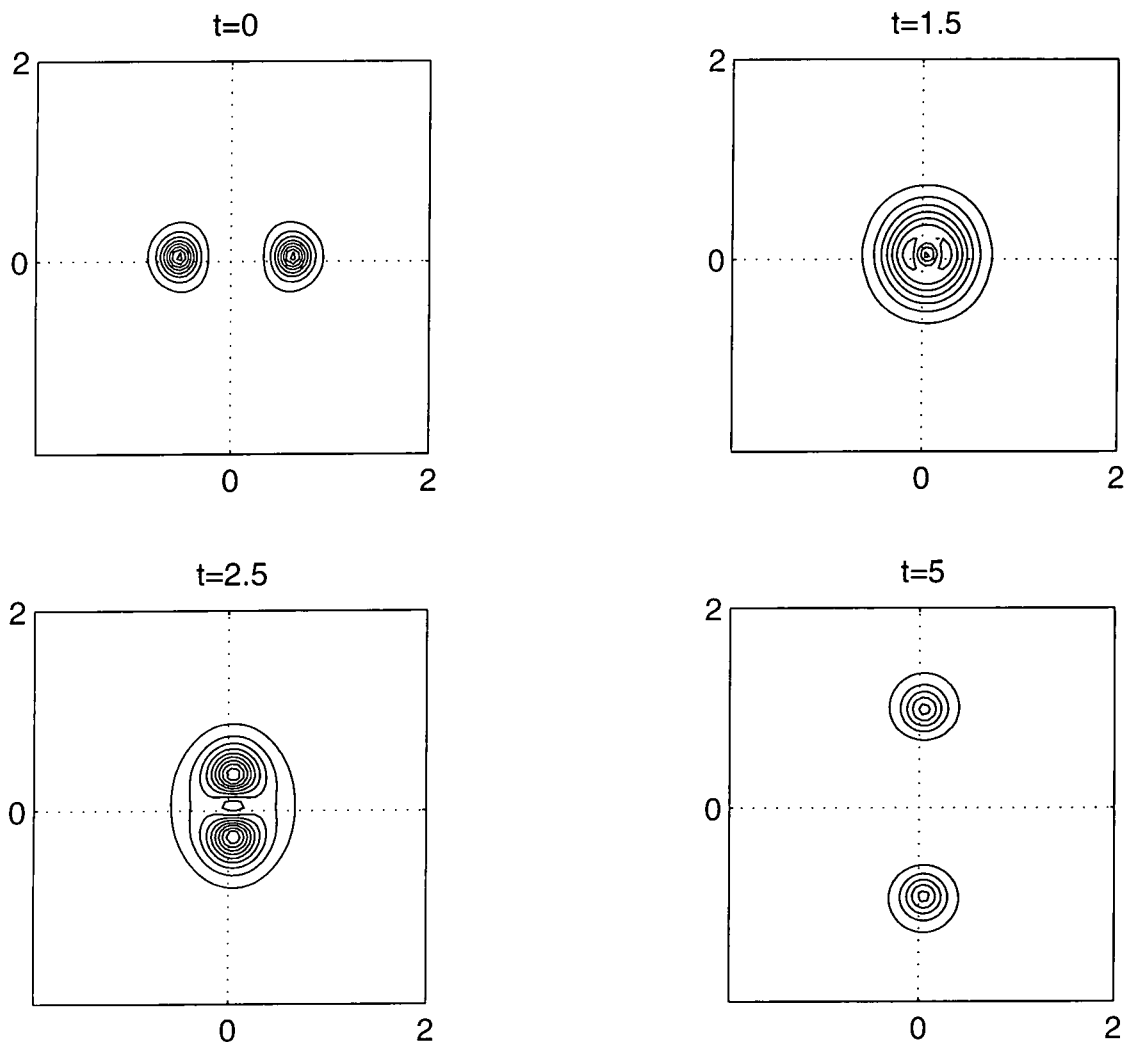


Figure 3.10: Contour plots for figure 3.9.

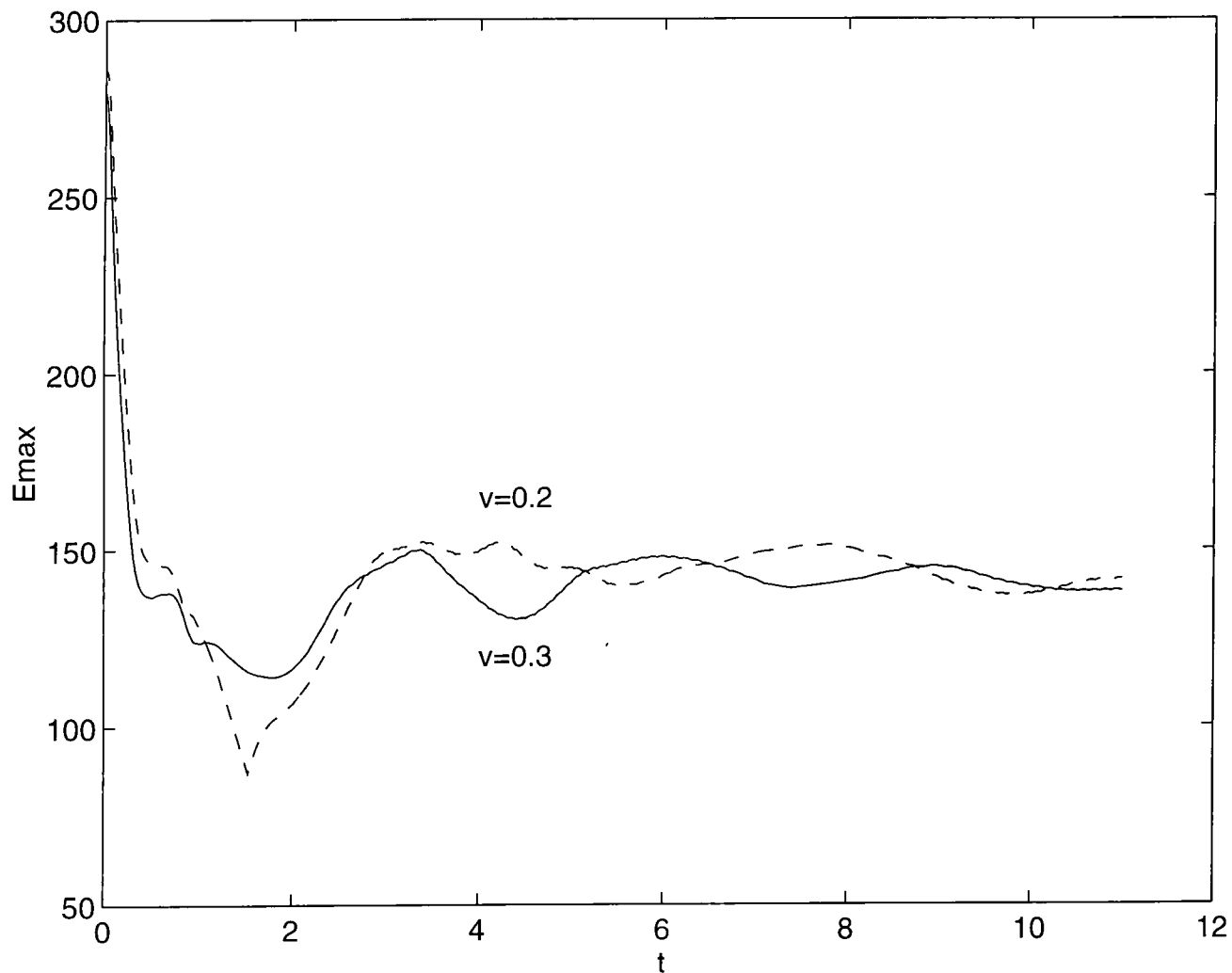


Figure 3.11: Amplitude of the total energy density corresponding to skyrmion scattering. A speed of 0.2 (0.3) leads to back-to-back (right angles) scattering. In both cases the lowest E_{max} occurs at impact time, when the two lumps coalesce. Compare with the unstable case of figure 3.6.

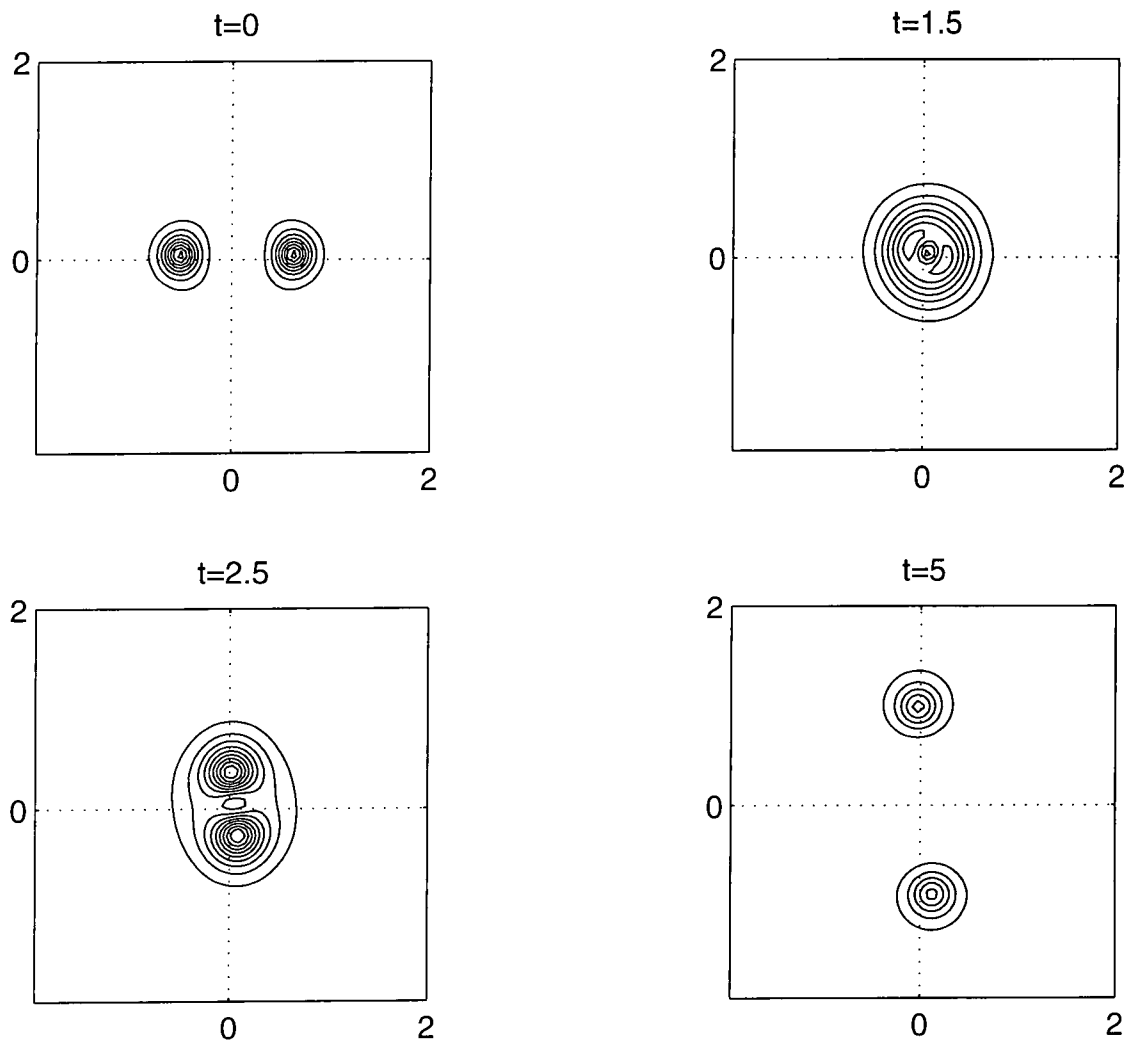


Figure 3.12: Non-zero impact parameter collision between skyrmions. The initial velocity is $\vec{v} = (0.3, 0.01)$.

Chapter 4

\mathbb{CP}^1 model on a torus

In this chapter we study the evolution properties of the non-linear $O(3)$ sigma-model when periodic boundary conditions are imposed. This amounts to defining the classical model on a two-dimensional torus, situation that looks more physical than the one on the sphere in the sense that the solitons are located in a finite volume from the outset. In any case, a comparison between both the toroidal and the spherical approaches is certainly of interest, if only to check the consistency of the two results. As in the previous chapter, we will be concerned with the stability and scattering properties of the system.

In the next section we present the $O(3)$ model on the torus, and explain the numerical set up in section 4.2. Solitons of degree one both in the $O(3)$ and its Skyrme version are discussed in section 4.3. The chapter closes with a study of the scattering situation, section 4.4.

4.1 The $O(3)$ model on a torus

The toroidal $O(3)$ model is defined as before by a lagrangian density of the form

$$\mathcal{L}_{O(3)}^{(T_2)} = \frac{1}{4}(\partial_\mu \vec{\phi}) \cdot (\partial^\mu \vec{\phi}), \quad (4.1)$$

where in (2+1) dimensions we have

$$x^\mu \equiv (x^0, x^1, x^2) = (t, x, y).$$

The field

$$\vec{\phi}(x^\mu) \equiv (\phi_1, \phi_2, \phi_3)$$

is a real vector in internal space and is restricted as usual to lie on the unit sphere $S^{(\Phi)}$:

$$\vec{\phi} \cdot \vec{\phi} = 1. \quad (4.2)$$

Let us write (4.1)-(4.2) together in terms of the action

$$S = \int_{T_2} dx dy \int dt \left[\frac{1}{4}(\partial_\mu \vec{\phi}) \cdot (\partial^\mu \vec{\phi}) + \varrho(x^\mu)(\vec{\phi} \cdot \vec{\phi} - 1) \right], \quad (4.3)$$

stressing that (x, y) belongs to the two-dimensional torus T_2 . Extremising the action and using (4.2) to eliminate the lagrange multiplier ϱ we get the field equation of motion

$$(\partial^\mu \partial_\mu - \vec{\phi} \cdot \partial^\mu \partial_\mu \vec{\phi}) \vec{\phi} = \vec{0}, \quad (4.4)$$

which for the static case simplifies to

$$\nabla^2 \vec{\phi} - (\vec{\phi} \cdot \nabla^2 \vec{\phi}) \vec{\phi} = \vec{0}. \quad (4.5)$$

For any value of t the configurations $\vec{\phi}$ are maps

$$T_2 \mapsto S_2^{(\Phi)}$$

that satisfy the periodic boundary conditions

$$\vec{\phi}(x + mL_1, y + nL_2) = \vec{\phi}(x, y), \quad (4.6)$$

where $m, n=0,1,2,\dots$ and L_1, L_2 are two primitive periods.

Recalling the relationship between (ϕ_1, ϕ_2, ϕ_3) and the CP^1 inhomogeneous coordinates W and \bar{W} :

$$\vec{\phi} = \left(\frac{W + \bar{W}}{|W|^2 + 1}, i \frac{-W + \bar{W}}{|W|^2 + 1}, \frac{|W|^2 - 1}{|W|^2 + 1} \right), \quad (4.7)$$

the equation of motion (4.5) adopts the form

$$W_{z\bar{z}} - \frac{2\bar{W}W_zW_{\bar{z}}}{|W|^2 + 1} = 0, \quad (4.8)$$

where $z = x + iy$ and a bar denotes complex conjugate.

Much as the similarity of (4.8) with its spherical counterpart (3.14) seems to be, their solutions are quite different owing to the boundary conditions imposed. In terms of W , equation (4.6) is replaced by

$$W(z + mL_1 + inL_2) = W(z), \quad (4.9)$$

our solitons being elliptic functions that may be expressed as [83]

$$W = \lambda \prod_{j=1}^{\kappa} \frac{\sigma(z - a_j)}{\sigma(z - b_j)}, \quad (4.10)$$

with the zeros (a_j) and poles (b_j) subject to the constraint

$$\sum_{j=1}^{\kappa} a_j = \sum_{j=1}^{\kappa} b_j. \quad (4.11)$$

The complex number λ is related to the size of the soliton and κ is the order of the elliptic function W : It is equal to the number of poles (which in turn is equal to the number of zeros), each pole/zero counted according to its degree of multiplicity. The function $\sigma(z)$ is the Weierstrass σ -function.

Equations (4.10)-(4.11) are valid in the whole plane but, due to the periodicity of the system, we can limit ourselves to consideration of their values within a fundamental cell (FC) delimited by the vertices

$$(0, 0), (L_1, 0), (L_1, L_2), (0, L_2). \quad (4.12)$$

Note that (4.10) is the elliptic analogue of the field (3.21) which expresses a rational function as a quotient of two polynomials. However, whereas in the latter case we can restrict ourselves to fields without poles and take $W = \lambda z$, the meromorphic nature of (4.10) cannot be dispensed of: Every non-constant elliptic function has poles. Indeed, some reflection shows that if $W(z)$ had no poles then it would be a bounded integral function in FC, and hence in the entire plane. By Liouville's theorem such a function cannot be but a constant (this theorem states that every integral function whose absolute value is always less than a fixed number is a constant).

The periodic solitons (4.10) have been studied in a variety of contexts. In reference [84], for example, they have been used to compute the contribution of instantons to the partition function.

It is important to bear in mind that $\sigma(z)$ is not an elliptic function itself but satisfies the pseudo-periodicity property [85]

$$\sigma(z + mL_1 + inL_2) = (-1)^{(m+n+mn)} \exp\left\{\frac{\pi}{L_1}(m-in)\left[z + \frac{1}{2}(mL_1 + inL_2)\right]\right\} \sigma(z). \quad (4.13)$$

The role of the selection rule (4.11) is now apparent: Substitution of (4.13) into (4.10) yields

$$W(z + mL_1 + inL_2) = \exp\left[\frac{\pi}{L_1}(m - in)\left(-\sum_j a_j + \sum_j b_j\right)\right] W(z),$$

which entails the requisite boundary condition (4.9) by virtue of (4.11).

In the present work the term ‘elliptic function’ denotes a doubly-periodic meromorphic function, *i.e.*, a single-valued doubly-periodic analytic function whose only possible singularities in a finite part of the plane are poles. In the literature, the σ -function, the theta functions and other related functions are not unfrequently dubbed ‘elliptic’ too.

Now, the Weierstrass’ σ -function is developable in a Laurent series of the form

$$\sigma(z) = \sum_{m,n=0}^{\infty} 2^{-(m+n)} a_{m,n} (g_2)^m (g_3)^n \frac{z^{(4m+6n+1)}}{(4m+6n+1)!}, \quad (4.14)$$

where

$$\begin{aligned} a_{0,0} &= 1, \\ a_{m,n} &= 3(m+1)a_{m+1,n-1} + \frac{16}{3}(n+1)a_{m-2,n+1} \\ &\quad - \frac{1}{3}(2m+3n-1)(4m-6n-1)a_{m-1,n}, \end{aligned} \quad (4.15)$$

it being understood that $a_{r,s}=0$ if either subscript is negative.

The quantities g_2 and g_3 , known as the invariants in the theory of elliptic functions, can be calculated via

$$\begin{aligned} g_2 &= 60 \sum_{m,n} \frac{1}{(mL_1 + inL_2)^4}, \\ g_3 &= 140 \sum_{m,n} \frac{1}{(mL_1 + inL_2)^6}, \end{aligned} \quad (4.16)$$

the summation being over all pairs m, n bar $m, n = 0$.

We shall consider a square torus ($L_1 = L_2 = L$) which corresponds to taking $g_3=0$ and $g_2 \in \mathfrak{R} - \{0\}$. In this so-called lemniscate case the expansion (4.14) simplifies to

$$\begin{aligned} \sigma(z) &= z \sum_{m=0}^{\infty} c_m z^{4m}, \\ c_m &= \frac{2^{-m}}{(4m+1)!} a_{m,0} (g_2)^m. \end{aligned} \tag{4.17}$$

The finite-energy configurations we want are harmonic maps from the two-torus to the two-sphere. Harmonic maps $\mathcal{N} \mapsto \mathcal{M}$ where both surfaces are compact and orientable have been extensively studied in differential geometry [37, 86]. When $\mathcal{M} = S_2$ these maps are partitioned into homotopy sectors parametrised by an invariant integral index, the Brouwer degree of the map. It is defined as usual by taking a volume-form from S_2 to \mathcal{N} via the pull-back map. For a given map $W : T_2 \mapsto S_2$ equation (2.11) dictates

$$Q^{(T_2)} = (\text{constant}) \int_{T_2} W^* w. \tag{4.18}$$

Pulling back the Kahler two-form

$$\omega = 4i \frac{d\xi \wedge d\bar{\xi}}{(1 + \xi\bar{\xi})^2}, \quad \xi \in S_2, \tag{4.19}$$

we obtain

$$Q^{(T_2)} = \frac{1}{\pi} \int_{T_2} \frac{|W_z|^2 - |W_{\bar{z}}|^2}{(|W|^2 + 1)^2} dx dy, \tag{4.20}$$

upon setting the constant in (4.18) equal to $1/8\pi$.

Writing the lagrangian (4.1) as

$$\mathcal{L}_{O(3)}^{(T_2)} = \frac{|W_t|^2 - 2|W_z|^2 - 2|W_{\bar{z}}|^2}{(|W|^2 + 1)^2}, \tag{4.21}$$

we see that the potential energy is given by

$$V_{O(3)}^{(T_2)} = 2 \int_{T_2} \frac{|W_z|^2 + |W_{\bar{z}}|^2}{(|W|^2 + 1)^2} dx dy \quad (4.22)$$

which, in conjunction with (4.20) produces

$$V_{O(3)}^{(T_2)} = \begin{cases} 2\pi Q^{(T_2)} + 4 \int_{T_2} \frac{|W_{\bar{z}}|^2}{|W|^2 + 1} dx dy, \\ 2\pi[-Q^{(T_2)}] + 4 \int_{T_2} \frac{|W_z|^2}{|W|^2 + 1} dx dy. \end{cases} \quad (4.23)$$

Our solitons ($Q^{(T_2)} > 0$) and anti-solitons ($Q^{(T_2)} < 0$) are respectively given by equations:

$$W_{\bar{z}} = 0, \quad W_z = 0, \quad (4.24)$$

previously encountered analyticity conditions.

We have pointed out in the context of the usual CP^1 theory (where the soliton solutions are harmonic maps from sphere to sphere) that the solutions to equation (3.19), the analogue of (4.24), are all the static solutions to (3.14). This is no longer true within the framework of the toroidal theory. There are several kinds of harmonic maps disobeying (4.24) but satisfying (4.8). An example is provided by the solutions to a certain pendulum problem in which equation (4.8) becomes the pendulum equation. Interestingly, the solutions in question turn out to be the Gauss maps of certain surfaces of revolution (the nodoid and the unduloid) known as Delaunay's surfaces [87, 88]. Equation (4.8) is the condition for the said surfaces to have constant mean curvature. The surfaces of Delaunay also appear as solutions to an isoperimetric problem in the calculus of variations, and are relevant in some problems of gas dynamics like soap bubbles and stems of plants. A harmonic

map which does not solve one of the equations (4.24) is not a holomorphic function, and does not represent a minimum of the energy.

4.2 Basic numerical set up

Heretofore we have discussed the static field configurations. Now we concentrate on their dynamics, paying particular attention to their stability, scattering properties, *etc.*. As our model is not integrable, the study of the evolution of our fields requires numerical techniques. We treat the configurations (4.10)-(4.11) as initial conditions for our evolution, studied numerically. After giving some initial velocity to the W fields, we switch to the ϕ -formulation via equation (4.7), and evolve $\vec{\phi}$ according to the equation of motion (4.4). Of course, in the Skyrme version of the model the equation employed will be the corresponding skyrmion equation.

Again we have recourse to the fourth-order Runge-Kutta method and approximate the spatial derivatives by finite differences. The laplacian is evaluated using three different formulae: The standard 9-point recipe and a couple of 13-point laplacians meant to further check our results. One of these 13-point operators employs particularly simple coefficients, and it will be educational to derive it here:

Replace the $x - y$ plane by a square mesh with spatial step a and consider a central point 0 surrounded by a dozen of points labelled 1-12 as in the schematic plot below

$$\begin{array}{ccccccc}
 & & & & 10 & & \\
 & & & & 6 & 2 & 5 \\
 & & & 11 & 3 & 0 & 1 & 9 \\
 & & & & 7 & 4 & 8 & \\
 & & & & & & & 12
 \end{array}$$

In terms of the central point 0 we have

$$\begin{aligned}
 \phi_1 &= \exp(a\partial_x)\phi_0, & \phi_3 &= \exp(-a\partial_x)\phi_0, \\
 \phi_2 &= \exp(a\partial_y)\phi_0, & \phi_4 &= \exp(-a\partial_y)\phi_0,
 \end{aligned}
 \tag{4.25}$$

where ϕ_k represents the function $\phi(x, y)$ at point k . Upon Taylor-expanding (around ϕ_0) the symmetrical sums

$$S_1 = \sum_{j=1}^4 \phi_j, \quad S_2 = \sum_{j=5}^8 \phi_j, \quad S_3 = \sum_{j=9}^{12} \phi_j,
 \tag{4.26}$$

some algebraic manipulation leads to

$$(\partial_{xx} + \partial_{yy})\phi_0 = \frac{4\phi_0 - S_1 - S_2 + S_3}{a^2},
 \tag{4.27}$$

where terms of order higher than a^2 have been omitted. Clearly, the coefficients entering the calculations are quite simple; our 13-point laplacian can be symbolically presented as

$$\nabla^2 = \frac{\begin{bmatrix} & & & & 1 & & \\ & & & & -1 & -1 & -1 \\ & & & 1 & -1 & 4 & -1 & 1 \\ & & & & -1 & -1 & -1 & \\ & & & & & & & 1 \end{bmatrix}}{a^2}.
 \tag{4.28}$$

For completeness let us also display the standard 9-point laplacian:

$$\nabla^2 = \frac{\begin{bmatrix} 1 & 4 & 1 \\ 4 & -20 & 4 \\ 1 & 4 & 1 \end{bmatrix}}{6a^2},
 \tag{4.29}$$

utilised in the studies of chapter 3 as well.

Our simulations are carried out in a 200×200 ($n_x = n_y = 200$) periodic lattice with coordinate steps $\delta x = \delta y = 0.02$ and $\delta t = 0.005$. The size of our torus is then $L = n_x \times \delta x = 4$. For a square torus the basic network (4.12) reduces to

$$(0, 0), (L, 0), (L, L), (0, L). \quad (4.30)$$

Unlike the simulations with non-periodic boundary conditions, the implementation of an absorption device in the mesh (4.30) is not required. The exception, however, is the single-soliton case of section 4.3, whose particular features necessitate, if only for a short while, a damping set up.

With the help of (4.15) the coefficients c_m in the expansion (4.17) can be computed. The first six are:

$$\left. \begin{aligned} c_0 &= 1 \\ c_1 &= -0.7878030 \\ c_2 &= -0.221654845 \\ c_3 &= 9.36193 \times 10^{-3} \\ c_4 &= 7.20830 \times 10^{-5} \\ c_5 &= 2.37710 \times 10^{-5} \end{aligned} \right\}, \quad (4.31)$$

where the simplifying value $g_2 = 1$ has been used. We have verified that the omission of higher terms in the series does not compromise much in accuracy. The seventh coefficient, for example, is the negligible 1.97×10^{-7} .

The numerical truncations errors gradually move the evolving configurations away from the constraint (4.2). We account for this by rescaling

$$\vec{\phi} \rightarrow \frac{\vec{\phi}}{\sqrt{\vec{\phi} \cdot \vec{\phi}}}$$

every few iterations. Before the rescaling operation we evaluate the quantity

$$\mu \equiv \vec{\phi} \cdot \vec{\phi} - 1$$

which, as in the simulations of chapter 3, serves as a guide to detect undesirable numerical deviations.

The parameter λ in (4.10) has been equated to unity in all our simulations. And, for the sake of easiness when checking out results, we have set the scale of the total energy so that it equals the value of the topological charge (this has been used in chapter 3 as well). In this way, $E_{total}=1$ for one-soliton cases and $E_{total}=2$ when two solitons are involved. Note also that the relationship $V_{O(3)}^{(T_2)} = 2\pi Q^{(T_2)}$ implies that all our energy density plots are basically topological charge density plots.

To close this section we note that the discretisation of the toroidal model introduces more perturbation into the system than in the planar format of chapter 3. Comparison of the respective soliton fields in both schemes so suggests. But in all processes studied the radiation waves remained quite low and the implicit disturbances proved to be immaterial.

4.3 Solitons of degree one

4.3.1 $O(3)$ case

From the theory of meromorphic functions we know that the sum of the residues B_j with respect to the poles situated in a FC (4.30) is given by

(suppose for definiteness that there are no poles at the boundary)

$$\sum_j B_j = \frac{1}{2i\pi} \oint_{FC} f(z) dz, \quad (4.32)$$

where $f(z)$ is an arbitrary elliptic function. Taking into account the facts

$$\int_L^{L+iL} f(z) dz = - \int_{iL}^0 f(z) dz,$$

$$\int_{L+iL}^{iL} f(z) dz = - \int_0^L f(z) dz,$$

we note that the integral in (4.32) is zero:

$$\begin{aligned} \sum_j B_j &= \frac{1}{2i\pi} \oint_{FC} f(z) dz \\ &= 0, \end{aligned} \quad (4.33)$$

signifying that, unless $f(z)$ is a constant, it must have at least either a single pole of order two or two simple poles: The simplest non-trivial elliptic function is at least of the second order. For suppose that $f(z)$ possesses only a single pole of order one. Then we have

$$\begin{aligned} f(z) &= \frac{B}{z-b} + \text{Regular part} \\ &= \text{Regular part} \quad [B = 0 \text{ from (4.33)}] \\ &\neq \text{elliptic function.} \end{aligned}$$

But if the single pole b in $f(z)$ is of a higher order, two say, we have:

$$\begin{aligned} f(z) &= \frac{A}{(z-b)^2} + \frac{B}{z-b} + \text{Regular part} \\ &= \frac{A}{(z-b)^2} + \text{Regular part} \quad [B = 0], \end{aligned}$$

which is certainly elliptic.

The above implies that the $O(3)$ model on the torus possesses no static analytic single-soliton solutions.

This fact may also be understood in the context of differential geometry: The harmonic maps $M \mapsto S_2$ (M an orientable Riemann surface) have holomorphic representatives (instantons) of any degree provided that it is greater than the genus of M [37, 86]. Clearly, for $M = T_2$ the Brouwer index of the maps must be greater than unity. It is important to realise that $Q^{(T_2)}$ in (4.20) is numerically equal to the order κ of (4.10) only when the latter is greater than one. Thus, an order-one solution carries degree zero, not one. Instanton solutions of zero degree on the torus are trivial. These are not to be confused with solutions of the type involved in the Delaunay problem described at the end of section 4.1, which also have degree zero. The latter are *not* constant functions since they are *not* holomorphic.

In order to study a single soliton-like configuration on T_2 , we ignore the selection rule (4.11) and take

$$W_1(z) = \frac{\sigma(z-a)}{\sigma(z-b)}, \quad a \neq b, \quad (4.34)$$

which describes a quasi-periodic soliton that instead of (4.9) satisfies

$$W_1(z + mL + i nL) = \exp\left[\frac{\pi}{L}(m - in)(b - a)\right]W_1(z). \quad (4.35)$$

Were a equal to b in (4.34) the field W_1 would be trivial. The condition $a \neq b$ allows the construction, out of W_1 , of a $Q^{(T_2)}=1$ soliton. Such a periodic configuration may be fabricated by taking a field whose values in

the sub-cell of vertices

$$(l, l), (L - l, l), (L - l, L - l), (l, L - l), \quad l \ll L, \quad (4.36)$$

are given by (4.34) and in the rest of the fundamental cell (4.30) are given by a suitably chosen interpolating function.

Commence by periodising W_1 along the abscissas with the help of the kink-like *ansatz*

$$\begin{aligned} W_h(x, y) &= A(y) \tanh[\alpha(x - L)] + B(y), \\ x \in [L - l, L + l], \quad y \in [0, L], \end{aligned} \quad (4.37)$$

where it is important to note that

$$[L - l, L + l] = [0, l] \cup [L - l, L],$$

which keeps us within the basic mesh. For each value of y the kink (4.37) will periodise the field (4.34) along the x -axis.

The complex functions $A(y)$ and $B(y)$ are obtained by demanding periodicity and continuity of (4.34) and (4.37):

$$\begin{aligned} W_h(l, y) &= W_h(l + L, y) \\ &= A(y) \tanh(\alpha l) + B(y) \\ &= W_1(l, y); \end{aligned} \quad (4.38)$$

$$\begin{aligned} W_h(L - l, y) &= A(y) \tanh(-\alpha l) + B(y) \\ &= W_1(L - l, y). \end{aligned} \quad (4.39)$$

Substraction and addition of (4.38) and (4.39) entail

$$\begin{aligned} A(y) &= \frac{W_1(l, y) - W_1(L - l, y)}{2 \tanh(\alpha l)}, \\ B(y) &= \frac{W_1(l, y) + W_1(L - l, y)}{2}. \end{aligned} \tag{4.40}$$

Therefore, our horizontally-periodic configuration is

$$W_H(x, y) = \begin{cases} W_1; & x \in [l, L - l], \quad y \in [0, L]; \\ W_h; & x \in [L - l, L + l], \quad y \in [0, L]. \end{cases} \tag{4.41}$$

Next periodise W_H along the ordinates with the assistance of

$$\begin{aligned} W_v(x, y) &= C(x) \tanh[\beta(y - L)] + D(x), \\ x \in [0, L], \quad y \in [L - l, L + l]. \end{aligned} \tag{4.42}$$

For each value of x the kink W_v will periodise W_H along the y -axis.

Demands of both periodicity and continuity on (4.41)-(4.42) give

$$\begin{aligned} W_v(x, l) &= W_v(x, l + L) \\ &= C(x) \tanh(\beta l) + D(x) \\ &= W_H(x, l); \end{aligned} \tag{4.43}$$

$$\begin{aligned} W_v(x, L - l) &= C(x) \tanh(-\beta l) + D(x) \\ &= W_H(x, L - l). \end{aligned} \tag{4.44}$$

Combining (4.43) and (4.44) we find

$$\begin{aligned} C(x) &= \frac{W_H(x, l) - W_H(x, L - l)}{2 \tanh(\beta l)}, \\ D(x) &= \frac{W_H(x, l) + W_H(x, L - l)}{2}. \end{aligned} \tag{4.45}$$

It turns out that the vertical periodisation on W_H produces a field W_p periodic in *both* x and y :

$$W_p(x, y) = \begin{cases} W_H; & y \in [l, L - l]; & x \in [0, L], \\ W_v; & y \in [L - l, L + l], & x \in [0, L], \end{cases} \quad (4.46)$$

configuration that represents the periodic one-soliton function that we are seeking.

The values of the parameters entering (4.46) are as follows: For the arguments in the kink configurations (4.37) and (4.42) we choose $\alpha=\beta=20$, and for the zero and pole of (4.34) we use

$$a = (2.05, 1.75), \quad b = (1.95, 2.25); \quad (4.47)$$

for the length l we take ten lattice points, so that $l = 0.2 \ll L = 4$.

We have numerically verified that the construct (4.46) has $Q^{(T_2)} \approx 0.9999\dots$, and therefore can be justly regarded as a map $T_2 \mapsto S_2$ of degree one.

Figure 4.1 illustrates the periodisation of W_1 for a representative line of the fundamental net, whereas a full picture of both the real and the imaginary parts of W_p is exhibited in figure 4.2.

Recall that our simulations are carried out in the ϕ -formulation, according to equation (4.4). The one-soliton configurations therein employed are periodic fields $\vec{\phi}_p$ obtained from W_p via (4.7):

$$\vec{\phi}_p = \left(\frac{W_p + \bar{W}_p}{|W_p|^2 + 1}, i \frac{-W_p + \bar{W}_p}{|W_p|^2 + 1}, \frac{|W_p|^2 - 1}{|W_p|^2 + 1} \right). \quad (4.48)$$

The components of (4.48) have interesting shapes, as shown in figure 4.3.

It is apparent from the above pictures that the periodisation procedure introduces some perturbation along the borders of the lattice in the form

of small folds. Under the numerical evolution these disturbances propagate towards the centre of the grid and collapse the lump of energy associated with the evolving fields. A picture showing the energy density corresponding to (4.48) can be appreciated in figure 4.4. As the initial condition for our system we would like to have a field whose energy density resembles a lump in the centre and is flat elsewhere, and see to what extent the shrinking of the soliton as described above can be reduced. Consequently, in order to minimise the effects of the said perturbations we try to improve the initial conditions by ironing out the folds. We do this in the spirit of section 3.4 by implementing a damping function χ that rescales

$$\partial_t \vec{\phi}_p \rightarrow \chi \partial_t \vec{\phi}_p, \quad \chi \leq 1,$$

throughout a narrow strip along the edges of our cell (4.30). The absorption is switched off at the time (t_0) when the folds have disappeared. In contrast with the soliton-lump of diagram 4.4, the flatness of the new initial structure along the edges can be appreciated in the upper half of figure 4.5.

We remind that the kinks W_h and W_v , responsible for the periodisation of the system, operate around the borders on a strip which is only 10% ($l = 0.2$) of grid size. We want this to be the case so that the periodised soliton (4.46) be only a small modification of the basic Weierstrass field W_1 , equation (4.34). For values $l > 0.2$ the kink folds are less pronounced but will not disappear unless l occupies a significant proportion of the net. On the other hand, smaller values of l give a greater perturbation at the edges of the mesh, perturbation which is then more difficult to deal with.

Our simulations show that during the preparatory stage the total energy

undergoes a small decrease, in conformity with the absorption that is taking place. Once the latter is turned off, the energy settles near the expected value of one (recall we have numerically normalised $E_{total} = Q^{(T_2)}$) and remains constant until the time (t_f) when the total energy density becomes so spiky that the numerical procedure breaks down [see the nether half of figure 4.5]. These results do not depend on how the initial conditions are prepared, nor on whether a 9-point or a 13-point nabla-squared operator is used in the simulations. In other words, the effects of the kinks on the shrinking of our soliton cannot be completely eliminated. Having performed many such simulations we are convinced that our results are genuine, *i.e.*, the shrinking is genuine and not a numerical artifact.

4.3.2 Skyrmion case

Next we look at possible ways to stabilising our periodic construct. Guided by the experience with the $O(3)$ model in the compactified plane (where stabilisation is achieved by the addition of two extra terms to the lagrangian -the Skyrme and the potential terms-) we consider the possibility of adding the Skyrme term alone. Adding such a term to the $O(3)$ lagrangian (4.1) we get:

$$\begin{aligned} \mathcal{L}_{sky}^{(T_2)} &= \frac{1}{4}(\partial_\mu \vec{\phi}) \cdot (\partial^\mu \vec{\phi}) \\ &- \frac{\theta_1}{4} [(\partial^\mu \vec{\phi} \cdot \partial_\mu \vec{\phi})^2 - (\partial^\mu \vec{\phi} \cdot \partial^\nu \vec{\phi})(\partial_\mu \vec{\phi} \cdot \partial_\nu \vec{\phi})], \end{aligned} \quad (4.49)$$

identical in form to the (3+1)-dimensional (2.42). As already discussed, the term in θ_1 fixes the height of the lumps of energy associated with the soliton

fields. Since in the present context the system is defined in a finite volume from the very beginning, the extended solitonic entities presumably will not expand indefinitely. Consequently, unlike the situation in the compactified plane, the addition of a θ_2 term should not be indispensable. Indeed, our results support this.

The equation of motion that follows from (4.49) is

$$\begin{aligned}
 \vec{0} = & (\partial^\mu \partial_\mu - \vec{\phi} \cdot \partial^\mu \partial_\mu \vec{\phi}) \vec{\phi} \\
 & + 2\theta_1 [\partial^\mu \partial_\mu \vec{\phi} (\partial^\nu \vec{\phi} \cdot \partial_\nu \vec{\phi}) + \partial_\nu \vec{\phi} (\partial_\mu \partial^\nu \vec{\phi} \cdot \partial^\mu \vec{\phi}) - \partial_\nu \partial_\mu \vec{\phi} (\partial^\nu \vec{\phi} \cdot \partial^\mu \vec{\phi}) \\
 & - \partial^\mu \vec{\phi} (\partial_\nu \partial^\nu \vec{\phi} \cdot \partial^\mu \vec{\phi}) + (\partial^\mu \vec{\phi} \cdot \partial_\mu \vec{\phi}) (\partial^\nu \vec{\phi} \cdot \partial_\nu \vec{\phi}) \vec{\phi} \\
 & - (\partial_\mu \vec{\phi} \cdot \partial_\nu \vec{\phi}) (\partial^\mu \vec{\phi} \cdot \partial^\nu \vec{\phi}) \vec{\phi}].
 \end{aligned} \tag{4.50}$$

In the convenient W -formulation the lagrangian reads

$$\begin{aligned}
 \mathcal{L}_{sky}^{(T_2)} = & \frac{|W_t|^2 - 2|W_z|^2 - 2|W_{\bar{z}}|^2}{(1 + |W|^2)^2} \\
 & - 8\theta_1 \frac{|W_z|^2 - |W_{\bar{z}}|^2}{(1 + |W|^2)^4} (|W_t|^2 + |W_z|^2 - |W_{\bar{z}}|^2),
 \end{aligned} \tag{4.51}$$

the corresponding static equation being

$$\begin{aligned}
 0 = & W_{z\bar{z}} - \frac{2\bar{W}W_zW_{\bar{z}}}{|W|^2 + 1} \\
 & + \frac{4\theta_1}{(|W|^2 + 1)^2} [2\bar{W}_{z\bar{z}}W_zW_{\bar{z}} - \bar{W}_{zz}(W_z)^2 - \bar{W}_{\bar{z}\bar{z}}(W_{\bar{z}})^2] \\
 & + W_{zz}\bar{W}_zW_{\bar{z}} + W_{\bar{z}\bar{z}}\bar{W}_{\bar{z}}W_z - W_{z\bar{z}}(|W_z|^2 + |W_{\bar{z}}|^2) \\
 & + \frac{2W}{|W|^2 + 1} (|W_z|^2 - |W_{\bar{z}}|^2)^2.
 \end{aligned} \tag{4.52}$$

Our computations reveal that thanks to the extra term the energy of the lump does not increase indefinitely, but instead it vibrates in a stable

manner as time goes by. In figure 4.6 we show the evolution of the amplitude of the total energy density and the corresponding total energy for the case $\theta_1 = 0.001$ (greater values of this parameter simply reduce the amplitude of the vibrations). Qualitatively similar pictures are obtained for values of θ_1 as small as ≈ 0.00015 , with the amplitude of the vibrations increased accordingly. Smaller values cannot refrain the soliton-hump from augmenting its height indefinitely and W_p is no longer stable.

The kinetic energy plots for figure 4.6 are depicted in figure 4.7: In the upper section we have the maximum value of the kinetic energy (K_{max}) as time progresses, whereas in the nether half the evolution of the total kinetic energy itself (K_{total}) is presented. Due to the already-discussed disturbances generated through the periodisation of the field (4.34), the radiation is quite big at the beginning. It then decreases under the action of the absorbing strip, which operates during the interval $t_f - t_0 = 0.8$. By this time the radiation is small enough and the damping can be switched off; the kinetic waves remain remarkably low afterwards, for the rest of the numerical simulation.

Note that W_p does not exactly satisfy the equation of motion (4.52), for the term

$$\frac{4\theta_1}{(|W|^2 + 1)^2} [-\bar{W}_{zz}(W_z)^2 + \frac{2W}{|W|^2 + 1}|W_z|^4]$$

does not vanish. Nevertheless, the smallness of θ_1 means that our Skyrme model is only a slight perturbation of $O(3)$, and hence our periodic one-soliton construction is a good, if approximate, solution.

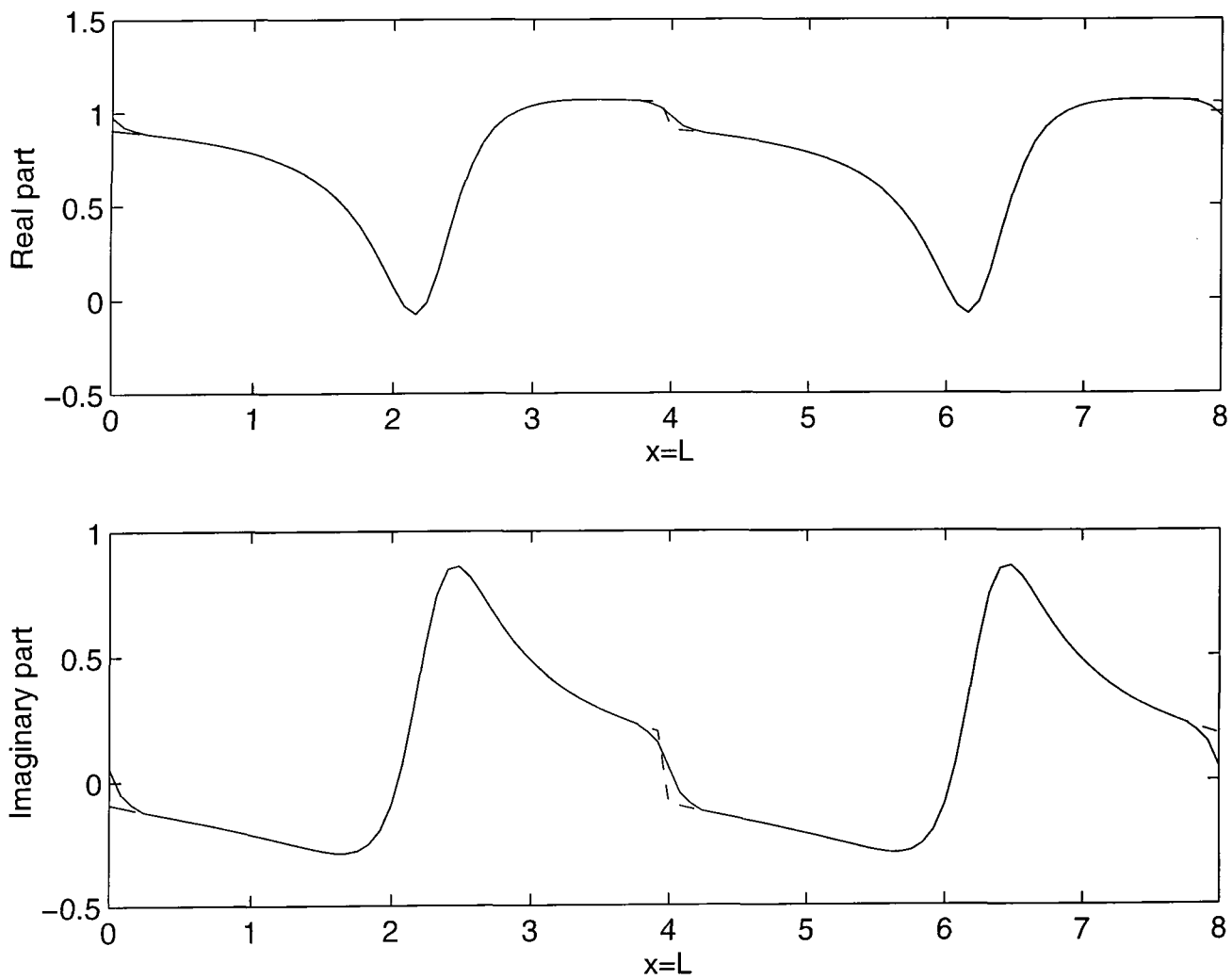


Figure 4.1: The non-periodic field W_1 (dashed line) and its periodised version W_p (solid line) along the line $y = 2$ of the fundamental cell.

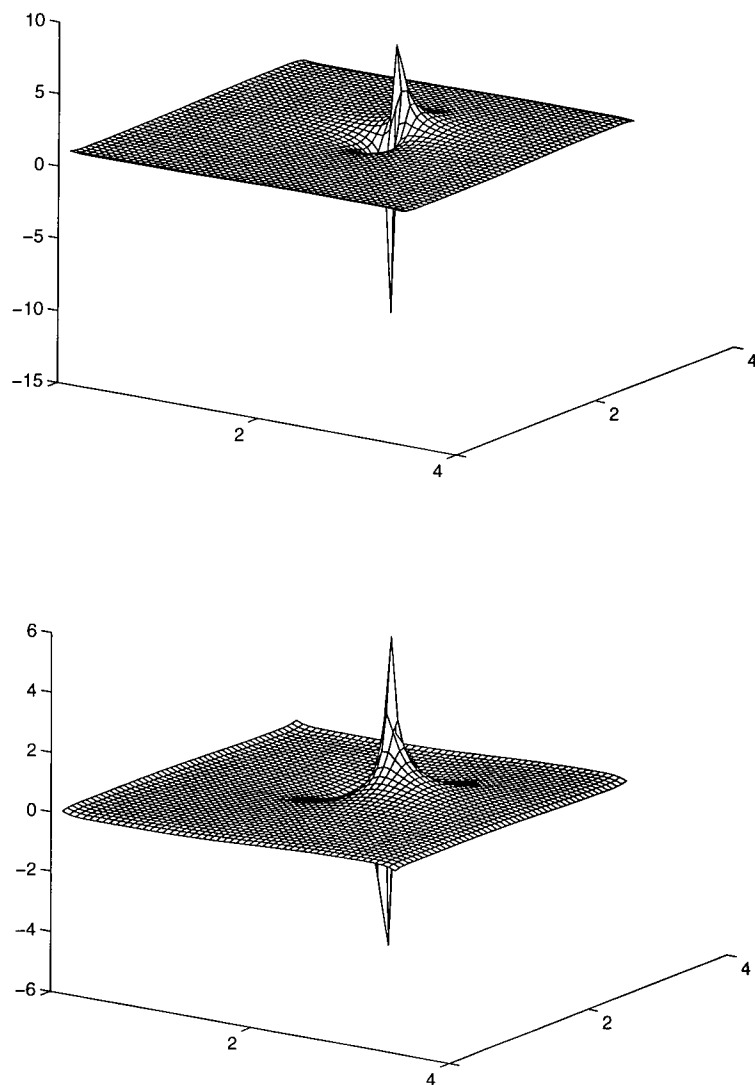


Figure 4.2: The real (above) and imaginary (below) parts of the periodic soliton field W_p . The periodisation procedure creates small folds at the borders.

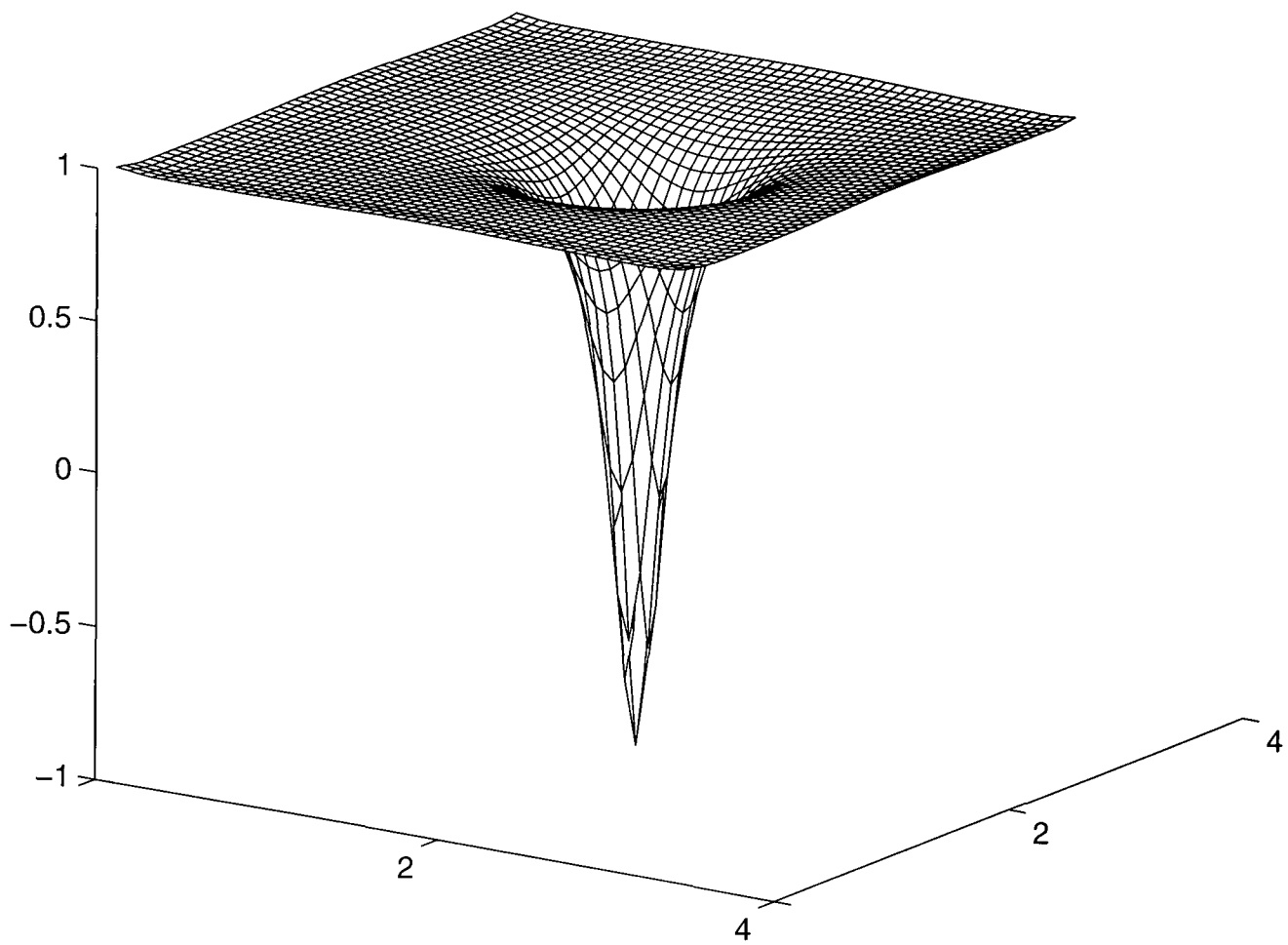


Figure 4.3: The first component of the periodic soliton $\vec{\phi}_p$. The components ϕ_2 and ϕ_3 are shown next.

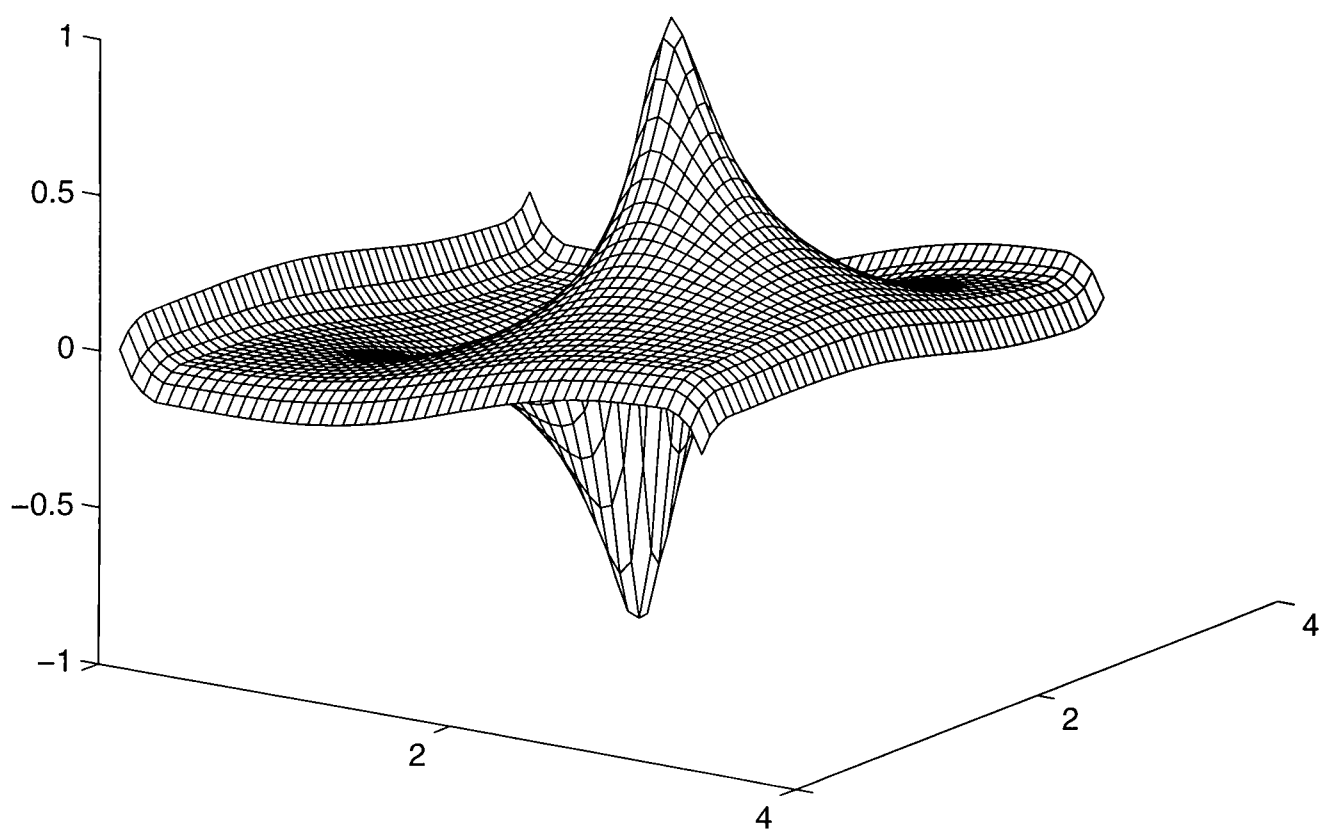


Figure 4.3: Continued. The second component of the field $\vec{\phi}_p$.

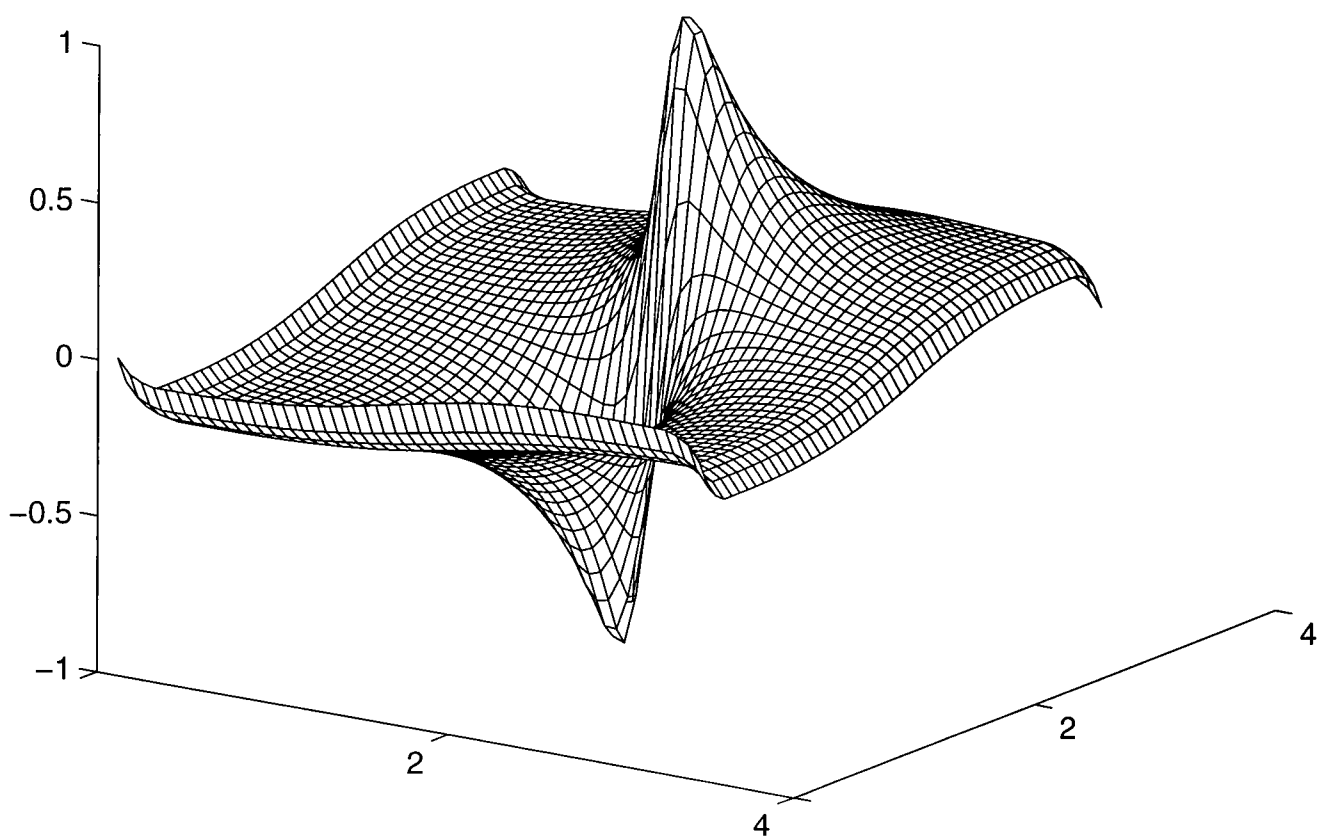


Figure 4.3: Continued. The third component of the periodic vector $\vec{\phi}_p$.



Total energy density

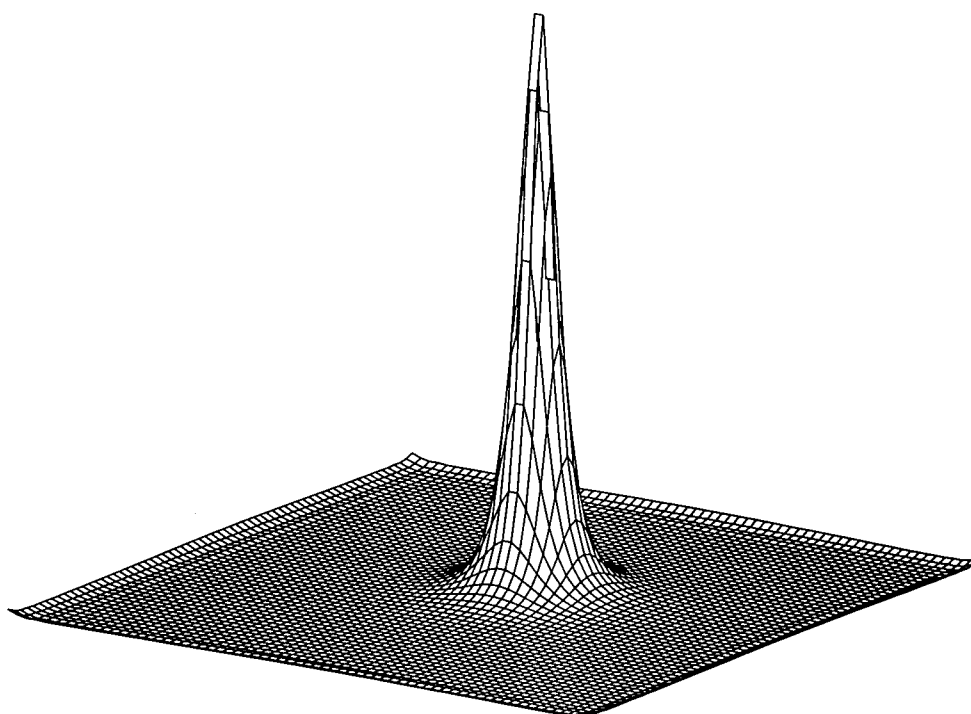


Figure 4.4: Total energy density at the initial time corresponding to the periodic field W_p . The folds at the edges, brought about by the periodisation procedure, must be eliminated in order to improve the initial conditions.

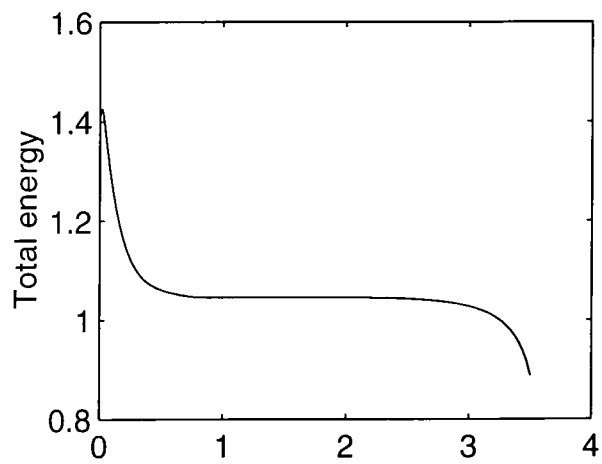
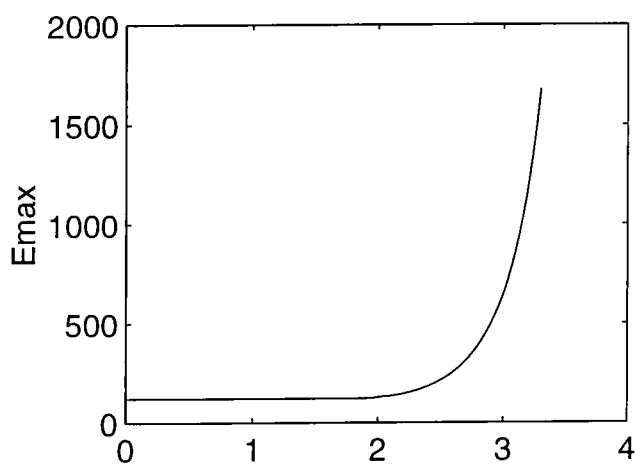
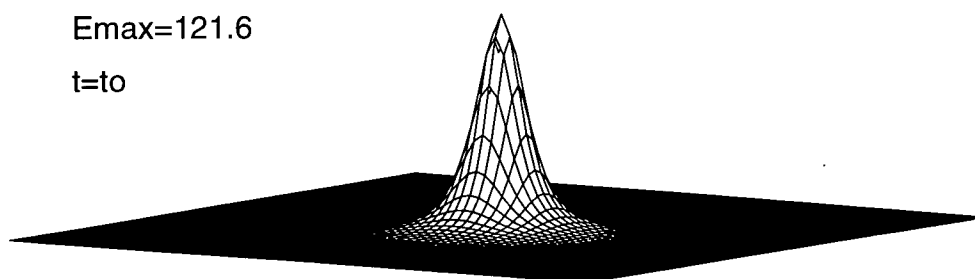


Figure 4.5: Above: Total energy density at $t_0=0.8$, corresponding to our prepared, improved initial one-soliton configuration. Below: The maximum value of the total energy density (E_{max}) and the total energy *vs.* t . The lump grows infinitely tall soon after $t_f \approx 3.5$, and the numerical procedure collapses.

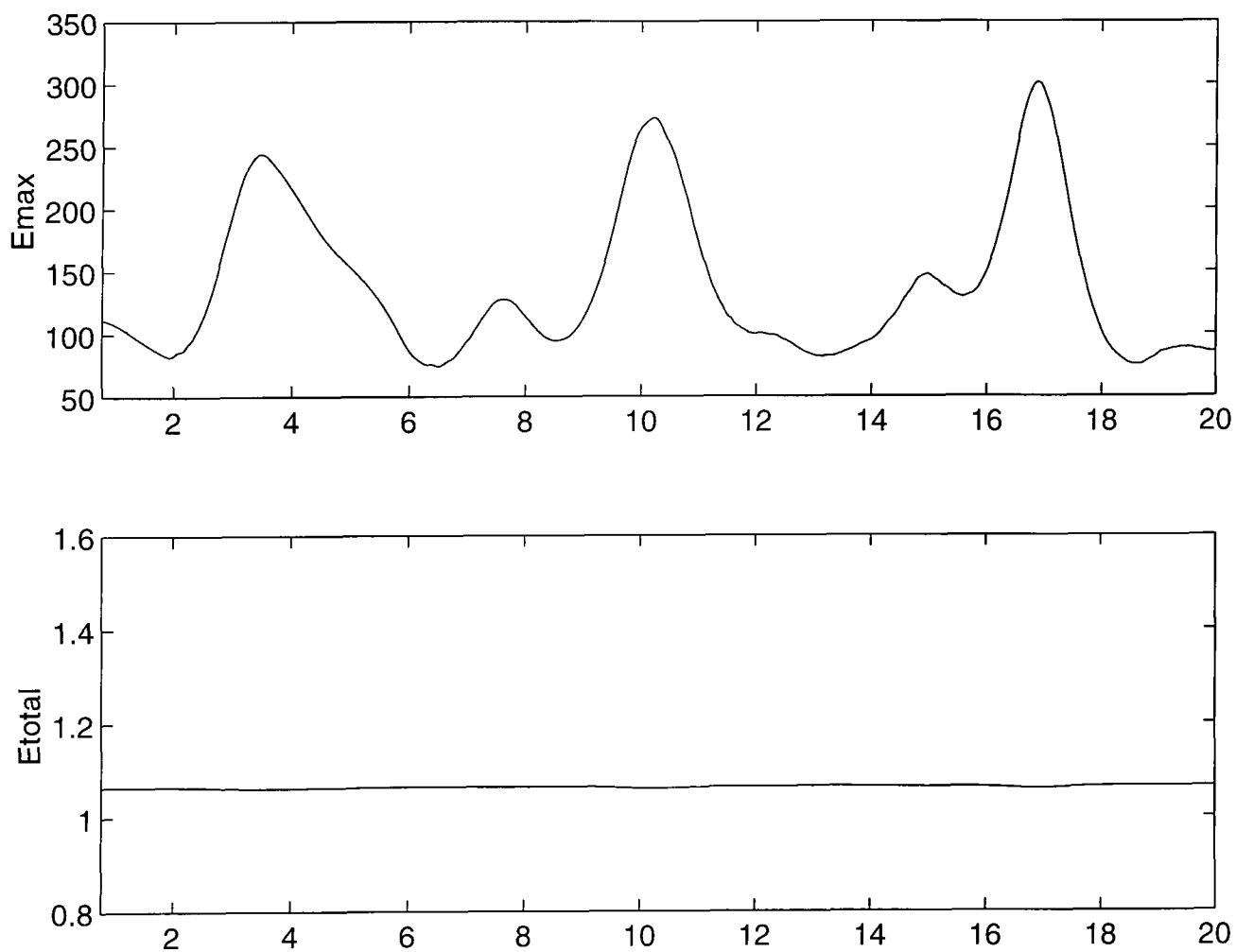


Figure 4.6: Modified $O(3)$ model for a single-lump with $\theta_1 = 0.001$. Above: Peak of the total energy density *vs.* t . The lump is now stable. Below: The corresponding total energy is now conserved throughout the numerical evolution. In both diagrams t runs from $t_0=0.8$ [compare with figure 4.5].

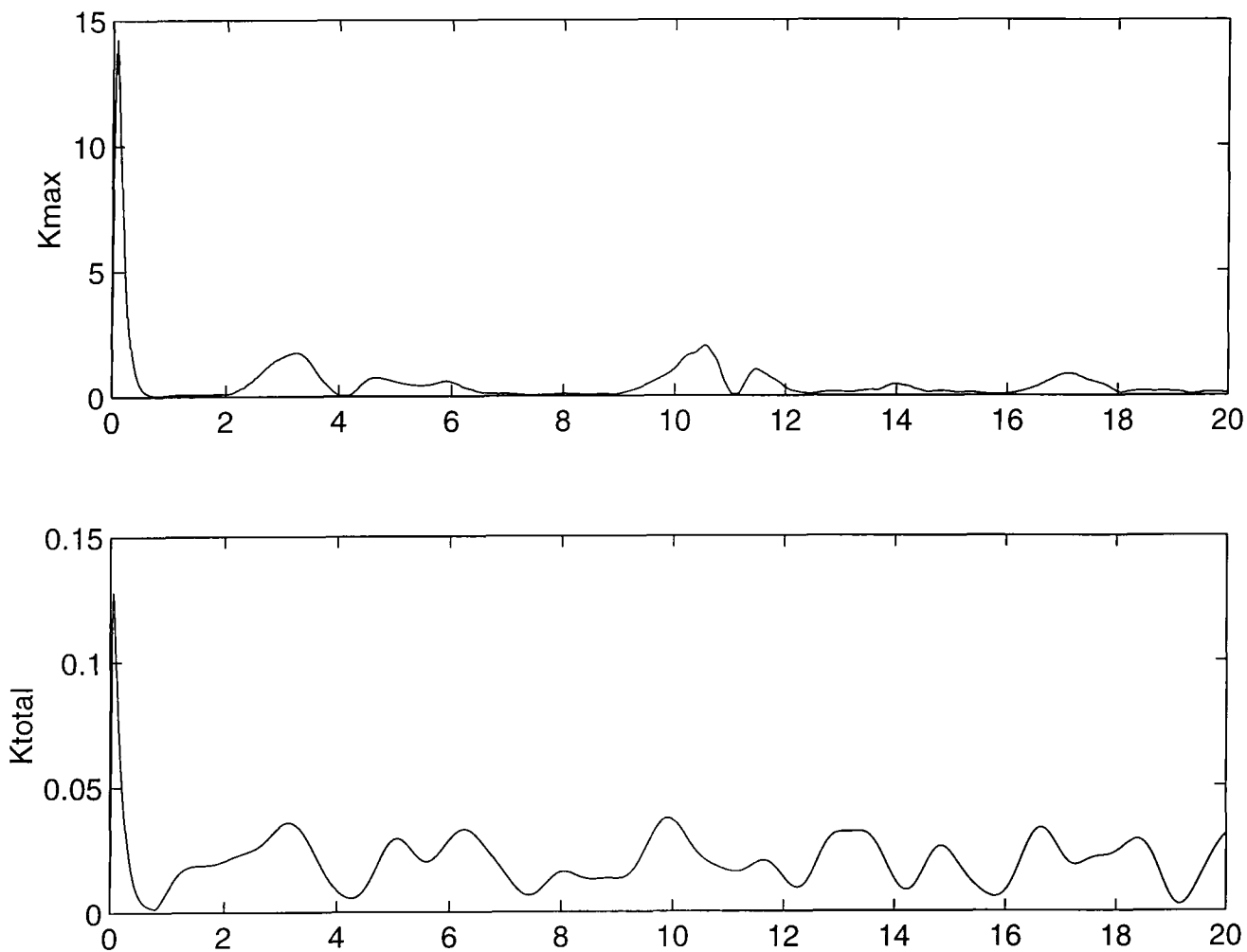


Figure 4.7: Kinetic plots for the single-skyrmion case of figure 4.6. Above: Peak of the kinetic energy density *vs.* time. Below: The corresponding total kinetic energy. In both diagrams the large values of the kinetic energy are during the preparatory stage ($t=0$ to $t_0=0.8$). Later on, the kinetic energy is derisory.

4.4 Solitons of degree 2

4.4.1 $O(3)$ case

We now move on to the interesting question of collisions, limiting ourselves to two solitons. It is to be stressed that the preparatory stage devised for the pathological single-soliton case of section 4.3 is not required for solitons of degree ≥ 2 .

Our initial two-soliton field is given by a function of the form (4.10)-(4.11) with $\kappa=2$:

$$W_2 = \frac{\sigma(z - a_1) \sigma(z - a_2)}{\sigma(z - b_1) \sigma(z - b_2)}, \quad a_1 + a_2 = b_1 + b_2. \quad (4.53)$$

First consider the situation where the solitons are symmetrically positioned along the horizontal axis and sent towards each other with initial relative velocity $\vec{v} = (0.2, 0)$. We select the zeros and poles to be:

$$\begin{aligned} a_1 &= (0.77, 1.95), & a_2 &= (3.25, 1.95); \\ b_1 &= (1.32, 1.95), & b_2 &= (2.70, 1.95). \end{aligned} \quad (4.54)$$

Note that we introduce the initial velocity into the system by evaluating at $t = 0$ the time derivative of equation (4.53) with

$$\begin{aligned} a_1 &\rightarrow a_1 + vt, & a_2 &\rightarrow a_2 - vt; \\ b_1 &\rightarrow b_1 + vt, & b_2 &\rightarrow b_2 - vt, \end{aligned} \quad (4.55)$$

That is, our initial values of $\partial_t W_2|_{t=0}$ are given by

$$\frac{\partial}{\partial t} \frac{\sigma(z - a_1 - vt) \sigma(z - a_2 + vt)}{\sigma(z - b_1 - vt) \sigma(z - b_2 + vt)} \Big|_{t=0}.$$

Our numerical output files indicate that the soliton-lumps gradually shrink and then undergo a gradual expansion as they approach one another. They

collide at the centre of the grid and transiently merge themselves into a ringish structure, where they are no longer distinguishable. At this point they reach their maximum breadth. After coalescing for a moment the humps of energy get narrower and narrower as they emerge at right angles to the initial direction of motion. Due to their instability, the shrinking process goes on until the solitons get so spiky that the numerical procedure is no longer reliable; this occurs for $t \approx 6$, when $\max|\mu|$ as defined in section 4.2 reaches $\approx 10^{-4}$ and higher. A depiction of this process is presented in figure 4.8: By $t = 5$ the lumps are re-emerging at ninety degrees with respect to the initial direction of motion. About a unit of time later, having displaced themselves a bit more in opposite senses along the ordinates, their increase in height is such that the computational code breaks down.

A numerically interesting feature of the periodic CP^1 model is that the scattering can also be observed when the solitons are sped ‘away’ from each other, towards the borders of the net. This is achieved by taking $v \rightarrow -v$ in (4.55). Again, we see scattering at 90° . A representation of this event can be viewed in figure 4.9, where the lumps appear in halves. By folding edge-to-edge any given picture in figure 4.9, as if deforming the flat T_2 into a cylinder, the halves coincide and reunite harmoniously. The evolution of the corresponding energy densities, total and kinetic, are exhibited in figure 4.10. Note that the soliton-lumps are depleted of very little radiation during the quasi-elastic process (before the collapse, that is, signalled by the familiar unlimited growth of the energy). In figure 4.11 the graphs of the total energy and the topological charge, for the process of illustration 4.9, are too shown as a function of time. The case of soliton-lumps colliding at the centre, figure

4.8, is also characterised by curves akin to those of figures 4.10 and 4.11. Note that this sort of border-scattering is a good way to test the correctness of our periodic lattice.

A typical head-on collision with the solitons initially placed along a diagonal is illustrated in figure 4.12. The initial state therein presented is achieved by the arrangement

$$\begin{aligned} a_1 &= (0.95, 0.75), & a_2 &= (3.05, 3.25); \\ b_1 &= (1.22, 1.95), & b_2 &= (2.78, 2.05). \end{aligned} \tag{4.56}$$

After directing the solitons away from the centre with initial velocity $\vec{v} = \sqrt{2}(0.1, 0.1)$ $-v=0.2$, they collide at the corner $(0,0)=(4,4)$ and reappear from $(0,4)=(4,0)$ at right angles to the initial direction of motion. Of course, all four corners are nothing but the same point: There the lumps meet, coalesce and scatter off as already explained. Shortly afterwards, the instability of the system manifests itself in the usual manner, reflected by the $O(3)$ curve in the graph $E_{max}(t)$ of figure 4.12. This diagram also includes the resulting curve of the stable Skyrme version, described later in subsection 4.4.2.

The proceedings for collisions involving a non-zero impact of parameter can be followed in the prototype display of figure 4.13: The extended objects come across non-frontally, rather mildly, preserving their integrity. They re-group and get passed each other separated by a certain vertical distance. As they do so, the lumps become thinner and thinner in the familiar $O(3)$ fashion.

We have also devoted attention to solitons situated in an arbitrary, non-symmetrical way within the network FC. We too found that the solitonic

entities scatter at ninety degrees when propelled against one another. In the next section we will further elaborate on this case.

We may interpret the instability of (4.53) under numerical simulations as follows: The lumps start off satisfying the selection rule $a_1 + a_2 = b_1 + b_2$, which links them in some manner. Due to inevitable round-off errors during the numerical simulation, the field gets perturbed and so it is only approximately described by the original field configuration. As the perturbation is quite small it will excite mainly the degrees of freedom which are zero modes of the original configuration. Thus, in particular, a_j and b_j will start evolving but in order to remain close to the original configuration they will keep the constraint unbroken. Such evolution may lead to a_j and b_j , pairwise, coming close together. This corresponds to the solitons shrinking. To see this note that $|a_j - b_j|/2$ determines the size of the j -th soliton. This shrinking is essentially of the same type as the shrinking of the solitons studied in chapter 3. We would like to stress that since analytical solutions exist in all topological sectors of index ≥ 2 , this lack of stability of our two-soliton system is of a different nature than the instability of the single-soliton configuration (and so non-existence of a one-soliton static solution) discussed in the previous section. There the solution does not exist on the lattice or in the continuum; here the solutions do exist in the continuum but are unstable and putting them on the lattice introduces a perturbation which sets off the instability. An alternative explanation is that during the time evolution the field may no longer obey the relation $a_1 + a_2 = b_1 + b_2$, and the extended structures may begin to move somewhat independently, away from the torus. In such circumstances, they become unstable and begin to shrink.

4.4.2 Skyrmion case

Let us now consider the Skyrme lagrangian (4.51) as applied to two solitons. Frontal collisions along the abscissas corresponding to the arrangement (4.53)-(4.54) unfold as in the pure $O(3)$ scheme. The Skyrme term, however, limits the shrinking of the lumps and renders them stable; their motion can now be followed for as long as desired. For instance, the skyrmions proceed as in figure 4.9 but, after 90° scattering at the lattice point $(0,2)=(4,2)$, they continue their journey and collide thrice more, reaching again their $t=0$ positions and going on to repeat this cycle anew, as suggested by figure 4.14. This notable multi-scattering phenomenon cannot be observed in the usual non-periodic CP^1 format.

All four snapshots in figure 4.14 correspond to coalescing skyrmions, shortly before scattering off. The indistinguishability of the lumps, come impact time, is also apparent from figure 4.14: The formation of four peaks characterises such occurrence. Observe also that the diameter of the ringish, volcano-like state that the lumps form when coming together is quite considerable, of the order of the lattice length L . This is further illustrated in figure 4.15.

All cases analysed in this section correspond to a value of the Skyrme parameter equal to $\theta_1 = 1/2000$, but the same qualitative behaviour is observed for values down to ≈ 0.00007 (with the amplitude of the vibrations being accordingly more pronounced). Smaller values of θ_1 cannot prevent the extended structures from getting too thin, and lead to the breakdown of our computational code.

Diagonal skyrmion collisions (that is, those in which the initial position of the extended objects is along a diagonal in the fundamental cell) develop in the same lines of the $O(3)$ situation sketched in figure 4.12. However, as exemplified by the dashed curve in the bottom-right side of that picture, this time the dynamic, solitonic quasi-particles are not unstable anymore.

Next consider the collision of two solitons located at arbitrary grid points, of which an example is provided by the parameters

$$\begin{aligned} a_1 &= (0.77, 1.30), & a_2 &= (3.25, 2.70); \\ b_1 &= (1.32, 1.95), & b_2 &= (2.70, 2.05). \end{aligned} \tag{4.57}$$

To calculate the velocity that will direct the skyrmions defined by (4.57) towards each other, we resort to the plot $x - y$ in the superior half of figure 4.16 and find

$$\tan(\zeta) \approx 2.09218476,$$

where ζ is the angle between the lump A and the abscissas. Setting the speed v equal to 0.2 and using

$$\begin{aligned} v &= \sqrt{(v_x)^2 + (v_y)^2} \\ &= v_x \sqrt{1 + \tan^2(\zeta)}, \end{aligned}$$

we obtain

$$\vec{v} = (0.08624827, 0.18044732).$$

We will however use the cruder approximation

$$\vec{v} = (0.0862, 0.1804), \quad v \approx 0.2. \tag{4.58}$$

whose corresponding impact parameter is very small but non-zero. This will be reflected in a scattering angle slightly less than 90° and in the colliding

lumps being not completely indistinguishable. When the collision is perfectly head-on, the coalescing solitons are not distinguishable and they emerge at exact right-angles to the original direction of motion. We have already seen this in both scattering cases shown previously. Our choice (4.58) allows to trace the path of each individual lump both before and after the impact.

In the upper-half of figure 4.16 we have two complementary graphs: The one in the left-hand-side exhibits the coordinates (x, y) of the amplitude E_{max} as a function of t , whereas the diagram on the right-hand-side plots x vs. y . The labels $A - E$ are a guide as to the path followed by one of the lumps, the route of the other being given by the corresponding symmetrical points: Labelling these points by $\tilde{A} - \tilde{E}$, the coordinates of a given point, A for example, are related to the coordinates of the corresponding site \tilde{A} by

$$x_A + x_{\tilde{A}} = L, \quad y_A + y_{\tilde{A}} = L \quad [L = 4]. \quad (4.59)$$

A skyrmion-lump starts at A and after 90° scattering (actually somewhat less than 90 degrees, as anticipated) around the centre it continues its itinerary to the position B , where it disappears to re-emerge at C . Thence the extended structure heads south-east and, having reached point D at $t_D \approx 14.5$, it suddenly changes its path to move south-west (point E), unequivocally signalling that a second 90° scattering has taken place. Regarding the other colliding entity, the one starting at $(x_{\tilde{A}}, y_{\tilde{A}}) \approx (1.5, 0.9)$, we can see that the said second clash changes its trajectory from the north-west to the north-east direction. Our numerical simulation terminates at $t_F \approx 30$, where F denotes the end of the leg started at E .

A 3-D picture of the above-described second scattering would not be easy

to decipher due to the expansion of the skyrmions. For instance, the distance from spot D to its counterpart \tilde{D} suggests the formation of a coalescing ring-like state of large periphery. Our numerical files show that at $t_D \approx 14.5$ (D impact time) E_{max} reaches its minimum value, 0.5623. An expansion of this kind can be appreciated from the dashed, skyrmion curve in the bottom-right of figure 4.12 [see also illustration 4.15].

Now imagine our flat manifold T_2 as the surface of a doughnut in \mathcal{R}_3 , obtained by rotating the circle of radius r and circumference $L = 4$ about a coplanar line (Z axis, say) that does not intersect it. The coordinates ($x \equiv \Upsilon, y \equiv \vartheta$) serve as the angle of rotation of the plane of the circle and the angle on the circle itself, respectively. The coordinates (X, Y, Z) of any point on the curved torus satisfy the standard equation

$$(\sqrt{X^2 + Y^2} - R)^2 + Z^2 = r^2, \quad (4.60)$$

where

$$\begin{aligned} X &= [R + r \cos(\vartheta)] \cos(\Upsilon), \\ Y &= [R + r \cos(\vartheta)] \sin(\Upsilon), \\ Z &= r \sin(\vartheta). \end{aligned} \quad (4.61)$$

The radius r is $L/2\pi \approx 0.63662$ and the distance from the centre of the circle to the axis of revolution (Z) is $R = 2r$.

The distance d from the origin $(X, Y, Z) = (0, 0, 0)$ to a soliton-lump on the toroidal surface can be calculated via

$$\begin{aligned} d &= \sqrt{X^2 + Y^2 + Z^2} \\ &= r \sqrt{5 + 4 \cos(\vartheta)}. \end{aligned} \quad (4.62)$$

Still referring to the general situation (4.57)-(4.58), from our numerical files or simply with the help of the top-right graph in figure 4.16, the approximate

values of the latitude $y \equiv \vartheta$ can be reckoned. Focusing ourselves on the A -lump, through formulae (4.61) and (4.62) we can tabulate some useful values in the accompanying table:

	ϑ	Z	d
A	3.1 (178.4°)	0.01	0.63
M	2 (114.6°)	0.57	1.16
D	0.46 (26.3°)	0.28	1.86
F	2.8 (160°)	0.2	0.7

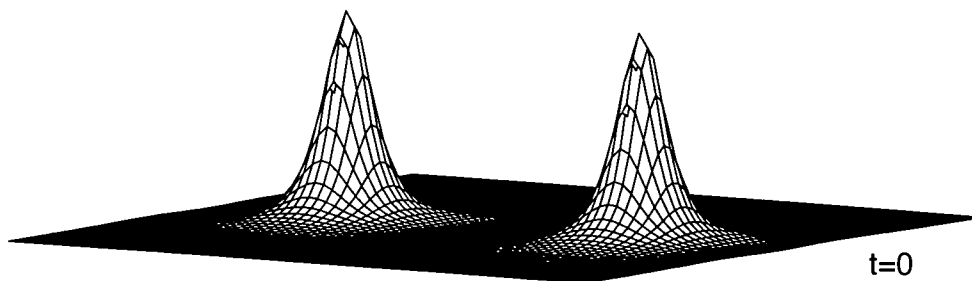
Sent from the vicinity of the centre in the polar illustration of the bottom-left side of figure 4.16, the skyrmion-lump A moves clockwise and meets its anti-clockwise travelling colleague at latitude $\vartheta_M = 114.6^\circ$ (M stands for ‘middle’). The A -soliton, after scattering as explicated earlier, continues its clockwise polar-trip, decreasing in latitude. Just going passed the 30° mark a second collision occurs: This time the lump reverses its ϑ -direction and marches on until the end of the simulated journey at site F , $(\vartheta_F, d_F) = (2.8, 0.7)$. The result is a circular trajectory.

Paying heed to the graph on the lower-half portion of figure 4.16, a similar analysis follows: Starting from around the valley of the curve $d(\vartheta)$, the dynamic skyrmion ascends to reach the top ($d_D = 1.86$), after experiencing the first 90° event at $\vartheta_M = 2$. The d -path of our extended object is reversed due to a subsequent collision: The skyrmion motions downhill, descending through the previously transited locus and stops at F , where the simulation ushers in.

With reference to the situation when the initial velocity equals zero, we recall from chapter 3 that in the non-periodic Skyrme model the solitons slightly move away from each other, thus demonstrating the presence of a

repulsive force between them. However, on the torus we have found that our skyrmions undergo no translation at all as time elapses. This might be related to the fact that there is no θ_2 term in the toroidal model (it might also be that the net repulsive force on a given lump is zero due to the presence of similar entities in neighbouring lattices). In further agreement with this result is the absence of a critical speed above (below) which the skyrmions would scatter at 90° (180°) to the initial direction of motion. Such a critical value was found to be ≈ 0.3 in the non-periodic, modified model of chapter 3. As thoroughly analysed in this now ebbing chapter 4, the toroidal model exhibits 90° scattering regardless (we have verified that values smaller than the speed of 0.2, employed all throughout this chapter, do not show otherwise).

$E_{\max}=118.2$



$E_{\max}=125.3$

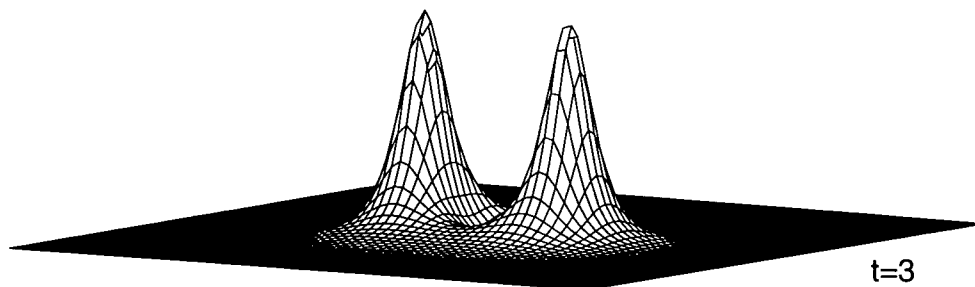


Figure 4.8: Total energy density corresponding to $O(3)$ solitons sent towards each other with $\vec{v} = (0.2, 0)$.

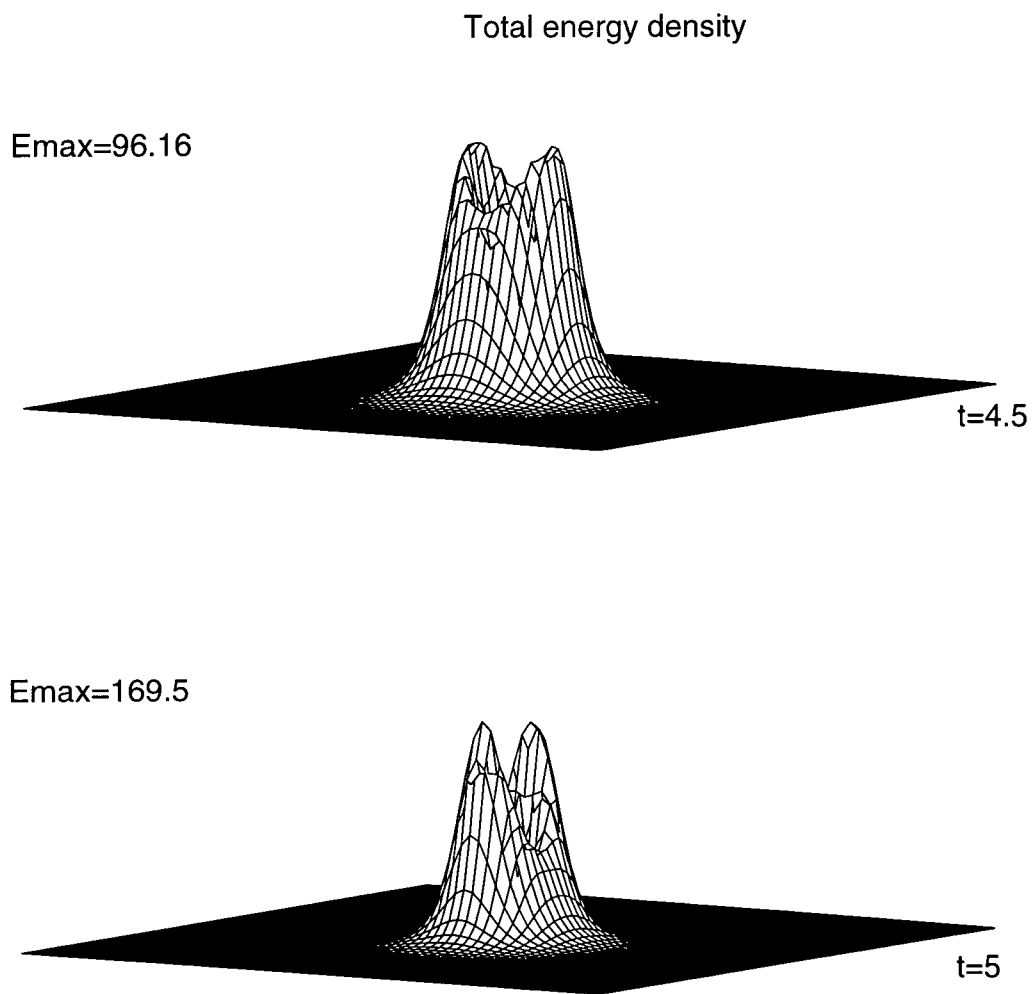
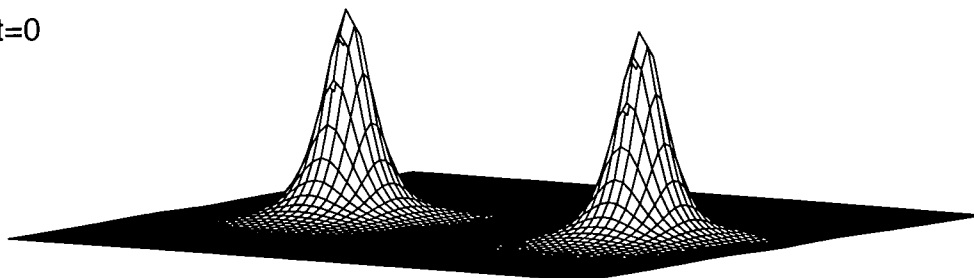


Figure 4.8: Continued. The extended structures scatter at 90° . They separate a moment later with their heights augmenting unstably until the lumps blow asunder.

$E_{\max}=118.2$

$t=0$



$E_{\max}=83.37$

$t=3.5$

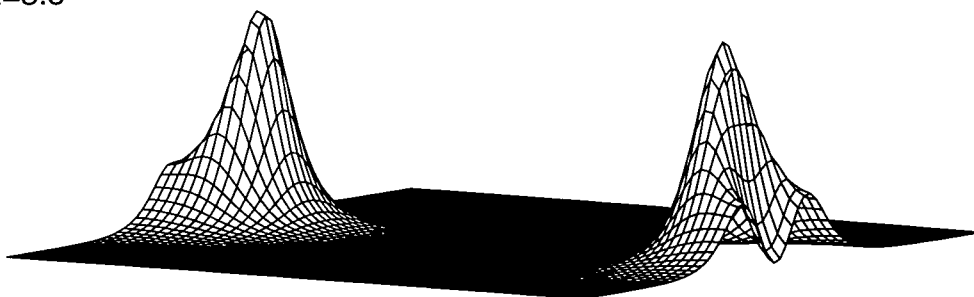


Figure 4.9: Total energy density corresponding to $O(3)$ solitons moving away from the centre with $\vec{v} = (0.2, 0)$. The amplitude of the lumps gradually decreases as they approach each other, reaching a minimum when they coalesce.

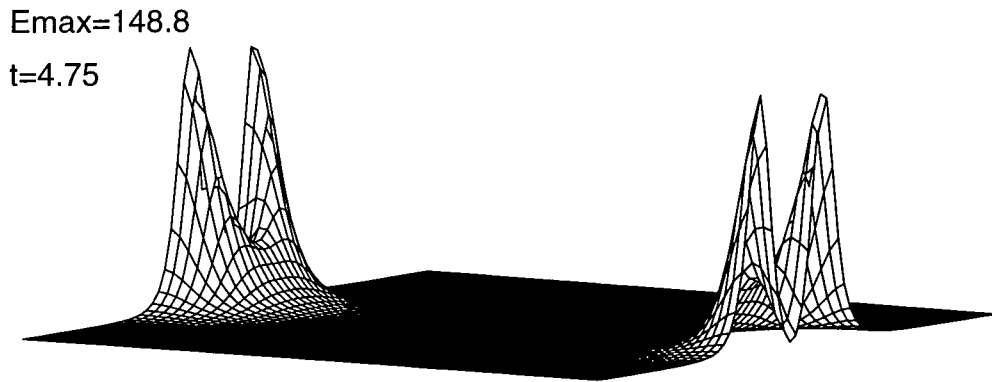


Figure 4.9: Continued. The solitons scatter at 90° . They become very spiky as time progresses but, as shown in figure 4.14, this is corrected by merely adding a Skyrme term to the lagrangian.

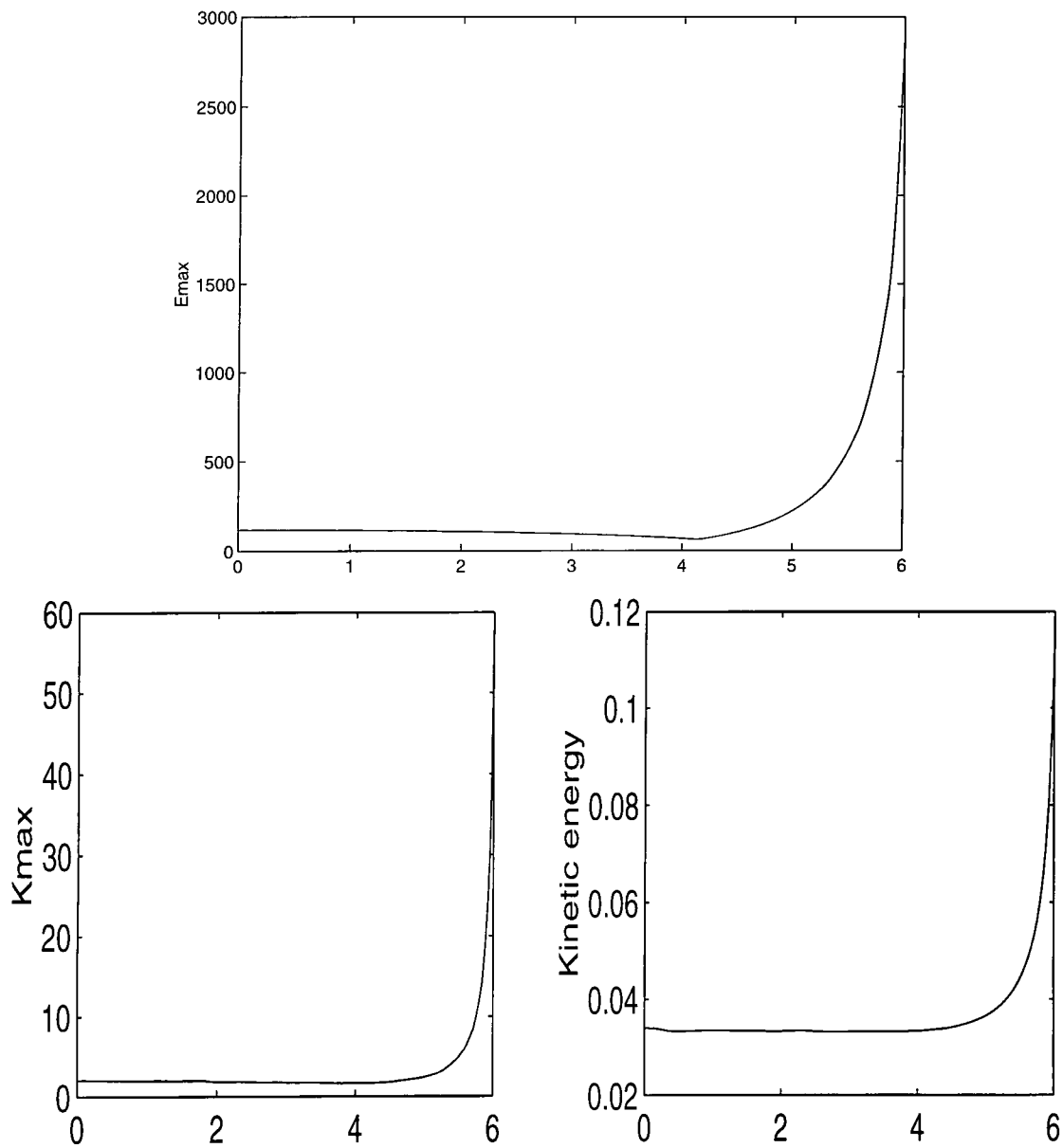


Figure 4.10: Graphs corresponding to the scattering shown in figure 4.9.

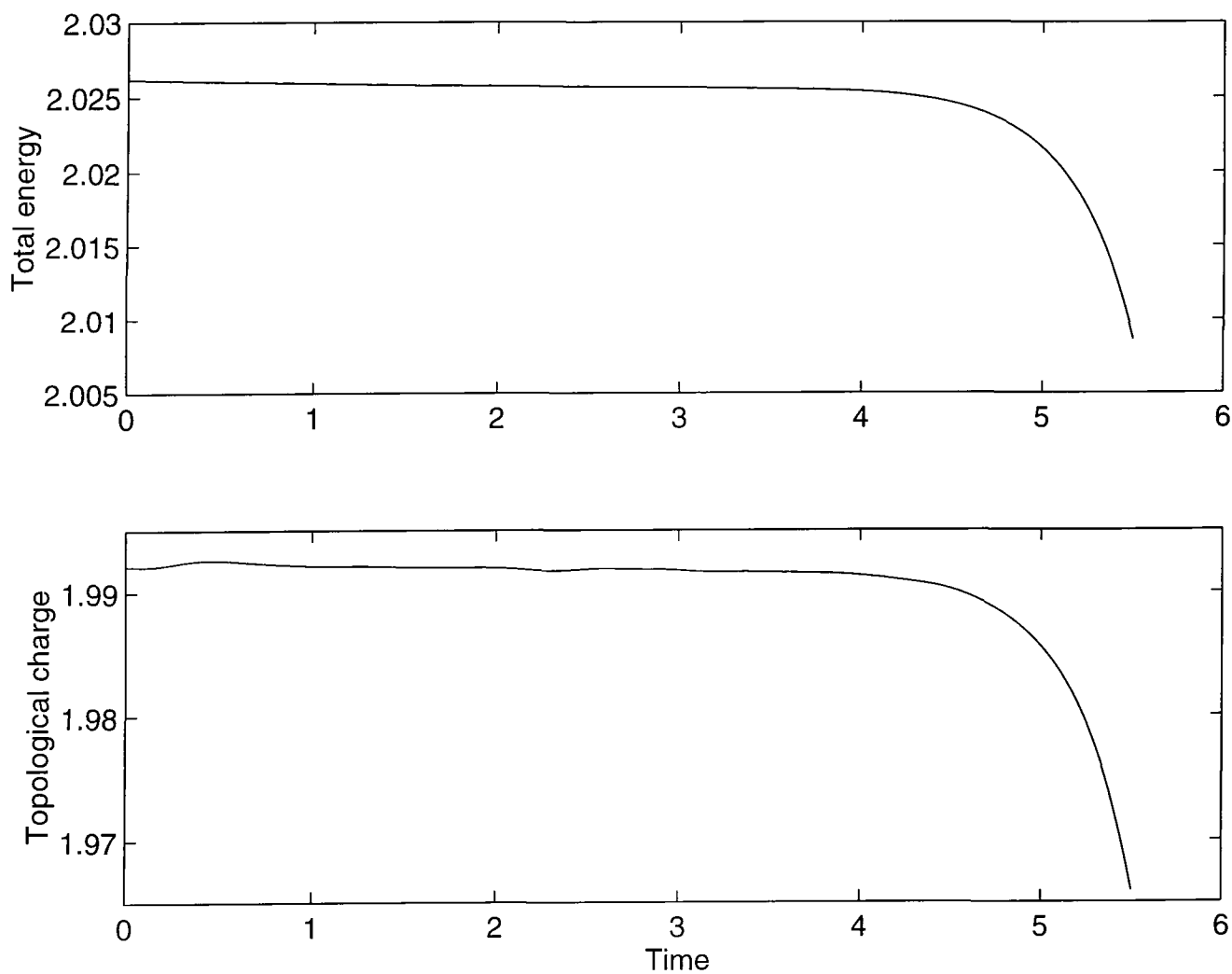


Figure 4.11: Conservation of energy and topological index. The slopes at the tail of the curves signal the occurrence of numerical errors as the solitons get too spiky.

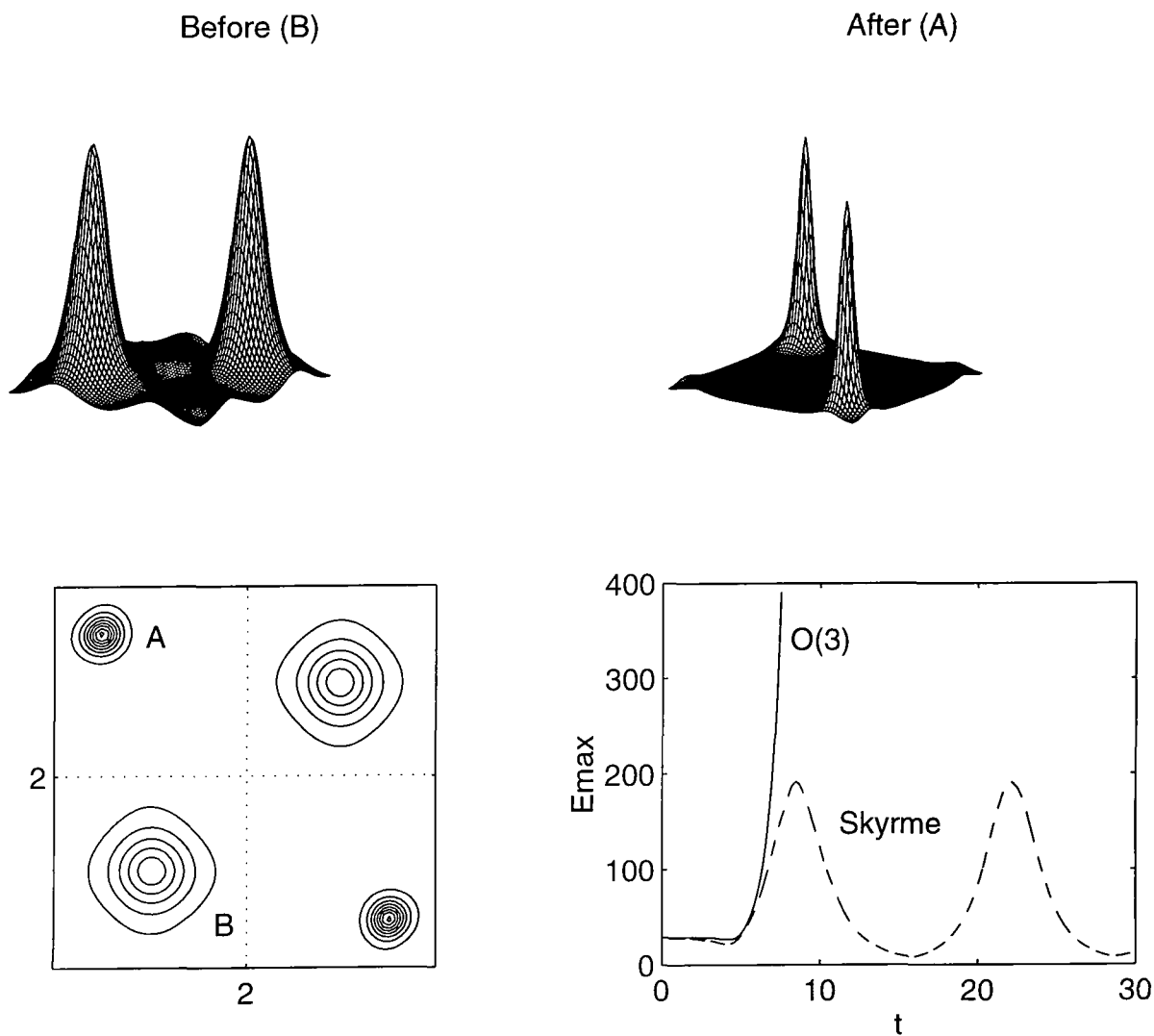


Figure 4.12: $O(3)$ solitons moving away from the centre along the $(0,0)-(4,4)$ diagonal (B). They collide at the corners and scatter at right angles (A). When the model is supplemented by a Skyrme term the lumps are stable, as shown in the accompanying graph $E_{max}(t)$ (broken curve).

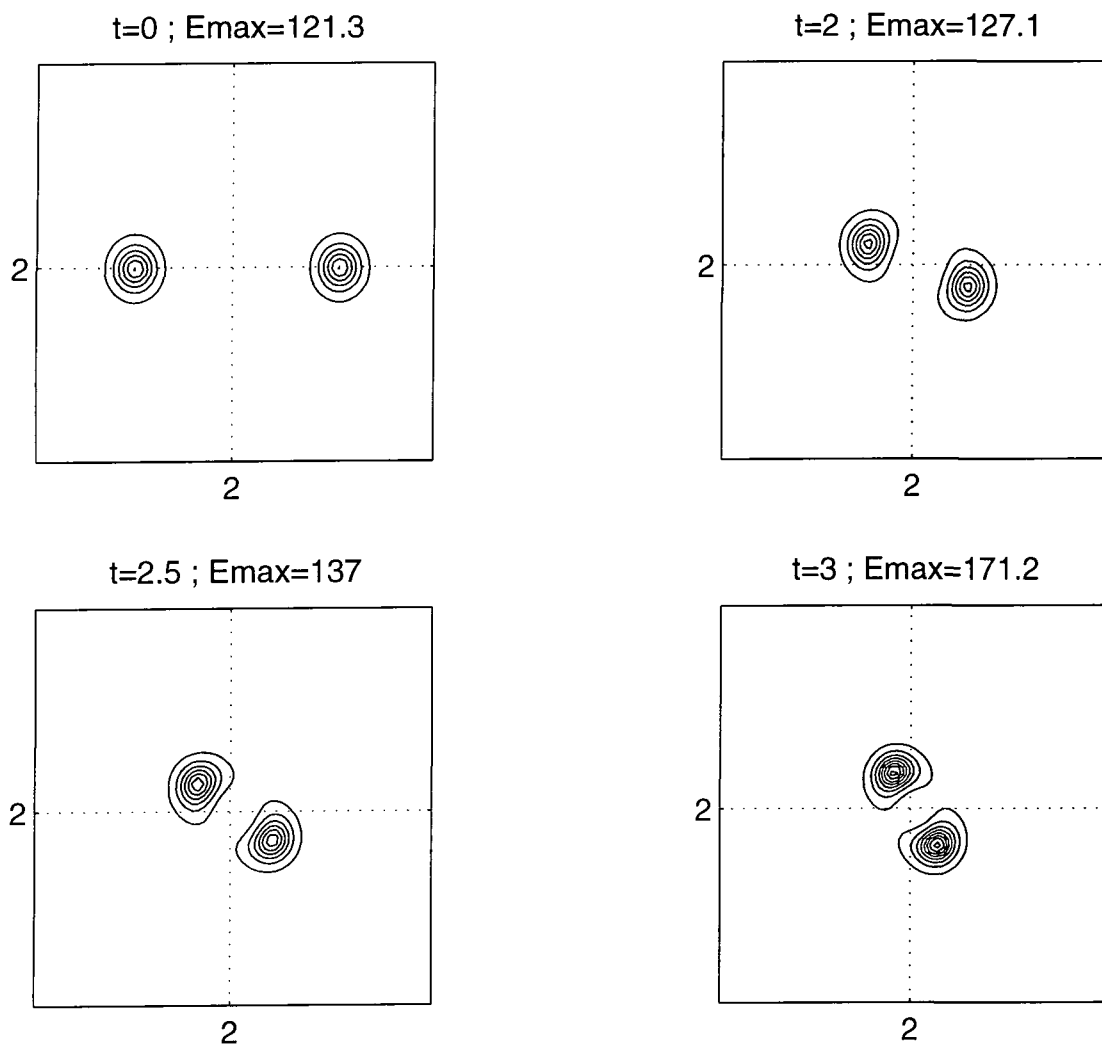


Figure 4.13: $O(3)$ collision for a relatively large impact parameter. The initial velocity is $\vec{v} = (0.3, 0.1)$.

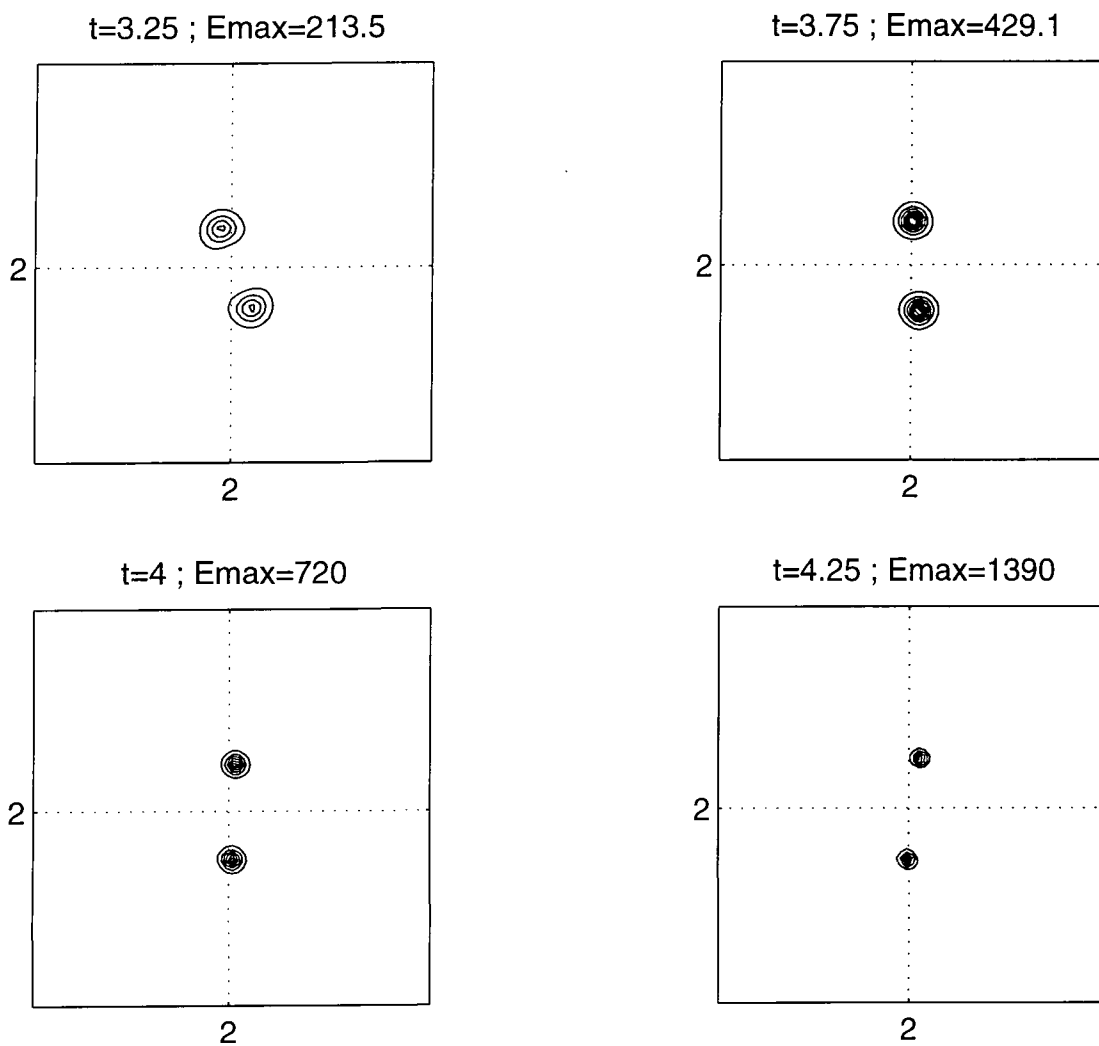


Figure 4.13: Continued. After a relatively mild scattering the solitons proceed in opposite senses whilst continuing to shrink.

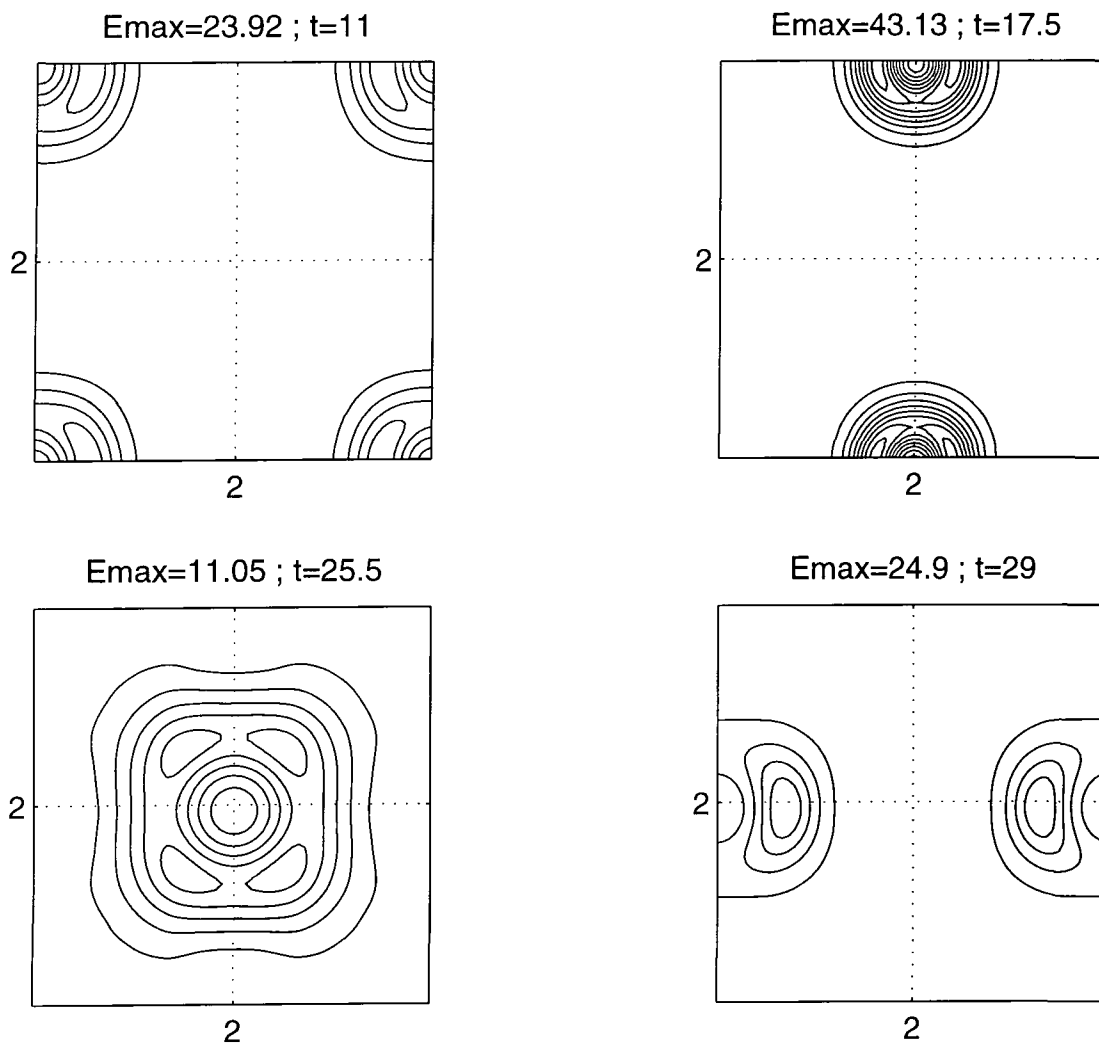


Figure 4.14: Skyrmion scattering ($\theta_1=1/2000$) for $\vec{v} = (0.2, 0)$. After scattering like the $O(3)$ solitons of figure 4.9, the skyrmions do not collapse but go on to collide at $t = 11, 17.5, 25.5$ and so forth. In every occasion they scatter at right angles. This cycle repeats itself indefinitely.

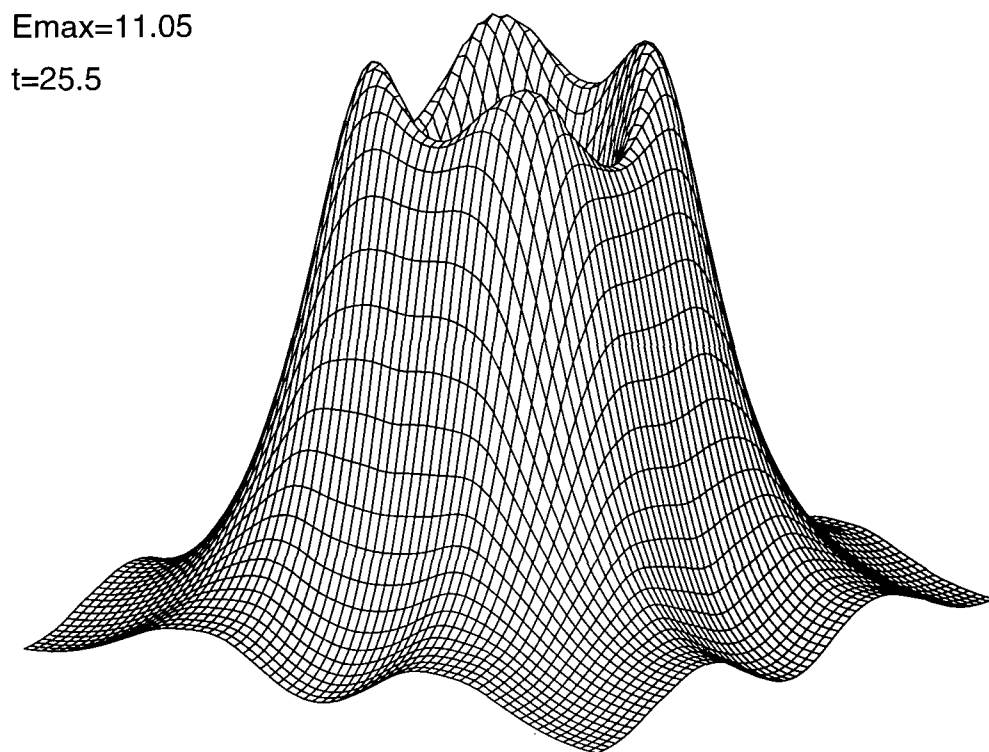


Figure 4.15: Three dimensional picture corresponding to the second collision of the event depicted in figure 4.14. The four peaks characterise the coalescing state, where the lumps can no longer be individually recognised. Note also that the united skyrmions occupy all the lattice area.

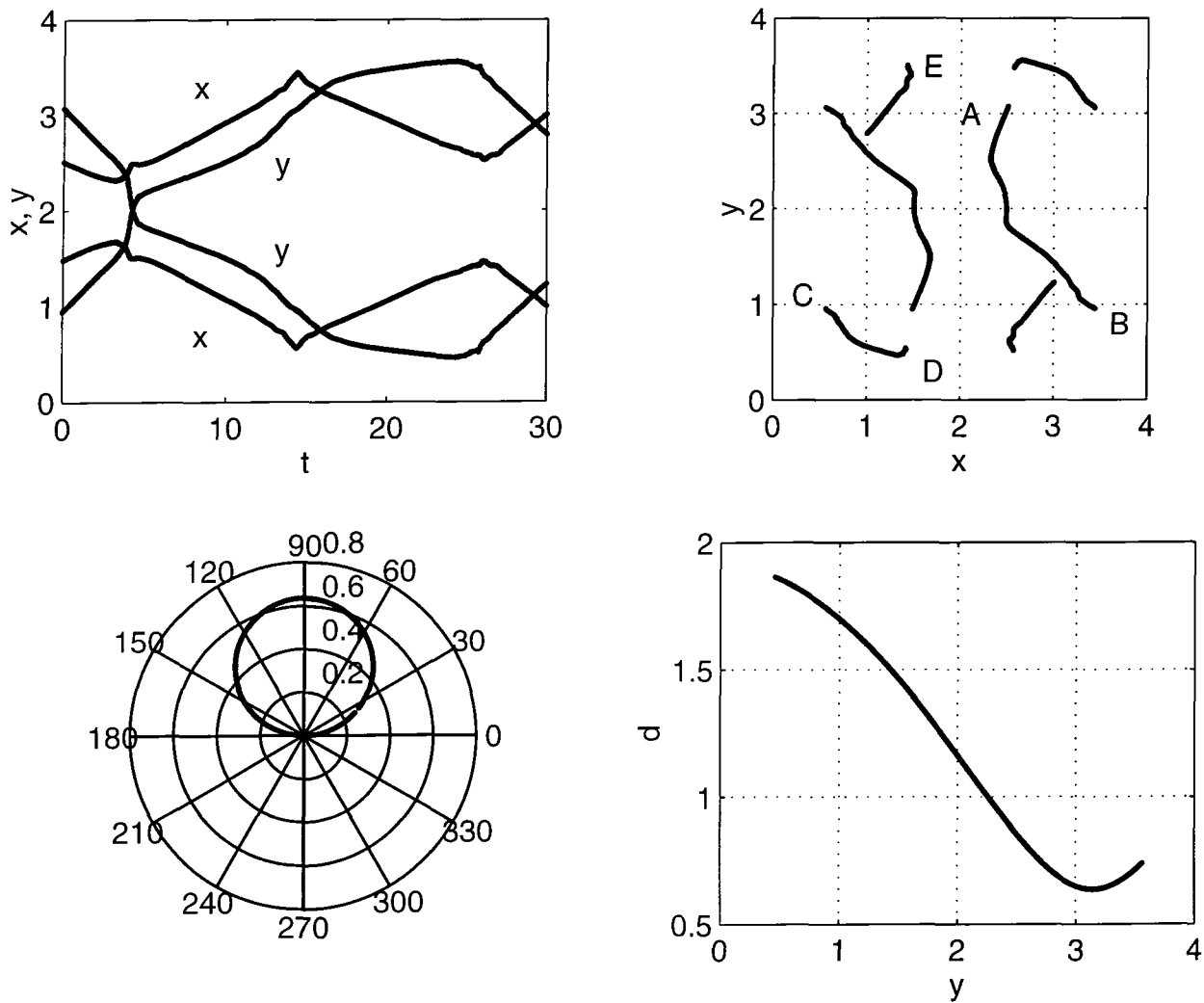


Figure 4.16: Trajectories of the position of E_{max} corresponding to head-on scattering of skyrmions arbitrarily situated in the basic cell. The labels A-E follow the itinerary of one of the lumps. The polar plot shows $Z = r \sin(\vartheta)$. The distance d is from the lumps to the origin $(0,0,0)$ of equations (4.58).

Chapter 5

Summary

We have performed a numerical study of some stability and scattering properties of both the non-linear $O(3)$ and the Skyrme model in (2+1) dimensions. This latter scheme, an extension of the former, is a low dimensional analogue of the nuclear skyrmion theory in four dimensional space-time. None of our two CP^1 systems is integrable, and their evolution in time has been made via numerical simulations.

The $O(3)$ solitons are not stable because they are invariant under scale transformations. Any perturbation causes the solitons' energy density to decrease (increase) its width (height) without limit. When the breadth is comparable to the lattice spacing the numerical code breaks down. An explicit perturbation can be introduced into the system by impinging the solitons with some initial velocity, but the implicit perturbation inevitably brought about by the discretisation procedure suffices to push to the fore the instability as already explained.

The $O(3)$ lumps have the property of scattering at 90° to the initial direction of motion when sent to collide head-on. Such systems are more perturbed than the static single-soliton case, but nevertheless their scattering can be arranged to happen before the instability takes over. Now, the judicious addition of extra terms to the $O(3)$ lagrangian can bring stabilisation to the model, a much desired asset for a theory to possess. In the usual case where the model is defined on compactified plane, represented numerically by a non-periodic lattice, two additional terms are necessary: A Skyrme-like (θ_1) and a potential-like (θ_2) term.

In chapter 3 we have exploited the non-uniqueness of the θ_2 term to write down a version of the planar Skyrme model with a rather general potential term. The numerical representation of this model introduces an implicit perturbation bigger than previously-studied choices for the θ_2 -term. However, such factor was not of the essence and our results did not differ qualitatively from those obtained with anteriority, in different versions of the model.

Restricting ourselves to solitons with topological charge $Q=1$ and 2, we found that the skyrmions are stable; their energy density profiles do not change appreciably in shape, nor they shrink or expand unduly with the passing of time. The single-skyrmion case was almost perfectly static, whereas the two-skyrmion situation evidenced a repulsive force between the extended objects when started off from repose. Further evidence of this repulsive interaction is seen in head-on collisions, when the skyrmion-lumps scatter back-to-back if the initial, boosting velocity is not greater than ≈ 0.3 . Otherwise they scatter at 90° .

In the $O(3)$ limit ($\theta_1=\theta_2=0$) scattering at 90° takes place for any non-zero initial velocity, *i.e.*, the soliton-lumps no longer repel each other. This is confirmed in the static $Q = 2$ case where the bell-shaped quasi-particles keep still as time goes by, before the instability breaks down the numerical code.

In chapter 4 we considered both CP^1 models defined on a flat torus, an unexplored scenario in the context of soliton stability/scattering. The numerical simulations in this case are carried out in a periodic fundamental mesh.

The toroidal theory possesses the distinctive feature of admitting analytic soliton solutions of topological degree ≥ 2 , only. Analytical solitons in the $Q = 1$ class do not exist, and those in the $Q = 0$ sector are trivial. This is because the periodic solutions are given by elliptic functions, the simplest of which are known to be of the second order. In the language of differential geometry, there are no holomorphic harmonic maps of degree one on the torus since its Euler number is zero.

Nonetheless, combining appropriate fields of the kink type with a one-pole quasi-periodic soliton configuration, we have been able to fabricate a doubly-periodic meromorphic solution of the $O(3)$ equation of motion in the $Q=1$ sector. But the periodisation procedure unavoidably unsmoothens the resulting energy-lumps around the borders of the fundamental cell. It turns out that our *ansatz* behaves unstably under numerical evolution, shrinking faster than its counterpart of chapter 3. Since, unlike the latter, single static solitons do not exist in the continuum on the torus, our results suggest that the instability of our periodic construct is intrinsic, rather than occasioned

by the numerical method utilised.

Notably, by supplementing the $O(3)$ lagrangian with merely a θ_1 term our solitonic *anstaz* becomes stable, prompting us to claim that it is a licit $Q = 1$ skyrmion on the torus. The sole addition of a Skyrme term also stabilises the pure $O(3)$ solitons in higher topological classes. The non-necessity of a θ_2 term to stabilise the $O(3)$ solitons is another peculiarity of CP^1 on the torus which, in this sense, resembles more closely the hadronic (3+1) dimensional Skyrme model (where no second extra term is needed, either).

In further contrast with the model in compactified plane, two skyrmions with no initial velocity showed that the net force between them is null, which is most likely linked to the absence of a θ_2 term in the toroidal model. As a consequence, there is no critical velocity below which the toroidal skyrmions will bounce back after the impact. This circumstance could be an advantage if one wishes (as in the geodesic approximation) to keep the radiation in the system as low as possible whilst studying CP^1 scattering. It would be interesting to simulate the evolution of our skyrmions with the presence of a θ_2 term, and study their behaviour when started off from rest and also in connection with the existence of a critical velocity.

Collisions on the torus showed scattering at right angles both in the pure $O(3)$ and modified schemes. In the pure model the lumps continue to shrink after the collision until the numerics collapses; in the stable Skyrme format the solitons course through indefinitely. Here, thanks to the periodicity of the network, yet another appealing characteristic of the toroidal model was observed: Multi-scattering. Indeed, after the first scattering the extended structures go on to repeat the quasi-elastic collision-cycle time and again. In

the pure $O(3)$ numerical dynamics these events do not occur, for the solitons blow up before the encore.

Another attractive feature is that collisions can also be studied when the solitons are sped ‘away’ from each other, boosted to meet one another at the borders of the basic grid. The picture is particularly worth viewing when the extended entities reach the edges of the nett: Each lump splits in two and the four bits (four in a soliton-soliton collision) move along the legs of the flat torus to later reunite in the subsequent clash and so on.

With respect to the instability of the toroidal $O(3)$ lumps for $Q > 1$, we must emphasise that it is of a different nature than the $Q = 1$ case. On the one hand, in sectors of charge greater than one, where analytical solutions do exist, the zeros (a_j) and poles (b_j) entering the static soliton-field solutions are subject to the selection rule

$$\sum a_j = \sum b_j,$$

condition that may not hold at later times. This would lead to the instability of the system. However, we favour the view in which the extended structures evolve respecting the abovesaid constraint but in such a way that $a_i \approx b_i$, reducing the breadth of the i -th lump and hence making it shrink. In any case, the aftermath is that the lumps become too spiky and break down the numerical procedure.

On the other hand, in the $Q = 1$ case (where no analytic static solution exists) there is no such selection rule. As a pedagogical exercise, these two kinds of instability can in turn be compared to the situation arising in the spherical model.

In this thesis we have not considered systems containing solitons of negative degree, *i.e.*, anti-solitons. It would be worthwhile to invest some time studying soliton-antisoliton CP^1 collisions, where annihilation features emerge. Inasmuch as this has already been investigated in the model defined in compactified plane [89], in simpler discrete versions than ours, we suggest to focus efforts on the toroidal model to start with. Amongst other things, a comparison of the results found in the above reference with those of the toroidal case would be worth making.

Regarding the model on the sphere, numerical simulations of the skyrmion model in an irregular lattice, *e.g.*, in a lattice where the boundaries are effectively shifted to infinity, have not been reported in the literature. This is something one may like to try out, but since the $O(3)$ two-soliton system in a finite grid is unstable whereas the two-skyrmion case is not (evidencing that the scale set by the grid is not responsible for the stabilisation of the latter), such line of investigation has perhaps only academic, formal value.

More appealing is the study of a $|Q|=1$ system assembled by combining two solitons with one antisoliton for instance, as suggested by Dr. Bernard Piette. Such topological class is specially interesting in the toroidal theory where a static analytic one-soliton solution by itself is not a possibility.

Another worthy follow-up to the present work would be to express the periodic solitons in term of Weierstrass' $\wp(z)$ function which, unlike our choice $\sigma(z)$, is elliptic itself and provides an example of a two-soliton solution. It is derived from $\sigma(z)$, equation (4.14), via

$$\wp(z) = -\frac{d}{dz}\left[\frac{d\sigma(z)/dz}{dz}\right].$$

However, note that $\wp(z)$ is even, and therefore cannot be applied to topological sectors of odd degree. An alternative to Weierstrass' functions is the utilisation of Jacobian elliptic functions. These have been employed to obtain a periodic sine-Gordon field from an instanton on the torus [90].

We opine that of some attractiveness would also be the problem of replacing the torus by a manifold \mathcal{N} with $g > 1$, where g is the genus of \mathcal{N} . We know from differential geometry that harmonic maps exist in the following cases:

- If $|Q| \geq g + 1$;
- if $|Q| = g$ and \mathcal{N} accepts a meromorphic function of degree 2;
- if $|Q| = g$ is even.

The attempt to find and study the dynamics of these soliton candidates would be educational, as so would be the possibility of fabricating numerical *ansatze* for the cases analytically ruled out by the above conditions. Our success in constructing (chapter 4) a good, approximate soliton of degree one on the torus encourages us to pursue the matter further.

Bibliography

- [1] Cova R. J. and Zakrzewski W. J., *Proc. Quantum systems, new trends and methods* 84 [Editors: A. O. Barut *et.al.*], World Scientific, Minsk (1994)
- [2] Cova R. J., *Helv. Phys. Acta* 68, 282 (1995)
- [3] Cova R. J. and Zakrzewski W. J., *Soliton scattering in the $O(3)$ model on a torus*, Durham preprint DTP 96-59 (1996)
- [4] Yang C. N. and Mills R. L., *Phys. Rev.* 96, 191 (1954)
- [5] Goldstone J., *Nuovo Cim.* 19, 154 (1961)
- [6] Higgs P. W., *Phys. Rev.* 145, 1156 (1966)
- [7] Rajaraman R., *Solitons and instantons*, North-Holland (1987)
- [8] Yakushevich L. V., *Q. Rev. Biophys.* 20, 201 (1993)
- [9] *Proc. Int. Cong. Math. Phys.* 691 [Editor: Iagolnitzer D.], International Press, Paris (1994)
- [10] Desurvire E., *Phys. Today* Jan (1994)

- [11] Russell J. S., *Rep. 14th Meet. Brit. Assoc. Adv. Sci.*, 311 York (1844)
- [12] Korteweg D. J. and de Vries G., *Philos. Mag. Ser. 5* 39, 422 (1895)
- [13] Zabusky N. J. and Kruskal M. D., *Phys. Rev. Lett.* 15, 240 (1965)
- [14] Miura R. M. *et. al.*, *J. Math. Phys.* 9, 1204 (1968)
- [15] Zakharov V. E. and Shabat A., *Sov. Phys. JETP* 34, 62 (1972)
- [16] Gardner C. S. *et. al.*, *Phys. Rev. Lett.* 19, 1095 (1967)
- [17] Lamb G. L., *Phys. Lett.* A25, 181 (1967)
- [18] Hirota R., *Phys. Rev. Lett.* 27, 1192 (1971)
- [19] Davey A. and Stewardson K., *Proc. Roy. Soc. Lond.* A338, 101 (1974)
- [20] Novikov S., *Theory of solitons*, Consultants Bureau, New York (1984)
- [21] 't-Hooft G., *Nucl. Phys.* B79, 276 (1974)
- [22] Polyakov A. M., *JETP lett.* 20, 194 (1974)
- [23] Polyakov A. M., *Nucl. Phys.* B120, 429 (1977)
- [24] Coleman S., *Uses of instantons in: The whys of subnuclear physics* [Editor: Zichichi A.], Plenum Press (1979)
- [25] Skyrme T. H. R., *Nucl. Phys.* 31, 556 (1962)
- [26] Holzwarth G. and Schwesinger B., *Rep. Prog. Phys.* 49, 825 (1986)
- [27] Witten E., *Nucl. Phys.* B160, 57 (1979)

- [28] Witten E., *Nucl. Phys.* B223, 422 (1983)
- [29] Chodos A. and Thor C. B., *Phys. Rev.* D12, 2733 (1975)
- [30] Gell-Mann M. and Levy M., *Nuovo Cimento* 16, 705 (1960)
- [31] Dzyaloshinskii I. *et. al.*, *Phys. Lett.* A127, 112 (1988)
- [32] Green A. G. *et. al.*, *Phys. Rev.* B53 11, 53 (1996)
- [33] Hobart R., *Proc. Phys. Soc.* 82, 201 (1963)
- [34] Derrick G. H., *J. Math. Phys.* 5, 1252 (1964)
- [35] Hector J. de Vega, *Phys. Rev. Lett.*, 18, 8 (1978)
- [36] Steenrod N., *The topology of fiber bundles*, Princeton Univ. Press (1951)
- [37] Eells J. and Wood J. C., *Topology* 15, 263 (1976)
- [38] Nakahara M., *Geometry, topology and physics*, IOP publishing, Bristol and Philadelphia (1990)
- [39] Goddard P. and Mansfield P., *Rep. Prog. Phys.* 49, 725 (1986)
- [40] Eichenherr H. and Forger M., *Nucl. Phys.*, B155, 381 (1979)
- [41] Zakrzewski W. J., *Low dimensional sigma models*, Adam Hilger (1989)
- [42] Dadda A. *et. al.*, *Nucl. Phys.* B146, 63 (1978)
- [43] Golo V. L. and Perelomov A. M., *Phys. Lett.* B79, 112 (1978)
- [44] Perelomov A. M., *Physica* D4, 1 (1981)

- [45] Dashen R. F. *et. al.*, *Phys. Rev.* D10, 4130 (1974)
- [46] Goldstone J. and Jackiw R., *Phys. Rev.* D11, 1486 (1975)
- [47] Polhmyer K., *Comm. Math. Phys.* 46, 207 (1976)
- [48] Luscher M. and Pholmeyer K., *Nucl. Phys.* B137, 46 (1978)
- [49] Barone A. *et. al.*, *Riv. Nuovo Cimento* 1, 227 (1971)
- [50] Bogomolny E. B., *Sov. J. Nucl. Phys.* 24, 449 (1976)
- [51] Speight J. M., *On the dynamics of topological solutions*, Ph. D. thesis Durham (1995)
- [52] Borchers M. S. and Garber W. D., *Comm. Math. Phys.* 72, 77 (1980)
- [53] Ward R. S., *J. Math. Phys.* 29, 386 (1988)
- [54] Ward R. S., *Phys. Lett.* A208, 203 (1995)
- [55] Nielsen H. B. and Olesen P., *Nucl. Phys.* B61, 45 (1973)
- [56] Ginzburg V. L. and Landau L. K., *Sh. Eksp. Teor. Fiz.* 20, 1064 (1950)
- [57] Adkins G. *et. al.*, *Nucl. Phys.* B228, 552 (1983)
- [58] Atiyah M. F. and Manton N. S., *Phys. Lett.* B222, 438 (1989)
- [59] Escola K. S. and Kajantie K., *Z. Phys.* 44, 347 (1989)
- [60] Jackson A. *et. al.*, *Nucl. Phys.* A432, 567 (1985)
- [61] Vinh Mau R. *et. al.*, *Phys. Lett* B150, 259 (1985)

- [62] Kopeliovih V. K. and Shtern B. E., *Sov. Phys. JETP Lett.* 45, 203 (1987)
- [63] Verbaarschot J. J. M. *et. al.*, *Nucl. Phys.* A468, 520 (1987)
- [64] Schramm A. J. *et. al.*, *Phys. Lett.* B205, 151 (1988)
- [65] Leese R. A. *et. al.*, *Nucl. Phys.* B442, 442 (1995)
- [66] Braaten E. and Carson L., *Phys. Rev.* D39, 838 (1989)
- [67] Braaten E. and Townsend S., *Phys. Lett.* B235, 147 (1990)
- [68] Battye R. A. and Sutcliffe P. M., *Phys. Lett.* B391, 150 (1997)
- [69] Perring J. K and Skyrme T. H. R., *Nucl. Phys.* 31, 550 (1962)
- [70] Belavin A. A. and Polyakov A. M., *JETP letters* 22, 245 (1975)
- [71] Woo G., *J. Math. Phys.* 18, 1264 (1977)
- [72] Din A. M. and Zakrzewski W. J., *Nucl. Phys.* B174, 397 (1980)
- [73] Leese R. A., Peyrard M. and Zakrzewski W. J., *Nonlinearity* 3, 387 (1990)
- [74] Leese R. A., *Nucl. Phys.* B344, 33 (1990)
- [75] Zakrzewski W. J., *Nonlinearity* 4, 429 (1991)
- [76] Leese R. A., Peyrard M. and Zakrzewski W. J., *Nonlinearity* 3, 773 (1990)

- [77] Azcárraga J. A., Rashid M. S. and Zakrzewski W. J., *J.Math.Phys.* 32, 1921 (1991)
- [78] Piette B. and Zakrzewski W. J., *Nucl. Phys.* B393, 65 (1993)
- [79] Sutcliffe P. M., *Nonlinearity* 4, 1109 (1991)
- [80] Campbell D. K. and Peyrard M., *Physica* D18, 47 (1986)
- [81] Shellar E. P. S. and Ruback P. J., *Phys. Lett.* B209, 262 (1988)
- [82] Atiyah M. F. and Hitchin N. J., *The geometry and dynamics of magnetic monopoles*, Princenton Univ. Press (1988)
- [83] Goursat E., *Functions of a complex variable* Dover Publications Inc., New York (1916)
- [84] Richard J. L. and Rouet A., *Nucl. Phys.* B211, 447 (1987)
- [85] Abramowitz M. and Stegun I. (editors), *Pocketbook of mathematical functions* Verlag Harri Deutsch (1984)
- [86] Eells J. and Lemaire L., *Math. Ann.* 252, 27 (1980)
- [87] Delaunay C., *J. Math. pure et appl. ser. 1* (6), 309 (1841)
- [88] Eells J., *The Mathematical Intelligencer* 9, 1 Springer Verlag New York (1987)
- [89] Peyrard M. *et. al.*, *Nonlinearity* 5, 563 and 585 (1992)
- [90] Sutcliffe P. M., *Nonlinearity* 8, 411 (1995)

